AN ABSTRACT OF THE DISSERTATION OF

Joseph J. Porter for the degree of Doctor of Philosophy in Biochemistry and Biophysics presented on November 16, 2018.

Title: Defining the Role of Tyrosine Nitration in Biology with Genetic Code Expansion.

Abstract approved:

_____

Ryan A. Mehl

The buildup of reactive oxygen species (ROS) and reactive nitrogen and oxygen species (RNS) is known as oxidative stress. Oxidative stress results in a wide variety of modification to biological macromolecules including nucleic acids, lipids, and proteins. For at least 30 years it has been known that high levels of oxidative stress leads to damage to cellular components resulting in cell death via apoptosis and necrosis. In perhaps the last 10 years it has become clear that ROS and RNS also mediate 'redox signaling' via specific macromolecule modifications. The formation of the oxidative post-translational modification (Ox-PTM) 3-nitrotyrosine (nitroTyr) in proteins serves as the main biomarker of oxidative stress and is present in over 50 disease pathologies. In the vast majority of these diseases it is not known if the nitroTyr is simply a bystander or is playing an active role driving disease progression. Genetic code expansion (GCE) has emerged as a method to install noncanonical amino acids (ncAAs) into proteins of interest. Here we develop several GCE systems for the incorporation of nitroTyr to address the role of tyrosine nitration in biology.

This dissertation presents studies aimed to both improve and develop GCE systems for encoding nitroTyr in *E. coli* and eukaryotic cells, and to apply this ability to studying the effect of tyrosine nitration on the calcium (Ca^{2+}) regulatory protein calmodulin (CaM). Four chapters of original work are presented in this dissertation

and include one review and three primary research reports. Three of the chapters (Chapters 2, 3, and 5) focus on the development and optimization of GCE systems for the incorporation of the nitroTyr, and the other chapter (Chapter 4) focuses on the application of the GCE systems to evaluate the nitroTyr Ox-PTMs in the regulatory hub protein, CaM, as the first report of regulating a protein function with the nitroTyr PTM. Chapters 2 and 3 are published; Chapters 4 and 5 are at the stage of manuscripts in preparation for submission. These central chapters are bookended by a brief introduction to oxidative stress and GCE (Chapter 1) and concluding remarks on my summary of the impact of this work, and perspective on future directions (Chapter 6).

In the first research chapter (Chapter 2), I review the strengths and weaknesses of GCE for the study of Ox-PTMs, provide an overview of the Ox-PTMs that have been genetically encoded and applications of GCE to the study of Ox-PTMs. The GCE systems for nitroTyr reviewed in Chapter 2, show clear phenotypic evidence that they cannot match the efficiency of natural translational systems, however the root causes of these efficiencies were unknown. In Chapter 3, I correlate the efficiency of *in vivo* GCE with kinetic constants derived from the *in vitro* aminoacylation reactions carried out by several nitrotyrosyl-aminoacyl-tRNA synthetases (nitrotyrosyl-aaRS-tRNA) derived from the *Methanocaldococcus janaschii* (*M. jannaschii*) tyrosyl-aaRS-tRNA. On the basis of these measurements I report that certain modifications made to the tRNA sequence thought to be necessary for maintaining translational fidelity are not necessary and negatively impact the efficiency of the system.

With these optimized tools in hand I applied them to addressing a major outstanding question in the oxidative stress field in chapter 4; can the oxidative stress induced nitrotyrosine PTM regulate protein function? As a way to address the question I investigated the effect of tyrosine nitration on the regulatory hub protein CaM. Tyrosine phosphorylation of CaM is known to modulate its regulation of intracellular Ca^{2+} signling. Proteomic studies have also revealed that both tyrosines in CaM are nitrated *in vivo*, although the impact of this modification is unknown. The effect of tyrosine nitration on the CaM target protein endothelial nitric oxide synthase

(eNOS) is of particular interest as this signaling protein can generate the oxidants that result in tyrosine nitration, potentially indicating a feedback loop and signaling microdomain. Using GCE I show that tyrosine nitration alters CaM regulation with regard to eNOS function *in vitro* and in eukaryotic cell lysate.

To extend this research further, I developed a system to genetically encode tyrosine nitration directly into proteins in eukaryotic cells (Chapter 5). This is an empowering technology for studying the impact of tyrosine nitration on regulation/dysregulation of cellular function in the native context of the modification. This technology is also of particular utility for the study of nitrated transmembrane proteins that need to be studied in eukaryotic cell culture or animal models.

Defining the Role of Tyrosine Nitration in Biology with Genetic Code Expansion

by
Joseph J. Porter

A DISSERTATION

submitted to

Oregon State University

in partial fulfillment of
the requirements for the
degree of

Doctor of Philosophy

Presented November 16, 2018
Commencement June 2019

Doctor of Philosophy dissertation of Joseph J. Porter presented on November 16, 2018

APPROVED:

Major Professor, representing Biochemistry and Biophysics

Head of the Department of Biochemistry and Biophysics

Dean of the Graduate School

I understand that my dissertation will become part of the permanent collection of Oregon State University libraries. My signature below authorizes release of my dissertation to any reader upon request.

Joseph J. Porter, Author

ACKNOWLEDGEMENTS

First, I would like to thank my advisor Ryan Mehl for always working to get the best out of me even though this was not always the easiest route to take. For pushing me to develop, think about, execute, and communicate science effectively. You gave me the opportunity to interact with many different scientists over the years through workshops you hosted and allowed me to go out to a wide variety of conferences over the years to both disseminate my work and broaden my scientific horizons. I was always given wide latitude to pursue the scientific goals we had outlined and I count that as the most significant milestone in my development as I can remember. For all of this and more I am immeasurably grateful.

I also need to thank you for fostering an amazing lab environment and attracting amazing people to work in the lab. I owe an immense debt of gratitude to Taylor Willi and Linda Benson for getting me up to speed on the day to day activity of lab when I was first starting and for laying much of the groundwork for what I was to do. From around the same time I also need to thank Chris Bazewicz and Arsalan Zolfaghari for always entertaining my questions about synthetic chemistry and entertaining me in other ways. In fact, there is a long line of synthetic chemists, Dakota Backus, True Gibson, Sam Hester, and Subhashish Jana, that consistently let me, out of my own curiosity, harass them about the wonders of chemical synthesis. My fellow graduate students in the Mehl lab, Robby Blizzard, Rachel Henson, Riley Bednar, Elise van Fossen, and by extension Phil Zhu, have all been a tremendous help and enjoyment over the years. My sometimes collaborator but mostly conspirator (and honorary Mehl lab member), Kelsey Kean has been an overflowing fount of structural biology knowledge among many other things. I owe a tremendous debt of gratitude to Hyo Sang Jang for his tireless work on covering everything I need on the eukaryotic cell front. I have also had the privilege of working with and training many outstanding undergraduate students in the lab, Taylor Bundy, Wes Brown, Max Paradiz, Hayati Wolfenden, Garth Kong, Austin Alexander, Sonia Grutzius, Jenna Beyer, and Jacob North.

I must thank many of those in the department especially Colin Johnson for access to knowledge on the wide world of calcium signaling and instrumentation, Joe Beckman for his fortitude to work on oxidative stress all these years and access to knowledge and instrumentation critical for my work, and Rick Cooley for his always insightful advice about how to conduct science. Outside of the department I would like to thank Denis Stuehr and Mahfuz Haque at the Cleveland Clinic for obtaining critical results related to my work in the Mehl lab and John Perona and Ben Rauch at Portland State University for what one might say is our shared hubris to re-engineer what mother nature has wrought, for our own benefit. I also thank Weihong Qiu and Chong Fang, my committee members not already mentioned, for their guidance throughout my graduate career.

I would like to thank my friends for all of the extracurricular activities during my time at OSU; Clay for moving all the way across the country with me; those from my cohort, Kelsey, Jillian, Bharath, Pam, and Nicole; those already in the department, Chelsea (and Ben), Murugesh, Steve (and Annie), Arden, Camden, Sara, Jared; and those who came later, Robby, Nathan, Andrew, Poppy, Allison, Riley (and Alexa), James, Shauna, Ally, Nathan, Heather, Elise, Amber, Kayla, Ruben, and Phil. You've all certainly spiced up my time here.

Of course, none of this would have been possible without funding sources and as such I would like to acknowledge the OHSU-MRF, NIH R01-GM114653, and the OSU department of Biochemistry and Biophysics.

I am forever grateful for the support of my family. Thank you Mom, Dad, and Emily; various aunts, uncles and cousins, and Grandpa and Susanna.

And last, but certainly not least, Mrs. Hershey and Mrs. Knight who many years ago opened my eyes to the wonders of chemistry and biology and set me on this path.

CONTRIBUTION OF AUTHORS

In Chapter 2, Ryan Mehl contributed to writing this paper. In Chapter 3, Ben Rauch planned and performed experiments; John Perona and Ryan Mehl planned experiments, analyzed data, and wrote the paper. In Chapter 4, Hyo Sang Jang and Mohammad Mahfuzul Haque planned and performed experiments and analyzed data; Denis J. Stuehr planned experiments and analyzed data; Ryan A. Mehl planned experiments, analyzed data, and wrote the paper. In Chapter 5, Hyo Sang Jang and Taylor S. Willi planned and performed experiments and analyzed data; Duy P. Nguyen and Elise Van Fossen planned and performed experiments; Ryan A. Mehl planned experiments, analyzed data, and wrote the paper.

TABLE OF CONTENTS

LIST OF FIGURES

Figure Page

LIST OF TABLES

Table Page

LIST OF ABBREVIATIONS

$^1O_2$	singlet oxygen
aaRS/tRNA	aminoacyl-tRNA synthetase-tRNA pair
Acd	acridonylalanine
ApoAI	apolipoprotein AI
BLI	bio-layer interferometry
Bpa	benzophenone
Ca^{2+}	calcium
CaM	calmodulin
Chlor	chloramphenicol
Cys-SO^-	cysteine sulfenate
Cys-SO_2H	cysteine sulfinic acid
Cys-SOH	cysteine sulfenic acid
dansyl-CaM	dansyl-calmodulin
DMNB-Br	4,5-dimethoxy-2-nitrobenzyl
DOPA	dihydroxyphenylalanine
DOPA quinone	dihydroxyphenylalanine quinone
eNOS	endothelial nitric oxide synthase
EPL	expressed protein ligation
GCE	genetic code expansion
GlnRS	glutaminyl-tRNA synthetase
H_2O_2	hydrogen peroxide
HOBr	hypobromous acid
HOCl	hypochlorous acid
Hsp90	heat shock protein 90
ITC	isothermal titration calorimetry
Kn	kanamycin
M. jannaschii	*Methanocaldococcus jannaschii*
Met-SO	methionine sulfoxide
Mj-RS 5b	*Methanocaldococcus jannaschii* nitrotyrosyl aminoacyl-tRNA synthetase 5b
MnSOD	manganese super oxide dismutase
Msr	methionine sulfoxide reductase
MsrA	methionine sulfoxide reductase A
MsrB	methionine sulfoxide reductase B
ncAA	noncanonical amino acid
NES	nuclear export signal
nitroTyr	3-nitrotyrosine
nitrotyrosyl-aaRS-tRNA	nitrotyrosyl-tRNA synthetase-tRNA pair

LIST OF ABBREVIATIONS (Continued)

nitroTyrRS	nitrotyrosyl-tRNA synthetase
NO_2	nitrogen dioxide
$O_2^{\bullet-}$	superoxide
$OH^{\bullet}$	hydroxyl radical
$ONOO^-$	peroxynitrite
orthog-tRNA	orthogonal-tRNA
Ox-PTM	oxidative post-translational modification
pCNF	*para*-cyano-phenylalanine
PCR	polymerase chain reaction
Prx	peroxyredoxin
PTK	protein tyrosine kinase
PTM	post-translational modification
PTP	protein tyrosine phosphatase
PylRS-tRNA	pyrrolysyl-aminoacyl-tRNA synthetase-tRNApyl pair
RNS	reactive nitrogen and oxygen species
ROS	reactive oxygen species
SCOT	succinyl-CoA:3-ketoacid-coenzyme A transferase
sfGFP	superfolder green fluorescent protein
SPPS	solid phase peptide synthesis
Srx	sulfiredoxin
Tet	tetracycline
tfmF	4-(trifluoromethyl)-phenylalanine
(TyrRS):$tRNA_{tyr}$	tyrosyl-aminoacyl-tRNA synthetase-tRNAtyr pair from *M. jannaschii*

Defining the Role of Tyrosine Nitration in Biology with Genetic Code Expansion.

Chapter 1

Thesis Overview

Oxidative stress

Oxidative stress, a term originally coined in 1985 has come to mean "An imbalance between oxidants and anti-oxidants in favor of the oxidants, leading to a disruption of redox signaling and control and/or molecular damage" [1]. Reactive oxygen species (ROS) and the closely related reactive nitrogen and oxygen species (RNS) are generated as natural byproducts of the normal metabolism of oxygen. The major biological oxidants include superoxide ($O_2^{\bullet -}$), hydrogen peroxide (H_2O_2), hydroxyl radical ($OH^{\bullet}$), singlet oxygen ($^1O_2$), hypochlorous acid (HOCl), hypobromous acid (HOBr), nitrogen dioxide ($^{\bullet}NO_2$) and peroxynitrite ($ONOO^-$ /ONOOH), along with downstream radical products. It has been known for some time that high levels of ROS and RNS production in the cell results in damage to biomacromolecules including nucleic acids, lipids, and proteins. If enough damage occurs cells will ultimately die whether via apoptosis or necrosis. When generated at low levels however, oxidants have been shown to be involved in cell signaling [1-2]. While the role of protein post-translation modifications (PTMs) in cellular signaling and regulation is perhaps best known from protein phosphorylation/ dephosphorylation [3], over time evidence for the role of oxidants in signaling has mounted and the idea of 'redox signaling' mediated by protein oxidative PTMs (Ox-PTMs) has become firmly entrenched [4]. Processes like transcriptional control, apoptosis, immunity, and differentiation are all dependent on the proper production and presence of ROS and RNS inside cells at a low level. It is imperative that cells maintain the correct redox balance, both to support normal cellular signaling and to prevent damage to the cellular components. It is important to understand the mechanisms underlying this redox balance, as disturbing it leads to cell dysfunction and ultimately disease. Oxidative stress is responsible to some level for the onset and/or progression of several diseases including cancer, diabetes, metabolic disorders, atherosclerosis, and cardiovascular diseases [5]. According to the CDC the economic impact of these diseases is on the order of one trillion U.S. dollars per year. While the exact contribution of oxidative stress to these conditions is not entirely clear, even a fraction of the responsibility for these diseases constitutes a significant economic burden.

Peroxynitrite and Protein Tyrosine Nitration

The powerful oxidant, peroxynitrite ($ONOO^-$), is a product of the reaction between the biological signaling molecule nitric oxide ($NO^\bullet$) and superoxide ($O_2^{\bullet-}$) [6]. In fact $NO^\bullet$ is the only molecule produced in high enough concentration and reacts fast enough with $O_2^{\bullet-}$ to outcompete the anti-oxidant enzyme superoxide dismutase, which dismutates $O_2^{\bullet-}$ to H_2O_2 [7]. While peroxynitrite is a strong oxidant and can react directly with electron-rich groups like sulfhydryls [8] and iron-sulfur clusters [9], it is surprisingly stable in solution and as such is unusually selective as an oxidant [10]. This selectivity underlies the importance of peroxynitrite as a mediator of biological processes; only specific biological sites are modified, resulting in a sufficient buildup of particular products to alter cellular function. A variety of protein sidechains are susceptible to modification by peroxynitrite, or downstream radical products of peroxynitrite, including cysteine, tyrosine, tryptophan, methionine, and histidine (for the products formed from the reaction of these amino acid sidechains with peroxynitrite, see chapter 2). Tyrosine does not react directly with peroxynitrite. Instead, tyrosine nitration occurs through a radical mechanism in which a hydrogen atom is abstracted from the phenol ring to form a tyrosyl radical that quickly combines with $^\bullet NO_2$ to produce 3-nitrotyrosine (nitroTyr) [11]. The formation of nitroTyr has served as a stable biomarker of oxidative stress, no doubt in part due to the development of antibodies to this Ox-PTM [12-13]. NitroTyr formation has been noted in at least 50 disease phenotypes and tends to correlate with disease progression [7]. A major challenge for those studying the nitroTyr modification is the installation method mediated by molecular species like peroxynitrite is capable of diverse chemical reactions, resulting in a heterogeneous mixture of protein products (Figure 1.1A). Determining the effect of specific modifications from this mixture with regards to cellular function is extremely challenging. To gain insight into the impact of Ox-PTMs like nitroTyr on cellular regulation and dysfunction leading to disease, methods to produce specifically modified proteins were developed. Genetic code expansion (GCE) has emerged as a method to generate proteins containing site-

specific tyrosine nitration through the co-translational installation of non-canonical amino acids (ncAAs) (Figure 1.1B) [14].

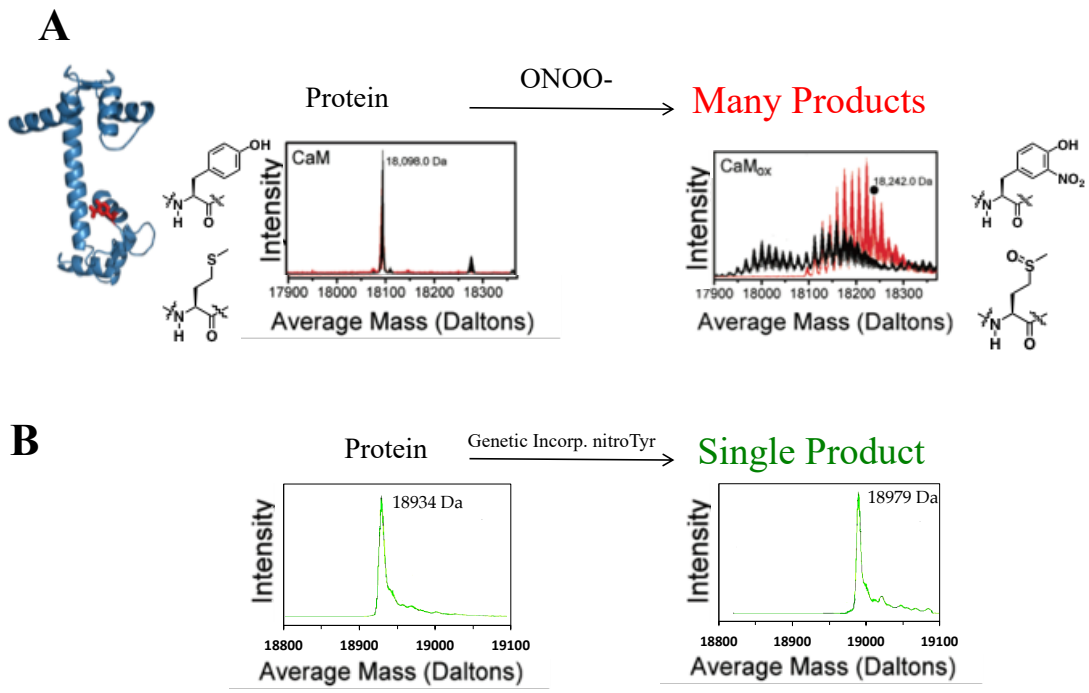

Figure 1.1. Genetic code expansion provides homogeneous site-specifically Ox-PTM modified proteins.
A. Exposure of calmodulin to peroxynitrite in vitro (contains 11 susceptible amino acids; 9 methionines, and 2 tyrosines) results in over 500 distinct oxo-forms shown here by mass spectrometry (Adapted from [Smallwood, et al, 2007]). The Ox-PTMs of tyrosine (nitroTyr) and methionine (methionine sulfoxide) seen in the oxidized calmodulin are shown at the right **B.** By contrast, installation of the Ox-PTM nitroTyr by genetic code expansion results in a site-specifically modified homogeneous product.

Genetically encoding oxidative stress

Natural translation relies on the function of many orthogonal systems for the correct conversion of the information present in a nucleic acid sequence into a specific protein chemical structure (e.g. the RNA triplet codon UAC coding for the amino acid tyrosine). For the correct encoding of all life, the fidelity of translation needs to be maintained. Fundamentally, genetic code expansion (GCE) extends these orthogonal systems and exploits the natural translational machinery to incorporate new unique chemical functionality into a protein of interest. This unique chemical

functionality ranges from unique chemical reactivity to act as a chemical handle (bioorthogonal reactivity), photoreactivity (photocrosslinkers or photocaged amino acids), or the altered chemical structure present in the sidechain of a post-translationally modified amino acid [15]. GCE requires that a new orthogonal aminoacyl-tRNA synthetase/tRNA (aaRS/tRNA) pair be transplanted into the organism of interest for recombinant protein expression. Generally, this aaRS/tRNA is obtained from an evolutionarily distant organism to ensure that distinct identity elements for the recognition of the tRNA are employed by the aaRS in order to have a truly orthogonal system and maintain translational fidelity [16]. The genetic code of *E. coli* was first expanded to include the ncAA *o*-methyltyrosine in 2001 by importing and evolving the tyrosyl aaRS/tRNA pair from the methanogenic archaeon *Methanocaldococcus janaschii* (*M. jannaschii*) [17]. The anticodon of the orthogonal tRNA was converted to CUA so that it would suppress the UAG stop codon, meaning that instead of encoding a translational termination signal, the UAG codon would instead code for *o*-methyltyrosine. Based on an *in* vivo orthogonality assay at the time it was thought that the *M. jannaschii* $tRNA^{Tyr}_{CUA}$ was not sufficiently orthogonal to the *E. coli* translational machinery. A library of tRNA mutants was generated and a selection performed to further orthogonalize the *M. jannaschii* $tRNA^{Tyr}_{CUA}$ [18]. This orthogonalized *Mj* $tRNA^{Tyr}_{CUA}$ was used for the next 15 years without any further characterization. In chapter 3, I show that some of the alterations made to increase orthogonality of this tRNA are unnecessary and deleterious to the function of the *M. jannaschii* tyrosyl-aaRS/tRNA pair for genetic code expansion.

The ability of an orthogonal aaRS/tRNA pair to incorporate an ncAA can be characterized by several metrics. The efficiency of the orthogonal aaRS/tRNA pair is the yield of full-length product and is dependent on the kinetics of the aaRS/tRNA as well as the rate that the ncAA-acylated tRNA moves through the rest of the translational machinery. The UP_{50} is the ncAA concentration at which half-maximal ncAA-containing protein is produced, useful for determining the amount of ncAA needed to supplement the media. Fidelity is a measure of the orthogonality of the aaRS/tRNA pair. The absolute fidelity of an aaRS/tRNA pair is the amount of full length protein product produced in the absence of ncAA [19]. Relative fidelity is the

amount of noncognate amino acid incorporated into the protein of interest in the presence of the ncAA of interest, a more useful metric as it more closely resembles the fidelity of the aaRS under conditions in which it will be used. Certain evolved orthogonal aaRS/tRNA pairs can incorporate a related family of ncAAs (e.g. *para*-substituted phenylalanines [20]), which is referred to as the permissivity of the aaRS/tRNA pair [21].

The first Ox-PTM genetically encoded was nitroTyr in 2008 using an evolved *M. jannaschii* tyrosyl-aaRS/tRNA pair [22]. This evolved pair was used to site-specifically incorporate nitroTyr for the first time into MnSOD at residue 34 and show that this modification impacts protein function [22]. A more efficient second generation *M. jannaschii* tyrosyl-aaRS/tRNA pair was evolved by altering the stringency of the selection scheme and employing a new final step to select efficient aaRSs based on a fluorescent reporter [19]. This new nitroTyr aaRS/tRNA pair was used to generate site-specifically nitrated heat shock protein 90 (Hsp90) at modification sites determined to be occurring under conditions of oxidative stress in motor neuron cells [23] and was also used to generate site-specifically modified apolipoprotein AI (ApoAI) at sites determined to be occurring during conditions of oxidative stress during atherosclerosis [24]. In both of these cases site-specific tyrosine nitration resulted in protein dysfunction, progression of disease, or cell death. While the second generation nitroTyr aaRS/tRNA pair was efficient enough to tackle the site-specific incorporation of nitroTyr for the recombinant expression of difficult proteins like Hsp90 and ApoAI, it is clear that the evolved system for nitroTyr incorporation cannot match the efficiency of natural aaRS/tRNA pairs [19]. Much of the effort going into the GCE field over the past 15 years has been focused on introducing new chemical functionality into proteins and comparatively little effort has been directed towards addressing the fundamental inadequacies underlying the current orthogonal systems. To more effectively study Ox-PTMs like nitroTyr we need more efficient tools. In chapter 3 I show for the first time that *in vitro* orthogonal aaRS/tRNA activity assays correlate with *in vivo* recombinant protein production for GCE and that changing the orthogonal tRNA sequence can lead to greater efficiency. With the new tools in hand I was able to begin to address a long-standing question in

the oxidative stress field, namely can tyrosine nitration regulate protein function in the context of cellular signaling?

Can the oxidative stress induced nitrotyrosine PTM regulate protein function?

In order to address this question, I chose to employ the protein, calmodulin (calcium-modulated protein; CaM). CaM possesses a number of qualities that make it an attractive candidate as a first foray into the world of regulatory tyrosine nitration. CaM is a central protein in calcium (Ca^{2+}) signaling, which in turn regulates a variety of biological processes including fertilization and proliferation, transcription, metabolism, contraction, and exocytosis [25]. CaM function is regulated by tyrosine phosphorylation indicating that its two tyrosines (Tyr99 and Tyr138) are regulatory sites. It has also been shown via mass spectrometry that these two tyrosines are nitrated under conditions of oxidative stress *in vivo* [26-27]. As a further indication that tyrosine nitration of these sites is regulatory in nature, a denitrase activity has been reported that returns nitrated CaM to the native tyrosine at these sites (analogous to a phosphatase for signaling via phosphorylation) [27].

CaM adopts a dumbbell shape with two terminal lobes connected by a long flexible helix. Each of the terminal lobes contains a pair of EF-hands. The EF-hand is a helix-loop-helix motif composed of approximately 30 amino acids that ligate Ca^{2+}, first seen in the structure of parvalbumin reported in 1973 [28-29]. Binding of Ca^{2+} to CaM induces conformational changes that expose hydrophobic patches on the surface of the protein and ultimately the ability to interact with targets domains. Binding to targets then induces a large conformational change of CaM, which bends to a variable extent, depending on the target in question, from an extended dumbbell shape to a more globular structure in which the two halves wrap around the target domain (Figure 1.2). CaM is ubiquitously expressed in all eukaryotes and is highly conserved, in fact the sequence of CaM is identical in all vertebrates [30]. CaM is encoded by three non-allelic genes, while the coding sequences differ substantially, the encoded protein is identical. Unlike some Ca^{2+} sensor proteins CaM functions to associate with many targets not based on sequence divergence but instead via structural plasticity [31]. The CaM central helix contains a flexible hinge region that confers

flexibility to the two lobes. This linker enables the CaM molecule to sample many conformations in which the two lobes adapt different relative orientations and variable spacing. The hydrophobic patches on the target binding sites of CaM, exposed following Ca^{2+} binding, contain many methionine residues. Methionine residues contain a flexible side chain, which confers yet another level of plasticity, enabling binding pockets of CaM to adapt to diverse target sequences and structures [31]. As CaM binds to many targets, post-translational modifications (PTMs) serve as another level of regulation to allow CaM to differentially regulate target protein function.

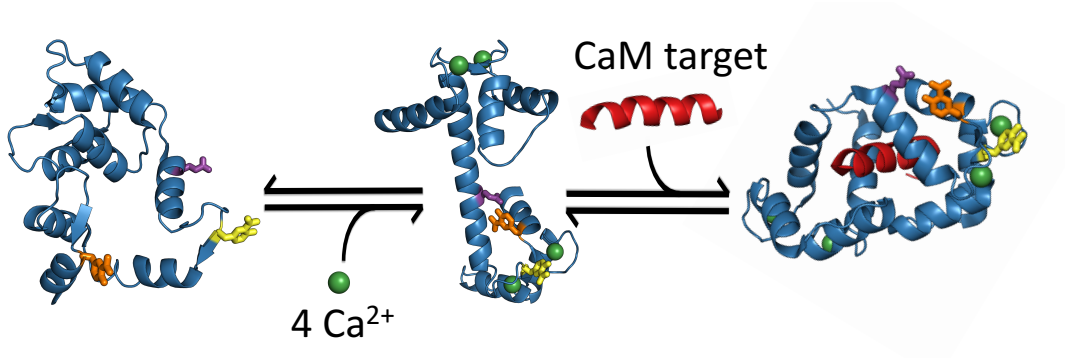

Figure 1.2. Structural changes to calmodulin following Ca^{2+} and target protein binding. Binding of Ca^{2+} to CaM induces conformational changes that result in the exposure of hydrophobic patches on the surface of the protein and ultimately target protein association. Binding to target proteins induces a large conformational change from a dumbbell shape to a more globular target-associated structure (ApoCaM structure, PDB 1QX5; Ca^{2+}-CaM structure, PDB 3CLN; Ca^{2+}-CaM-eNOS structure, PDB 1NIW).

The interaction of CaM with its targets is regulated by a number of PTMs, including phosphorylation. Because CaM regulates at least 200 protein targets, PTMs serve as another level of regulatory control over specific CaM-dependent signaling pathways. Of the 18 amino acids in CaM that are putative sites of phosphorylation, 8 undergo phosphorylation by known kinases [32]. Both of the tyrosines on CaM are known to undergo phosphorylation by receptor protein tyrosine kinases (endothelial growth factor receptor; insulin receptor) and non-receptor kinases (Src family kinases, Jak2, and p38Syk) [33]. Tyrosine phosphorylation of mammalian CaM has

been shown to affect target interaction and activation *in vitro* [34]. CaM is modified by several other modifications including lysine trimethylation, proteolytic cleavage [35], and Ox-PTMs like methionine sulfoxide, and as previously mentioned, tyrosine nitration [26-27, 36-38].

CaM regulates the activity of many proteins including endothelial nitric oxide synthase (eNOS) [34]. ENOS is particularly interesting in the context of CaM nitration as it produces both the chemical species needed to produce peroxynitrite [39], is a major player in Ca^{2+} signaling as it sequesters a significant portion of the intracellular CaM pool [40], and is known to be regulated by CaM tyrosine phosphorylation [34-35]. ENOS catalyzes the NADPH-dependent conversion of L-arginine into L-citrulline generating nitric oxide and when uncoupled, superoxide. As eNOS generates both the chemical species involved in the nitration of CaM, and nitrated CaM alters the regulation of eNOS (shown in chapter 4), this system could serve as a microdomain, commonly seen in redox signaling [41]. ENOS is regulated by a wide variety of processes beyond the association of Ca^{2+}-CaM in the cell, including other proteins partners (Hsp90 and caveolin) [42], subcellular localization [43], and PTMs including phosphorylation [44-45]. Because of the complexity of eNOS regulation I was also interested in assessing the role of CaM tyrosine nitration in eNOS signaling in the context of the entire cellular environment. For this I needed to develop a GCE system for the genetic incorporation of nitroTyr in eukaryotic cell culture (outlined in chapter 5).

Development of a system for incorporation of nitrotyrosine in eukaryotes

The *M. jannaschii* aaRS/tRNA developed for nitroTyr is orthogonal in *E. coli*, however it is not orthogonal in eukaryotic cells. The pyrrolysine aaRS/tRNA pair from several species of methanogens was discovered in 2002 and quickly adapted for GCE [46-47]. This orthogonal aaRS/tRNA is of particular utility, as the molecular biology "workhorse", *E. coli*, is used to develop orthogonal pairs with specificity for new ncAAs. The aaRS/tRNA pair developed in *E. coli* can then be transplanted into eukaryotic cells, where the pyrrolysine aaRS/tRNA pair is also orthogonal [48-49].

While much of the work of developing a new pyrrolysine-derived aaRS/tRNA pair specific for a new ncAA is done in *E. coli*, there are unique challenges to be overcome in employing these systems in eukaryotic cells.

The ratio of aaRS to tRNA expressed is particularly important to optimize in eukaryotes. Levels of orthogonal tRNA expression are generally the bottleneck in efficiency for GCE in eukaryotes and delivery of multiple copies of orthogonal tRNA is necessary [50]. While the pyrrolysine tRNA is expressed via extragenic promoters in its native context, eukaryotes use intragenic A- and B-box promoters within the tRNA sequence for tRNA expression [48]. This necessitates coopting RNA polymerase III promoters (generally the U6 or H1 promoter) [51]. Even expression of the gene of interest containing an amber stop codon (UAG) can present a challenge as there is a surveillance system present in eukaryotes known as nonsense-mediated decay that degrades mRNA containing in-frame stop codons within the coding region of the gene sequence [52-53]. The delivery of ncAAs to eukaryotes can also be a limiting factor as some ncAAs are poorly bioavailable (i.e. not taken up the cells) or are toxic to the cells at levels necessary for effective incorporation.

Despite these challenges implementing GCE in eukaryotic cells, we were able to implement a pyrrolysine aaRS/tRNA pair in HEK293T cells specific for nitroTyr incorporation (chapter 5). Using this system, we showed site-specific nitroTyr incorporation into sfGFP in HEK293T cells, validated by mass spectrometry. We were then able to produce the physiologically nitrated proteins, 14-3-3 and manganese super oxide dismutase (MnSOD), site specifically-nitrated using our GCE system. This GCE system opens up our ability to study the impact of site-specific tyrosine nitration, for instance, by performing pull-downs of 14-3-3 nitroTyr-130 to determine the impact of this site of nitration on the 14-3-3 interactome. We will also have access to production of site-specifically nitrated full-length transmembrane proteins, many of which are known to be nitrated to unknown effect.

Chapter 2

Genetic Code Expansion: A Powerful Tool for Understanding the Physiological Consequences of Oxidative Stress Protein Modification

Joseph J. Porter and Ryan A. Mehl

Published in *Oxidative Medicine and Cellular Longevity, 2018, Apr 23, 7607463*

Abstract

Post-translational modifications resulting from oxidation of proteins (Ox-PTMs) are present intracellularly under conditions of oxidative stress as well as basal conditions. In the past, these modifications were thought to be generic protein damage, but it has become increasingly clear that Ox-PTMs can have specific physiological effects. It is an arduous task to distinguish between the two cases, as multiple Ox-PTMs occur simultaneously on the same protein, convoluting analysis. Genetic code expansion (GCE) has emerged as a powerful tool to overcome this challenge as it allows for the site-specific incorporation of an Ox-PTM into translated protein. The resulting homogeneously modified protein products can then be rigorously characterized for the effects of individual Ox-PTMs. We outline the strengths and weaknesses of GCE as they relate to the field of oxidative stress and Ox-PTMs. An overview of the Ox-PTMs that have been genetically encoded and applications of GCE to the study of Ox-PTMs, including antibody validation and therapeutic development, is described.

Introduction

It is accepted that post-translational modifications resulting from oxidation (Ox-PTMs) damage proteins and harm cells. Whether Ox-PTMs can modulate the function of proteins in a specific manner like other PTMs has been a long-standing question [54]. Recent studies have demonstrated that site-specific protein Ox-PTMs can lead to notable gain-of-function alterations that are connected to disease phenotypes. Enzymatic pathways that remove Ox-PTMs have also been identified, providing evidence for dynamic homeostasis with implications for the cellular function of these modifications. Major challenges exist in evaluating effects of Ox-PTMs because of the diversity of mechanisms by which they are formed. The Ox-PTMs result from reactive oxygen species (ROS) [superoxide ($O_2^{\cdot -}$), hydrogen peroxide (H_2O_2), and hydroxyl radical ($OH^{\cdot}$)] and reactive nitrogen and oxygen species (RNS) [nitric oxide ($^{\cdot}NO$), nitrogen dioxide ($^{\cdot}NO_2$), peroxynitrite (ONOO-/ONOOH)], and other downstream products interacting with a variety of amino acid residues [2, 55-60].

Elucidating the function of PTMs are notoriously challenging to evaluate because generating the modified proteins *in vivo* or *in vitro* results in a heterogeneous mixture of modified and unmodified proteins. The situation for oxidative stress PTMs is notably more dire because the installation method, diverse and non-specific chemical reactions from ROS and RNS, produces a heterogeneous mixture of Ox-PTMs on proteins containing multiple different modifications (Figure 2.1). Each different Ox-PTM needs to be assessed for site-specificity and abundance to identify its effects on protein function. Genetic code expansion (GCE) is particularly well suited to meet these challenges since at its core GCE co-translationally installs the Ox-PTM as a noncanonical amino acid (ncAA). This allows for facile production of homogenously modified protein at genetically programed sites, enabling new approaches for studying Ox-PTMs. GCE can validate Ox-PTM residues identified in oxidative stress conditions and explore the functional consequences of a single site of modification. GCE can also be used to develop assays for a particular site of modification on a particular protein, and to generate controls for evaluating the selectivity and effectiveness of antibodies for Ox-PTMs. Since GCE functions by generating ncAA-protein in living prokaryotes and eukaryotes it also allows for the *in vivo* study of homogeneous site-specifically modified protein.

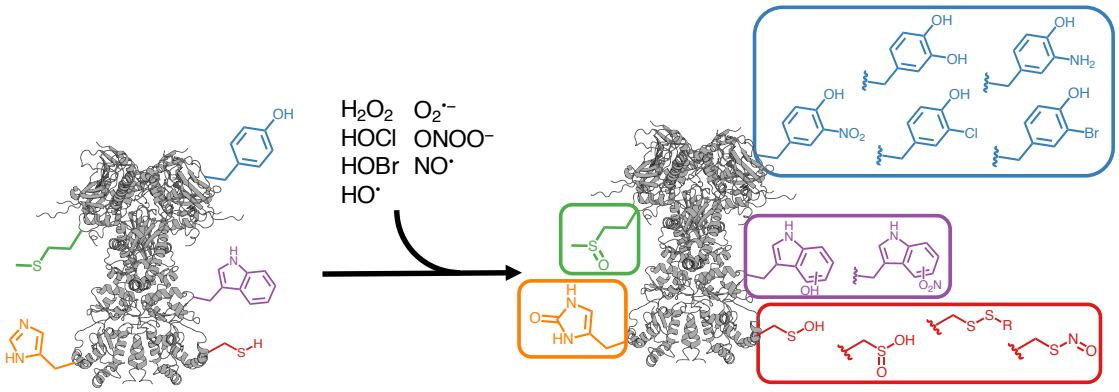

Figure 2.1. A variety of biological oxidants are capable of modifying susceptible amino acid sidechains to their Ox-PTM counterparts.
The major groups of amino acids modified are the sulfur containing amino acids (cysteine and methionine) and the aromatic amino acids (tyrosine, tryptophan, and histidine).

A survey of the literature produces at a minimum 65 reported Ox-PTMs (Figure 2.1, Supplementary Figure 2.1, and Supplementary Table 2.1). A number of excellent reviews on the ROS and RNS exist and as such we will not discuss them here [7, 61]. Identification of sites and identities of Ox-PTMs has also blossomed as a field of study and these have been reviewed elsewhere [62-63]. It is critical to note from studies on the identification of Ox-PTMs that these modifications are often not stable to purification from their native environments and require specialized stabilization or trapping methods [64]. This is important for GCE as these particularly sensitive Ox-PTMs will likewise require chemical caging strategies or stable mimetics for successful genetic incorporation. In this review, we summarize the relevant literature at the intersection of GCE and Ox-PTMs, focusing on the most abundant Ox-PTMs and those amenable to GCE technology (Figure 2.1). Ox-PTMs of low stability or amino acid crosslinks which are not applicable to GCE will not be discussed (**3**, **7**, **9**-**10**, **16**, **18**-**20**, **22**, **24**-**26**, **31**-**35**, **37**-**39**, **41**-**44**, **46**-**65** in Figure 2.2). This review will also highlight the strengths and shortcomings of GCE as applied to the study of Ox-PTMs, outline some of the important considerations when employing GCE, and describe exciting future applications of GCE technology for the oxidative stress field.

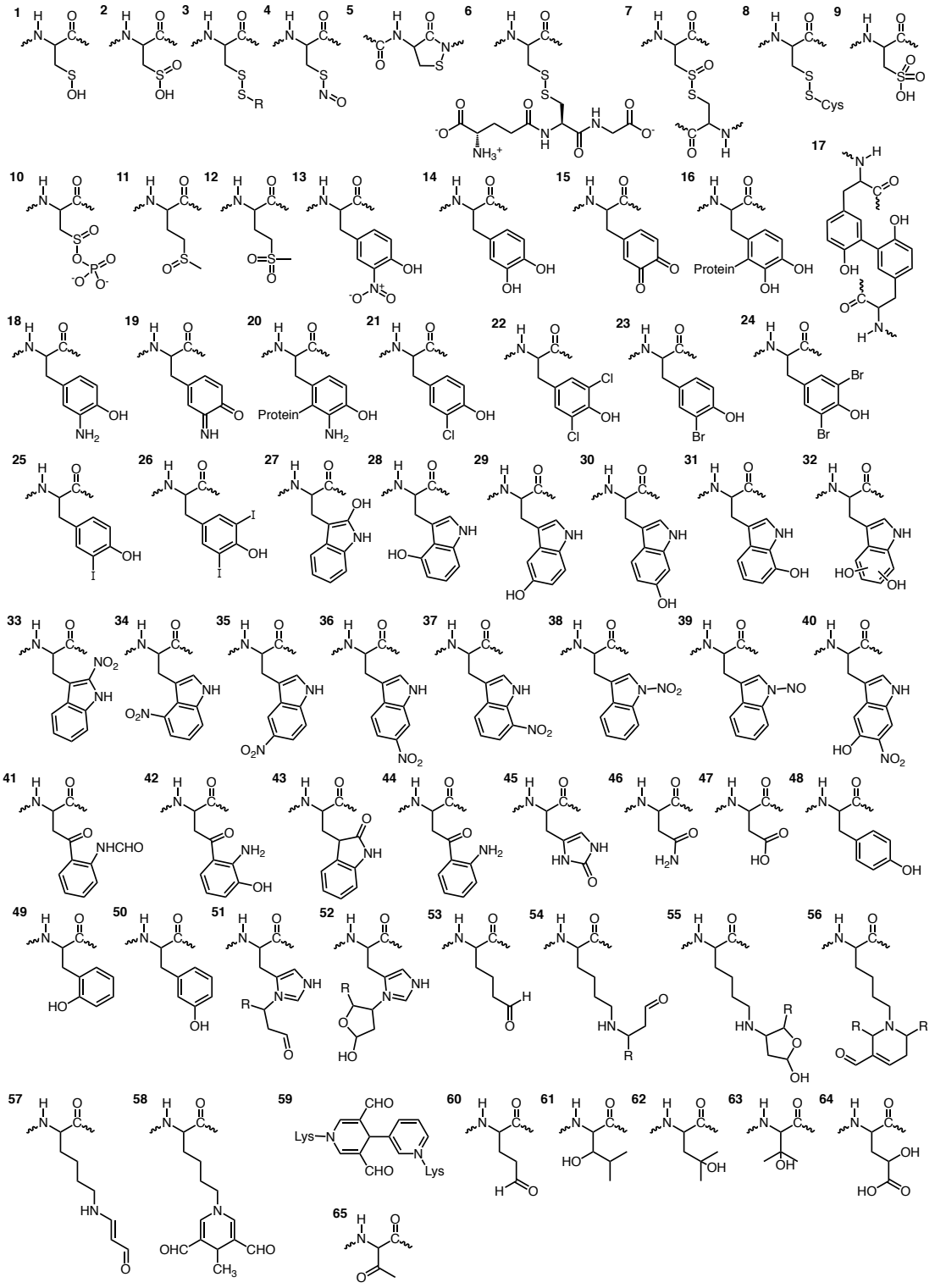

Figure 2.2. Ox-PTMs identified on proteins isolated from conditions of oxidative stress or following *in vitro* reaction with ROS or RNS.

For the list of Ox-PTM names and references see the supplementary information table 1.

Genetic Code Expansion Orthogonal Systems

The ability to site-specifically incorporate non-canonical amino acids (ncAAs) into proteins in living cells has emerged as a powerful method to probe protein structure and function [14, 65]. This capability has been extended to the incorporation of many different PTMs including Ox-PTMs. While cell-free protein synthesis is also developing as a powerful approach for generating modified proteins [66], GCE is a technology that must work inside a living cell. A first consideration for GCE is that the Ox-PTM must be chemically synthesized as an amino acid, which can be challenging for some modifications. The modified amino acid must also be stable to cell culture conditions and be internalized in a cell to concentrations adequate for translation. The stability of an Ox-PTM to cell culture conditions should be evaluated because many Ox-PTMs are redox sensitive and can be toxic to cells at media concentrations needed for GCE (0.1-1.0 mM). Provided the Ox-PTM amino acid can pass these initial steps then selection of GCE components specific for the new amino acid is possible.

Central to GCE technology is an engineered aminoacyl-tRNA synthetase-tRNA pair (aaRS-tRNA) that encodes an ncAA in response to a nonsense (often the amber stop codon) or a frameshift codon (Figure 2.3). To maintain translational fidelity the aaRS-tRNA pair must also not cross-react with any endogenous aaRS-tRNA pairs in the host organism i.e. this aaRS-tRNA pair must be orthogonal. In general, evolution of an orthogonal aaRS-tRNA pair in a cell requires importing this pair from another domain of life, as the aaRS-tRNA identity elements for recognition are divergent enough to maintain orthogonality. All of the aaRS-tRNA pairs employed so far for GCE were derived from an aaRS-tRNA pair for a canonical amino acid and were altered to instead recognize and charge an ncAA onto the orthogonal tRNA. Generally, this strategy has been more successful when the ncAA of interest resembles the original canonical amino acid (e.g. a modified TyrRS may only accept aromatic amino acids). As this trend exists it is important to know what orthogonal systems have been used in the past when considering a heretofore unincorporated ncAA. Five main orthogonal pairs have been used, an archaeal TyrRS-tRNA$_{CUA}$ pair from *Methanocaldoccocus janaschii* (*Mj*) has been used extensively in *E. coli* and

other bacteria [67]; an *E. coli* LeuRS-tRNA$_{CUA}$ and an *E. coli* TyrRS- tRNA$_{CUA}$ pair have been used in eukaryotes [68-69]; a pyrrolysl-aaRS-tRNA pair (PylRS-tRNA$_{CUA}$) derived from several methanogenic archaea (notably *Methanosarcina barkeri* and *Methansarcina mazei*) is orthogonal in both *E. coli* and eukaryotes [48, 70]; and a liberated *E. coli* TrpRS-tRNA$_{CUA}$ pair orthogonal in both *E. coli* and eukaryotes [71].

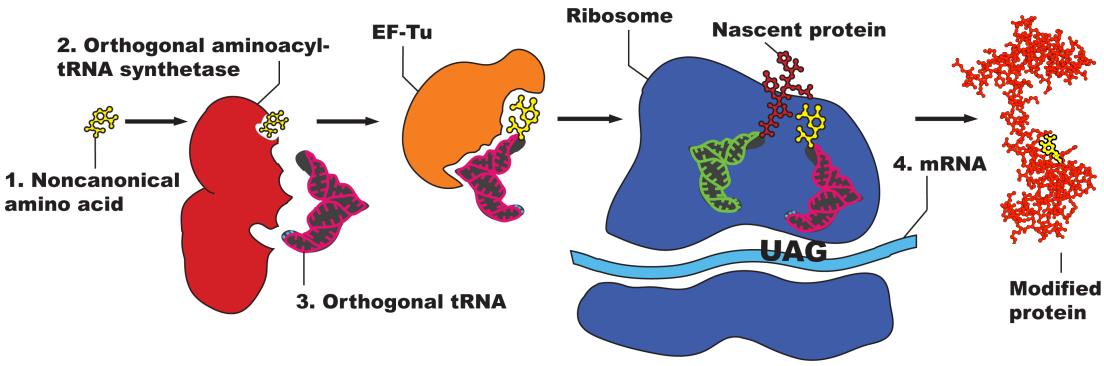

Figure 2.3. Components necessary for genetic code expansion.
These include the noncanonical amino acid of interest **1.**, an orthogonal aminoacyl tRNA synthetase-tRNA pair **2.** and **3.**, and an mRNA with an amber stop codon at the site of interest **4.**

Developing Orthogonal Pairs

Initially, all orthogonal aaRS-tRNA pairs must be evolved to efficiently incorporate an ncAA of interest. A library of mutations at certain positions is constructed and a double sieve selection scheme is employed to enrich aaRSs variants that incorporate the ncAA of interest but not any of the canonical amino acids [67]. Following a successful selection, several parameters may be used to characterize the effectiveness of the developed aaRS-tRNA pair. The efficiency of the orthogonal pair is a measure of the amount of full-length protein produced in the presence of ncAA and is often described by the fluorescence of a reporter protein like GFP or the yield of a purified protein of interest. Fidelity is a parameter that measures the orthogonality of the system. The absolute fidelity of an aaRS-tRNA pair is the amount of full-length protein product produced in the absence of ncAA [21]. Relative fidelity is the amount of non-cognate amino acid incorporated in the protein of interest in the presence of the ncAA of interest. Relative fidelity is a more useful parameter for characterization of an aaRS-tRNA pair as it more closely resembles the

fidelity of the aaRS under conditions in which it will be used. This parameter is measured by whole protein or tryptic digest mass spectrometry of the purified protein of interest to determine the amount of ncAA incorporation as compared to canonical amino acid. Oftentimes an evolved orthogonal pair can incorporate a related family of ncAAs e.g. *para*-substituted phenylalanines [20]. This characteristic is called permissivity (sometimes referred to as polyspecificity) of an orthogonal pair [21].

Other Considerations and Alternatives to Genetic Code Expansion

There are factors beyond the aaRS/tRNA pair that are also critical for GCE. For a given ncAA to be incorporated by an evolved aaRS-tRNA pair, the ncAA has to meet a set of translational compatibility criteria. The bioavailability of the ncAA has to be taken into account as it must diffuse into, be transported into, or be synthesized within the cell. This is particularly an issue for highly charged amino acids which generally do not diffuse across membranes and a suitable endogenous transporter does not exist. Further, the ncAA of interest needs sufficient stability to persist intracellularly for a timescale on the order of hours to days in order to be incorporated into a protein via translation. Following aminoacylation of the tRNA by the aaRS, the EF-Tu must transport the aminoacyl-tRNA to the ribosome. The EF-Tu has been finely tuned for natural translation and, while it tolerates many ncAAs, those that are highly charged or particularly large are not effectively transported by the EF-Tu. The amino acyl-tRNA then must be decoded on the ribosome. Finally, the installed ncAA also needs to be stable on the protein enabling protein purification and characterization.

A variety of strategies have been employed to overcome these issues with GCE in regard to particular ncAAs. One solution to poor cellular uptake is conversion of the desired ncAA into a dipeptide. Dipeptides have been shown to increase uptake of highly charged or otherwise poorly internalized amino acids via transporters [72-73]. Alternatively, methylation of the carboxylic acid of certain ncAAs also increases uptake in mammalian cell culture. A third solution is to generate a biosynthetic pathway for the desired ncAA so that it is generated inside the cell of interest [74-75]. Generally, structural mimics or chemically caged derivatives of ncAAs are used in

order to increase stability. For phosphorylated amino acids, both chemical caging [76] and structural mimetics [73, 77] have been used to stabilize the ncAA to allow for ncAA incorporation and characterization of PTM-proteins. Another strategy employed to increase the life time of genetically encoded PTM is to knock down the cell's PTM removal pathways. The lifetime of phosphoserine on proteins is increased by removal of endogenous serine phosphatases, allowing for genuine phosphoserine incorporation [77]. Generally, the EF-Tu transports ncAA aminoacylated-tRNAs efficiently enough to allow for incorporation but some charged ncAAs have required EF-Tu engineering. For initial studies on incorporation of phosphoserine it was thought that it was necessary to evolve the EF-Tu to allow for the transport of phosphoserylated-tRNA, however later studies indicated that while this evolved EF-Tu does transport phosphoserylated-tRNA more efficiently, evolution of the EF-Tu was not strictly necessary [77-78]. The ribosome needs to accommodate the ncAA-tRNA and catalyze peptide chain formation. Chemically acylated tRNA and cell-free synthesis has confirmed the ribosome is very permissive and ncAAs >700 Da in size have been incorporated without issue [66]. While an ncAA size limit has been identified for the ribosome exit tunnel using cell-free protein synthesis methods, the vast majority of alpha L-noncanonical amino acids are accepted. Finally, the newly synthesized protein is released from the ribosome and folded, processed, and trafficked to its appropriate location. Since GCE incorporates Ox-PTMs into the primary sequence, altered protein folding pathways and cofactor loading are possible from the modified protein.

Alternative methods to GCE have been developed that may be applicable for particularly metabolically unstable or toxic ncAAs or toxic proteins. Expressed protein ligation (EPL) has emerged as another powerful method to study Ox-PTMs [79]. This method allows the vast chemical space open to solid phase peptide synthesis (SPPS) to be coupled with the robustness of recombinant protein expression. As the ncAA is incorporated via SPPS and then native chemical ligation, novel aaRS/tRNA pairs do not need to be generated. In addition, provided the sites of modification are within <30 amino acids from one another it is trivial to incorporate multiple ncAAs. Successful generation of modified histones with EPL also highlight

some of the drawbacks of EPL, the site of interest should be within ~50 residues of the N- or C-terminus or a synthesis with three peptides is required, the protein of interest should be able to be refolded from denaturants, and there is some level of sequence requirement both for the intein to generate the α-thioester and for the presence of a cysteine at the site of ligation [80-81]. The EPL strategy has been used to yield milligram quantities of α-synuclein nitrated selectively at Y39 or Y125 allowing biophysical and biochemical studies of site-specific nitration on α-synuclein structure and function [82]. It is also important to note that the standard desulfurization reaction conditions originally used reduced the incorporated nitrotyrosine to aminotyrosine. This reduction during the desulfurization reaction was prevented with the addition of 2-nitrobenzylamine hydrochloride.

Oxidative Modifications of Sulfur Containing Residues

Cysteine Ox-PTMs are abundant modifications with the cysteine sulfur existing in several different oxidation states. Cysteine sulfenic acid (Cys-SOH, **1**) is directly generated by the oxidation of cysteine by two-electron oxidants, particularly H_2O_2. The propensity of Cys residues to undergo oxidation is influenced generally by the thiol nucleophilicity, the surrounding protein microenvironment, and the proximity of the target thiol to the ROS source [83]. Accordingly, the susceptibility to oxidation is usually correlated with the Cys pKa. Further, increasing evidence shows that ROS signaling responses are compartmentalized and that spatial regulation of Cys oxidation is key for signaling [84-85]. Cys-SOH can be overoxidized to cysteine sulfinic acid (Cys-SO_2H, **2**). As the H_2O_2 mediated pathway of Cys-SOH oxidation proceeds through the sulfenate anion (Cys-SO^-), the pKa of Cys-SOH should influence this reaction [85]. With a pKa of ~2, Cys-SO_2H exists exclusively in a deprotonated state at physiological pH. The sulfinate group is usually not reducible by typical cellular reductants and as such its further oxidation to sulfonic acid appears to be the only relevant reaction in cells [86]. All of which points to the importance of temporal and spatial control of these protein modifications and the need for tools that enable further investigation.

Cys-SOH has been identified in a relatively small number of proteins and the identification of this modification remains difficult. The first general analysis of known Cys-SOH modification sites included 47 proteins characterized by crystallography to contain the modification [87]. On the other hand, Cys-SO_2H was long considered merely an artifact of protein purification. Increasing evidence however indicates that hyperoxidation to Cys-SO_2H in cells is not a rare event. In fact, quantitative analysis of rat liver proteins has shown that ~5% of Cys residues exist as Cys-SO_2H [88]. The discovery of sulfiredoxin (Srx), an enzyme that in an ATP-dependent protein reduces Cys-SO_2H to Cys-SOH on some peroxiredoxins, has indicated that Cys-SO_2H plays a biological role in the redox regulation of peroxiredoxin function [89].

The same electrostatic interactions on the protein that affect the pKa of the Cys thiol also influence the stability of the Cys-SOH. The major factor that increases Cys-SOH stability (or lifetime on a protein) is the absence of proximal thiols capable of generating an intramolecular disulfide (**8**). It has been also reported that limited solvent access and nearby H-bond acceptors also contribute to Cys-SOH stabilization. In addition to the reaction of Cys-SOH with neighboring cysteine thiols, backbone amide nitrogens can readily react with Cys-SOH to yield a cyclic sulfonamide species (**5**) [90-91]. If Cys-SOH modifications are not removed by neighboring Cys residues or amide nitrogens they can be enzymatically removed. Thioredoxin can directly reduce Cys-SOH to Cys-SH and Cys-SOH reacts with glutathione to form a mixed disulfide (**6**), which is later reduced by glutaredoxin. Based on the rate of formation and repair by these mechanisms, the cellular lifetime of sulfenic acid is on the order of minutes, consistent with the lifetime of many PTMs, including phosphorylation [83]. In A431 cells a peak of protein sulfenylation was observed five minutes after endothelial growth factor stimulation, with a subsequent decay over 30 minutes [85]. Due to the low stability and high turnover rates, monitoring their formation is problematic by direct mass analysis of Cys-SOH. Currently, the use of chemical probes is the only suitable technique to monitor Cys-SOH formation [92]. The low biological stability of Cys-SOH presents a significant challenge to GCE, however chemical caging strategies and structural mimetics have been used to overcome this

challenge [73, 76-77]. Since Cys-SO_2H is notably more stable there is a good chance this oxidation state can be directly incorporated via GCE, although modulation of Srx proteins may be necessary.

The biological impact of protein Cys-SOH formation has been particularly well outlined in protein tyrosine phosphoregulation. Cysteine oxidation controls the activity of both protein tyrosine kinases (PTKs) as well as protein tyrosine phosphatases (PTPs). Sulfenylation of the PTP catalytic Cys residue (pKa 4-6) has emerged as a dynamic mechanism for the inactivation of this protein family [93]. In comparison to PTPs which are always inactivated by ROS, oxidation of PTKs can result in either enhancement or inhibition of kinase activity [94-95]. It is well established that ROS play a regulatory role for some ion channels, although little is described in terms of the molecular basis for this regulation [96]. Peroxiredoxins (Prxs) are important mediators of H_2O_2 signaling as they both maintain low levels of H_2O_2 and are themselves modified to Cys-SOH and Cys-SO_2H to modulate H_2O_2 levels [97].

Cysteine is also S-nitrosylated following the production of NO (**4**), with implications regarding the influence of NO in cellular transduction [98]. Proteins with a wide variety of functions are found to be endogenously S-nitrosylated in intact cellular systems [99]. Much like other Ox-PTMs it has become clear that S-nitrosylation and de-nitrosylation are regulated spatially and temporally in the cell [100]. Using the biotin switch methodology (or variations thereof), multiple proteins with the Cys-SNO modification have been isolated [76]. Among the identified proteins is GAPDH, which transnitrosylates and alters the enzymatic activity of SIRT1 [101]. Effector mechanisms for S-nitrosylation include protein-protein interactions, subcellular localization of proteins, and ubiquitylation-dependent protein degradation, which underlie a variety of cellular processes including apoptosis, metabolism, and membrane trafficking. This modification has been implicated in pathophysiological conditions including multiple sclerosis, Parkinson's disease, and asthma [102-103]. As this Ox-PTM is unstable, genetic incorporation will likely require generation of a structural analogue similar to the methods employed for incorporation of phosphotyrosine and phosphoserine [76-77]. Clearly both cysteine

oxidation and S-nitrosylation based Ox-PTMs are of significant biological interest and this is a field ripe for the development of GCE tools.

Methionine sidechains also contain a sulfur atom susceptible to oxidation. ROS and reactive chlorine species are a major source of methionine oxidation yielding methionine sulfoxide (Met-SO, **11**) [104-105]. Methionine is a strongly hydrophobic residue and is generally buried, which protects it from oxidation, although those few surface exposed Met residues are susceptible to oxidation. Methionine oxidation yields two stereoisomers of the sulfoxide, S- and R- forms. Met-SO formation results in a much more hydrophilic amino acid than Met, which may affect protein structure. Although Met-SO is a fairly stable product, the sulfur can be further oxidized by strong oxidants to the sulfone (Met-SO_2, **12**), however this occurs to a low extent [61]. Met-SO_2 is considered an irreversible reaction product and cannot be converted back to Met by cellular reductants. In much the same way as Cys Ox-PTMS, tools to study Met Ox-PTMs are necessary in order to further explore the implications of these modifications.

Under conditions of H_2O_2 treatment in which Jurkat T-cells were 90% viable, more than 2000 oxidation-sensitive Met residues were identified in the proteome. The majority (84%) of Met-containing peptides contained a low degree of Met-SO (less than 30% oxidized), while only the remaining 16% of peptides were oxidized to a high degree (up to 100% Met-SO) [106]. This significant level of Met oxidation in biological systems requires robust enzymatic repair mechanisms. Methionine sulfoxide reductases (Msrs) efficiently repair Met-SO to Met and are present in all aerobically respiring organisms [107]. Met-SO reductase A and B (MsrA and MsrB) are the prototypical Msrs for the two Met-SO epimers and while they are similar in neither sequence nor structure, they do share common mechanisms to reduce Met-SO to Met [108].

Methionine oxidation is associated with the aging process and several pathophysiological conditions such as neurodegenerative diseases and cancer [109-110]. Previously, Met-SO formation under these conditions was regarded only as protein damage. However, Met oxidation is now being acknowledged as a mode of triggering protein activity. The kinase CaMKII and the transcription factor HypT

were both found to be activated following oxidation of particular methionines [111-112]. The polymerization of actin has also been shown to be regulated by the redox state of Met residues, mediated by the concerted and stereo-selective action of Mical proteins and MsrB1 [113].

Oxidized cysteine or methionine residues have yet to be incorporated by GCE. While this should not be an insurmountable challenge, sulfur containing Ox-PTMs do present stability issues. Cys-SOH is not stable on proteins in living cells so genetic incorporation will require a chemical caging strategy or the use of a mimetic, analogous to what has been done for stable mimetics of phosphorylated serine, threonine, and tyrosine [73, 75-77]. A photocaged Cys-SOH on the protein Gpx3 has been prepared by alkylation of catalytic Cys32 with dimethoxy-*o*-nitrobenzyl bromide (DMNB-Br), followed by oxidation with H_2O_2. While the photo-caged cysteine sulfenic acid free amino acid was also synthesized with the goal to genetically encode this amino acid, to date it has not been incorporated via GCE [114]. In order to successfully incorporate Met-SO, modulation of cellular Msrs levels will be imperative in order to purify intact modified protein similar to the hurdles of removing cellular phosphatases when incorporating phosphorylated amino acids [77].

Ox-PTMs of Aromatic Residues

While the role of sulfur oxidation has been extensively studied, the biological role of Ox-PTMs on aromatic residues is less clear. Residues susceptible to oxidative or nitrosative modifications include tyrosine, tryptophan, and histidine.

Protein tyrosine nitration (nitroTyr, **13**) occurs under basal physiological conditions and is several-fold enhanced under conditions of increased oxidant and ˙NO formation. Much like other Ox-PTMs, the distribution of tyrosine nitrated proteins is largely dependent on the proximity to sites of RNS generation [115]. With the advent of proteomic analyses, it has been observed that protein tyrosine nitration occurs on a subset of proteins, and within those proteins, only a subset of tyrosines are nitrated [64, 116-119]. Based on current evidence, the mechanism of protein tyrosine nitration in biological systems is mediated by free radical reactions, implying

an intermediate tyrosyl radical and subsequent reactions with either ˙NO or ˙NO_2 [11]. Other Ox-PTMs may result from this general reaction mechanism as tyrosyl radical may also react with ROS to form L-3,4-dihydroxyphenylalanine (DOPA, **14**) or another nearby tyrosine to form the protein cross-link dityrosine (**17**) [120-121]. Tyrosine is also susceptible to modification by myeloperoxidase- and eosinophil peroxidase-derived hypochlorous and hypobromous acid to form 3-chlorotyrosine (**21**) and 3-bromotyrosine (**23**) [64]. As with all Ox-PTMs it is difficult to establish direct and quantitative relationships between extent of nitration on specific proteins and biological responses in cells and the influence of protein tyrosine nitration is often obscured by the multiplicity of oxidative modifications. GCE has already begun to untangle some of this complexity [22-24, 122].

Mass spectrometry indicates that protein-bound nitroTyr is present in plasma and tissue at levels on the order of 1 μmol of nitroTyr/mol of tyrosine under normal conditions and increases up to 100-fold under conditions of oxidative stress [123-124]. Over 60 individual proteins have been determined to contain nitroTyr [7] of which several have been investigated further with GCE. Less is known about the abundance of other tyrosine Ox-PTMs although in general they appear to be less abundant and appear on fewer proteins [64].

In contrast to the previously discussed Ox-PTMs, nitroTyr and the other tyrosine Ox-PTMs are generally stable modifications requiring protein turnover to remove the Ox-PTM modified proteins from the cellular protein pool [125]. A “denitrase” activity, capable of returning nitroTyr to the native tyrosine, has been reported multiple times although the enzyme(s) responsible has not been isolated [27, 126-128]. Tyrosine nitration is abundant in aging tissue and has been linked to pathological conditions including neurodegeneration, atherosclerosis, and cancer [7, 129]. While tyrosine nitration was traditionally thought of as global oxidative damage that accumulates under conditions of oxidative stress, it has become clear that some proteins with nitroTyr modifications at specific sites are capable of mediating biology [23-24, 122]. Currently, it is unclear the structural consequences of adding a meta nitro group to a tyrosine on the proteins that have this clear gain-of-function. The most obvious two options for altering protein structure are from the pKa change to

tyrosine and new interactions afforded by the nitro group. Nitration of tyrosine lowers the pKa of the amino acid from ~10 to near neutral pH, imparting a negative charge, while the nitro group also adds significant steric bulk and new hydrogen bonding groups. GCE is uniquely positioned to determine the structural consequences of PTMs because structural mimics of a PTM can be installed to probe if one chemical feature of a PTM is more critical than another. Possible biological effects due to these alterations to tyrosine properties include changes in protein activity (gain- or loss-of-function), increased protein immunogenicity, interference in tyrosine-kinase-dependent regulation, modulation of protein assembly or polymerization, facilitation of protein degradation (turnover), or formation of proteasome resistant protein aggregates [130]. GCE has provided tools to further the molecular understanding of protein tyrosine nitration and development of new tools promises further control over the study of biological processes associated with this Ox-PTM.

High levels of protein tyrosine halogenation have been detected in several inflammatory conditions including arthritis, some types of cancer, heart disease, cystic fibrosis, and asthma [131-133]. Protein tyrosine halogenation *in vivo* is a result of the reaction of myeloperoxidase-derived HOCl or eosinophil peroxidase-derived HOBr, yielding 3-chlorotyrosine (**21**) and 3-bromotyrosine respectively (**23**). HOCl and HOBr are strong oxidants and possess potent antibacterial properties, as such they are generated as components of mammalian host defense [134-135]. However, overproduction or misplaced induction can lead to accumulation of protein modification seen in the above inflammatory conditions. The 3-chlorotyrosine modification along with 3-nitroTyr has been noted in ApoA1 [131, 136]. The interest in these Ox-PTMs has led to the generation of a PylRS-pylT pair that efficiently incorporates both 3-chlorotyrosine and 3-bromotyrosine.

The same conditions that result in protein tyrosine nitration also result in oxidation and nitration of tryptophan residues. A variety of products result from the *in vitro* reaction of tryptophan with biologically relevant RNS (**27-44**) but of those hydroxytryptophan and nitrotryptophan have been detected in samples from tissue or cell culture, specifically 2-hydroxytryptophan (**27**), 4-hydroxytryptophan (**28**), 5-

hydroxytryptophan (**29**), or 6-hydroxytryptophan (**30**), 6-nitrotryptophan (**36**), and 5-hydroxy-6-nitrotryptophan (**40**) [59, 64, 137].

While tyrosine and tryptophan Ox-PTMs occur under the same conditions, several MS studies have indicated that tryptophan modifications are on the order of 10- to 1000-fold less abundant than tyrosine modification [138-139]. No direct repair mechanisms for tryptophan Ox-PTMs have been noted, indicating the only path to remove these Ox-PTMs is protein turnover. Although Ox-PTMs occur at a lower rate on tryptophan than on tyrosine, these modifications likely modulate cellular regulation as tryptophan resides are particularly important for specific protein-protein interactions and protein-small molecule recognition [140-141]. At least one instance of 5-hydroxy-6-nitrotryptophan formation has been reported in the mitochondrial metabolic enzyme Succinyl-CoA:3-ketoacid coenzyme A transferase (SCOT). This age-dependent Ox-PTM leads to a 30% increase in SCOT enzymatic activity and is thought to play a protective role, allowing the heart to better utilize ketone metabolism for energy production [142].

While a novel GCE system for incorporation of tryptophan derivatives has been published and shown to utilize 5-hydroxytryptophan as a substrate, it has not yet been utilized to investigate the effects of this Ox-PTM [71]. As tryptophan Ox-PTMs are generally stable to cellular conditions and the tryptophan-based system can be evolved for other tryptophan based ncAAs, this system will likely be applicable to the study of tryptophan Ox-PTMs.

Oxidation of histidine to 2-oxohistidine (**45**) occurs through a radical mechanism in protein, particularly near metal binding sites or in tissue exposed to UV radiation [143]. This Ox-PTM has been noted to occur significantly in Cu, Zn-SOD [144]. Little is known about how widespread this modification is or how it impacts biological function [145]. While a variety of histidine mimics have been genetically encoded via GCE, 2-oxohistidine has not yet been encoded genetically [146]. As 2-oxohistidine is stable enough on proteins to be characterized by x-ray crystallography [147] and given the aforementioned orthogonal system for modified histidine incorporation, it is likely that 2-oxohistidine will be amenable to incorporation by GCE.

Ox-PTMs that have been incorporated by GCE

The first PTM genetically encoded was nitroTyr by Neumann and coworkers in 2008 and to date has been the most utilized GCE system for probing Ox-PTMs. An *Mj* orthogonal pair was evolved and subsequently used to confirm a loss of function in site-specifically nitrated MnSOD [22]. Through a novel selection scheme, a second generation *Mj* nitroTyr-RS was then generated with roughly an order of magnitude greater efficiency for producing nitroTyr-proteins [21]. This second generation *Mj* nitroTyr-RS was used to generate all 5 forms of nitrated Hsp90 found in endogenously nitrated Hsp90. This allowed each different site-specifically nitrated form of Hsp90 to be characterized for functional changes *in vitro* and cellular toxicity *in vivo* in different mammalian cell lines. Three of the five nitrated forms had no apparent effect when delivered into PC12 cells at physiologically relevant levels. For nitrated Hsp90 a toxic gain of function and motor neuron cell death occurs if Hsp90 is nitrated at either tyrosine 33 or tyrosine 56 in less than 5% of the cellular pool of Hsp90 [23]. This is a key advance in the study of Ox-PTMs because it is the first example of a toxic gain-of-function confirmed from a single site of modification on a protein. Antibodies to nitrated Hsp90 were then generated and using GCE were validated to recognize site-specific nitroTyr-33-Hsp90 and nitroTyr-56-Hsp90. These antibodies, now confirmed to recognize the nitration of a specific sites on Hsp90, have been used to monitor formation of toxic nitrated Hsp90 in tissue and track these oxoforms in other pathological states. It was further shown that nitration of Hsp90 at tyrosine 33 downregulates mitochondrial activity [122]. This nitroTyr GCE system has also been used to investigate physiological role of tyrosine nitration in apolipoprotein A1 (ApoA1), a serum protein that facilitates systemic lipid trafficking. Using mass spectroscopy, three tyrosine residues in ApoA1 were identified as nitration sites. Genetic code expansion allowed the generation and characterization of each nitrated form of ApoA1 and only one nitrated tyrosine had an effect on ApoA1 activity. GCE was used to show that site-specific nitration of ApoA1 at tyrosine 166 results in a 90% reduction in LCAT activity [24]. A site-specific antibody for ApoA1 nitroTyr-166 was also generated in order to monitor this Ox-PTM in the context of

atherosclerotic tissue. These antibodies specific for ApoA1 nitroTyr-166 confirmed that only this nitrated variant was removed from human serum and was enriched in atherosclerotic plaques by 1000-fold over non-nitrated ApoA1.

The ability to incorporate the structurally similar 3-chlorotyrosine and 3-bromotyrosine Ox-PTMs with GCE would enable the characterization of these modifications in disease. However, the first and second generation *Mj* nitroTyr synthetase is not permissive to these ncAAs, and synthetases generated for halotyrosine using the Mj synthetase system resulted in poor efficiency and fidelity. However, selections for a 3-chlorotyrosine synthetase from the PylRS/pylT pair have yielded aaRSs that have good efficiency and fidelity for halogenated tyrosines. Proteins with site-specifically incorporated 3-chlorotyrosine and 3-bromotyrosine have indicated that currently available commercial antibodies to these modifications are not specific or are not sensitive to these modifications alone. GCE now presents the opportunity to improve on the specificity and sensitivity of antibodies for these modifications.

GCE has also been applied to the site-specific incorporation of the redox-active amino acid DOPA (**14**). The site-specific incorporation of DOPA is challenging because when this amino acid is added to media it can react with cellular components yielding the oxidized ncAA (DOPA quinone, **15**) that can serve as an electrophile [148]. To overcome the side reactions in media, a photocaged DOPA has also been encoded [149]. While the GCE of photocaged DOPA was developed for the production of recombinant bio-adhesives not for studying oxidative stress, this tool could also be used to evaluate the effects of DOPA containing proteins in disease.

Application of GCE to the Study of Ox-PTMs

It has long been known that ROS and RNS modify protein amino acids, but it has been challenging to determine the extent of their biological role and abundance. Identifying Ox-PTM formation on a protein is the first step of any investigation into Ox-PTMs followed by verification of biological relevance. The nitroTyr Ox-PTM can be used as an example of how the synergy of new detection methods and GCE can advance the understanding of Ox-PTMs. The earliest manuscripts outlining detection

of nitroTyr in proteins were based on methods using HPLC/UV-Vis and amino acid analysis because this Ox-PTM possesses a significant absorbance at 430 nm [150-151]. A September 2017 Pubmed literature survey revealed 5522 manuscripts published with the term “nitrotyrosine” in the title or abstract. In the first 24 years of research involving nitroTyr, less than 2% of present publications on nitroTyr were published, which was followed by a virtual explosion in the number of papers published on nitroTyr in the ensuing years. This rapid increase in nitroTyr research coincides nicely with the development of the first nitroTyr antibodies by Joe Beckman and coworkers in 1994 (Figure 2.4A) [152]. NitroTyr antibodies have been used to detect this modification in tissue via immunohistochemistry, for identification of proteins via western blot, and for enrichment of proteins for proteomic methods. Due in part to access to antibodies as a detection method, nitroTyr now serves as a general biomarker for oxidative stress [153].

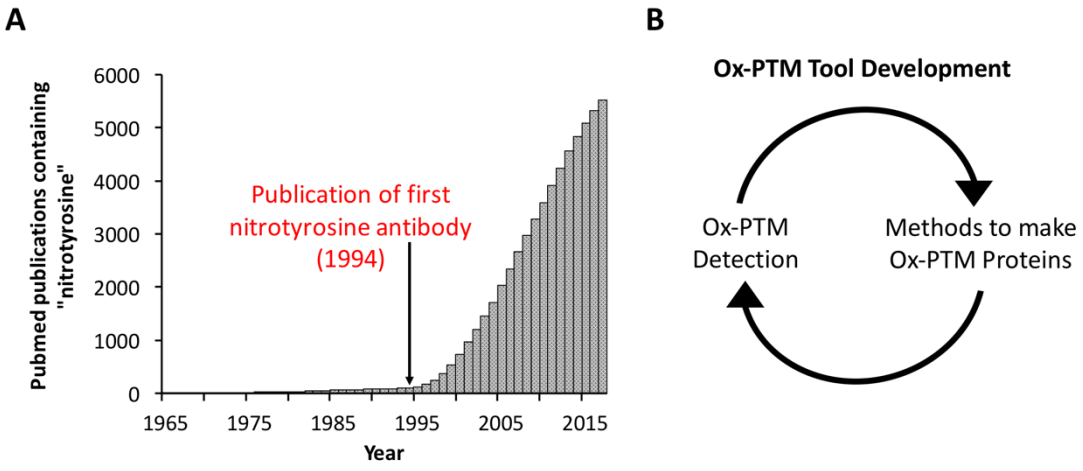

Figure 2.4. The interplay between GCE and other methods to study Ox-PTMs.
(**A**) Total number of publications on Pubmed containing the word ’nitrotyrosine’ in the title or abstract published up to the year indicated. The publication of the first nitrotyrosine antibody by Beckman and coworkers in 1994 is denoted with an arrow. (**B**) The cycle of development of chemical biology tools for studying Ox-PTMs. New methods like development of antibodies allow easier detection of Ox-PTMs, which naturally lead to increased interest and development of new chemical biology tools, including GCE, for studying Ox-PTMs. Tools like GCE allow for development of better detection methods, which further reinforces the cycle.

The increased interest in the nitroTyr Ox-PTM has spurred numerous methods for identifying nitroTyr proteins including HPLC-based techniques for quantifying total nitroTyr in tissues and lysates and various mass spectrometry methods for identifying sites of nitroTyr modification in proteins [62, 154]. The interest in nitroTyr and its detection in a variety of pathological conditions created the need to generate homogeneous nitrated proteins for characterization which led directly to the first GCE system for nitroTyr incorporation [22]. GCE clearly enables characterization of how a specific Ox-PTM on a protein alters its function but it also allows for analysis of the antibodies generated to detect Ox-PTM proteins. With access to site-specific and homogeneous Ox-PTM protein generated from GCE the specificity and sensitivity of Ox-PTM antibodies can be determined. The original nitroTyr antibodies generated were a foundational advancement in studying oxidative stress but as the field progresses improved antibodies for studying Ox-PTMs are needed. While the development of nitroTyr antibodies lead to the incorporation of nitroTyr via GCE, better detections methods for nitroTyr can now be developed using site-specifically modified protein from GCE (Figure 2.4B).

It has become very clear through GCE that nitroTyr antibodies have wildly different sensitivity depending on the site of protein nitration. All of the currently available Ox-PTM antibodies were developed prior to GCE of Ox-PTM and were validated using methods available at the time of their development [13]. Now GCE allows for verification that Ox-PTM antibodies are selective for one type of Ox-PTM over others of similar structure. Since antibodies are often generated to proteins that have been exposed to ROS and RNS reagents, not homogeneous Ox-PTM proteins, the resulting antibody specificity might be to a different Ox-PTM than intended. For example, the nitroTyr monoclonal antibody (clone 1A6) indicated a nitrated protein was present in aged rat heart mitochondria, but this protein was instead found to contain 5-hydroxy-6-nitrotryptophan, which closely resembles the nitroTyr sidechain [142].

A powerful application of GCE is the ability to confirm that an Ox-PTM modification at a specific location in a protein is detected by an antibody. While nitroTyr-antibodies are specific for the nitroTyr modification they do not detect all

sites of nitration equally. In addition, if there is the ability to detect the modification at one location on a protein and not another this can be verified with GCE. A specific peptide sequence containing the desired Ox-PTM can be used to generate antibodies and then the Ox-PTM antibodies can be screened for selectivity against homogeneous protein generated with GCE. Antibodies specific for nitroTyr-33-Hsp90, nitroTyr-56-Hsp90, and ApoA1 have been generated using this approach [23-24, 122]. These site-specific antibodies have been used to determine the extent of nitration of specific sites in Hsp90 in different cellular contexts and conditions. Unsurprisingly, there exists clear peptide context dependent sensitivity to the function of nitroTyr antibodies, that is to say, the amino acid sequence of the protein surrounding the Ox-PTM site plays a role in antibody detection sensitivity. In addition to the development of site-specific antibodies, the ability of GCE to produce homogeneously nitrated proteins allows for the characterization of this context dependence that was not possible with existing techniques. While much of the past work on detection of Ox-PTMs with antibodies has focused on nitroTyr, further development of GCE for other Ox-PTMs will lead to exciting advances in Ox-PTM antibody development and validation, particularly for cysteine and methionine oxoforms.

As Ox-PTMs are relevant to disease the Ox-PTM-proteins and their function represent a new class of possible therapeutic targets. Any Ox-PTM-protein that shows an undesirable gain-of-function or new interaction could be a therapeutic target. Ox-PTMs present a unique situation insofar as they are not directly enzymatically catalyzed and therefore the PTM “writer” (e.g. kinase) cannot be directly inhibited. This requires the oxidized protein itself to be directly inhibited. For instance, nitrated Hsp90 found in motor neurons under pathological conditions such as ALS and spinal cord injury may present a target for intervention [23]. It has become increasingly clear that the site of protein Ox-PTMs are an important determinant of their biological role. With this in mind, the use of GCE for site-specific PTM incorporation as a means of screening for potential therapeutics against specific Ox-PTMs has been acknowledged [155]. This is clear in the case of Hsp90, which is endogenously nitrated on five tyrosines and of them only nitration of tyrosine 33 and 56 lead to motor neuron cell death, while nitration of tyrosine 33 downregulates mitochondrial

activity [23, 122]. Given this clear functional specificity from site-dependence of nitrated Hsp90 it will be desirable to develop sequence-specific inhibitors that target site-specific Ox-PTM proteins. As GCE can produce all possible form Ox-PTM forms, the technology will allow for screening of therapeutic compounds against site-specific oxoforms.

Conclusions and Perspective

The study of protein Ox-PTMs is hampered by access to defined Ox-PTM-proteins. GCE is uniquely suited to overcome this roadblock because it generates site-specific and homogenous Ox-PTM proteins. GCE has been applied to protein tyrosine nitration both to investigate biological effects of particular sites of modification on key proteins and to provide defined Ox-PTM-proteins for validating nitroTyr antibodies. Every newly identified Ox-PTM-protein that shows a gain of function can be considered as a therapeutic target since it forms under oxidative stress conditions. As seen with nitrated Hsp90 and ApoA1, the ability to generate Ox-PTM-proteins opens the ability to develop screens for therapeutics and identify their molecular role in disease.

Thus far, the development of GCE methods for Ox-PTMs has relied on researchers from both the oxidative stress field and the GCE fields. NitroTyr was identified in biological samples as a major marker for oxidative stress which prompted those in GCE to develop methods for site-specific incorporation of this Ox-PTM. As those in the oxidative stress field embraced the use of the GCE methods for challenging problems, the GCE tools required refinement and improvement. With this in mind, significant advances in the Ox-PTM field will likely rely on synergy between developments in GCE technology and those applying the tools to challenging Ox-PTM problems.

Acknowledgements

We thank Richard Cooley, Elise van Fossen, and Sara Clark for critical review of the manuscript. This work was funded by National Institutes of Health Grant RGM114653A (to R.A.M.).

Supplementary Table S2.1. The list of Ox-PTMs identified following oxidative stress in cells or exposure of protein *in vitro* to ROS and RNOS.

Number	**Ox-PTM Name**	**Reference**
(**1**)	cysteine sulfenic acid	[2, 3]
(**2**)	cysteine sulfinic acid	[2, 3]
(**3**)	cysteine mixed disulfide	[4]
(**4**)	S-nitrosyl cysteine	[3]
(**5**)	cysteine cyclic sulfenamide	[2, 3]
(**6**)	cysteine glutathionylation	[3]
(**7**)	cysteine thiosulfinate	[2]
(**8**)	cysteine disulfide	[2-4]
(**9**)	cysteine sulfonic acid	[2, 3]
(**10**)	Prx cysteine phosphoryl sulfinic enzyme intermediate	[2]
(**11**)	methionine sulfoxide	[4, 5]
(**12**)	methionine sulfone	[5]
(**13**)	3-nitrotyrosine	[6]
(**14**)	3,4-dihydrophenylalanine (DOPA)	[6]
(**15**)	dopaquinone (DQ)	[6]
(**16**)	DQ protein conjugate adduct	[6]
(**17**)	3,3'-dityrosine	[6]
(**18**)	3-aminotyrosine	[6]
(**19**)	Quinone imine (QI)	[6]
(**20**)	QI protein conjugate adduct	[6]
(**21**)	3-chlorotyrosine	[6]
(**22**)	3,5-dichlorotyrosine	[6]
(**23**)	3-bromotyrosine	[6]
(**24**)	3,5-dibromotyrosine	[6]
(**25**)	3-iodotyrosine	[6]
(**26**)	3,5-iodotyrosine	[6]
(**27**)	2-hydroxytryptophan	[4, 7]
(**28**)	4-hydroxytryptophan	[4, 7]
(**29**)	5-hydroxytryptophan	[4, 7]
(**30**)	6-hydroxytryptophan	[4, 7]
(**31**)	7-hydroxytryptophan	[4, 7]
(**32**)	dihydroxytryptophan	[7]
(**33**)	2-nitrotryptophan	[7]
(**34**)	4-nitrotryptophan	[7]
(**35**)	5-nitrotryptophan	[7]
(**36**)	6-nitrotryptophan	[7]
(**37**)	7-nitrotryptophan	[7]
(**38**)	1-nitrotryptophan	[7]
(**39**)	1-nitrosotryptophan	[7]

Number	Ox-PTM Name	Reference
(**40**)	5-hydroxy-6-nitrotryptophan	[7]
(**41**)	N-formylkynurenine	[4, 7]
(**42**)	3-hydroxykynurenine	[4]
(**43**)	Oxindole-3-alanine	[7]
(**44**)	kynurenine	[7]
(**45**)	2-oxohistidine	[4, 8]
(**46**)	Asparagine (Ox-PTM histidine)	[4]
(**47**)	Aspartate (Ox-PTM histidine)	[4]
(**48**)	4-hydroxyphenylalanine	[4]
(**49**)	2-hydroxyphenylalanine	[4, 6]
(**50**)	3-hydroxyphenylalanine	[4, 6]
(**51**)	2-alkenal Michael adduct (Ox-PTM histidine)	[8]
(**52**)	4-hydroxy-2-alkenal Michael adduct (Ox-PTM histidine)	[8]
(**53**)	Aminadipic semialdehyde (Ox-PTM lysine)	[4, 8]
(**54**)	2-alkenal Michael adduct (Ox-PTM lysine)	[8]
(**55**)	4-hydroxy-2-alkenal Michael adduct (Ox-PTM lysine)	[8]
(**56**)	FDP adduct (Ox-PTM lysine)	[8]
(**57**)	N-propenallysine	[8]
(**58**)	DHP adduct (Ox-PTM lysine)	[8]
(**59**)	pyridium DHP (Ox-PTM lysine)	[8]
(**60**)	Glutamylsemialdehyde (Ox-PTM arginine)	[4]
(**61**)	3-hydroxyleucine	[4]
(**62**)	4-hydroxyleucine	[4]
(**63**)	3-hydroxyvaline	[4]
(**64**)	4-hydroxyglutamic acid	[4]
(**65**)	2-amino-3-ketobutyric acid	[4]

Chapter 3

Improved Incorporation of Noncanonical Amino Acids by an Engineered $tRNA^{Tyr}$ Suppressor

Benjamin J. Rauch*, Joseph J. Porter*, and Ryan Mehl

*These authors contributed equally to this work

Published in *Biochemistry, 2016, 55, pp 618-628*

Abstract

The *Methanocaldcoccus jannaschii* tyrosyl-tRNA synthetase (TyrRS):tRNA^{Tyr} cognate pair has been used to incorporate a large number of noncanonical amino acids (ncAAs) into recombinant proteins in *Escherichia coli*. However, the structural elements of the suppressor tRNA^{Tyr} used in these experiments have not been examined for optimal performance. Here, we evaluate the steady-state kinetic parameters of wild-type *M. jannaschii* TyrRS and an evolved 3-nitrotyrosyl-tRNA synthetase (nitroTyrRS) toward several engineered tRNA^{Tyr} suppressors, and we correlate aminoacylation properties with the efficiency and fidelity of superfolder green fluorescent protein (sfGFP) synthesis in vivo. Optimal ncAA-sfGFP synthesis correlates with improved aminoacylation kinetics for a tRNA^{Tyr} amber suppressor with two substitutions in the anticodon loop (G34C/G37A), while four additional mutations in the D and variable loops, present in the tRNA^{Tyr} used in all directed evolution experiments to date, are deleterious to function both *in vivo* and *in vitro*. These findings extend to three of four other evolved TyrRS enzymes that incorporate distinct ncAAs. Suppressor tRNAs elicit decreases in amino acid K_m values for both TyrRS and nitroTyrRS, suggesting that direct anticodon recognition by TyrRS need not be an impediment to superior performance of this orthogonal system and offering insight into novel approaches for directed evolution. The G34C/G37A tRNA^{Tyr} may enhance future incorporation of many ncAAs by engineered TyrRS enzymes.

Introduction

Site-specific incorporation of noncanonical amino acids (ncAAs) with genetic code expansion offers substantial potential for the development of new designer proteins for insights into cellular processes [156-158] and is also a key foundational technology in synthetic biology [159]. The key requirement for all new coding applications is the design of novel aminoacyl-tRNA synthetases (aaRS) that can ligate one or more ncAAs to a unique tRNA that reads an unused codon triplet or quadruplet [160-163]. Novel aaRS-tRNA pairs must efficiently function in both aminoacylation and downstream protein synthesis steps *in vivo*, including interactions with elongation factors and the ribosome.

Directed evolution has been used to derive engineered aaRS enzymes capable of introducing >100 ncAAs into proteins in bacterial and eukaryotic cells [17, 69, 161, 164]. The first step in the directed evolution process is to modify an aaRS-tRNA pair so that it is orthogonal to the naturally occurring aaRS-tRNA systems in the host cell [161]. Orthogonality requires that the new aaRS does not attach the ncAA to any endogenous cellular tRNA at rates that would compromise the specificity of protein synthesis *in vivo* or result in heterogeneous incorporation of the ncAA. In addition, proper functioning of the new orthogonal pair demands that an endogenous aaRS does not efficiently aminoacylate the new tRNA with a canonical amino acid [17-18]. The second step of directed evolution is to alter the active site of the aaRS so that it will accommodate the desired ncAA and attach it to the cognate tRNA while excluding other amino acids [161]. Although a number of aaRS-tRNA systems have been examined as candidate scaffolds for directed evolution [16], two that reliably pass both engineering steps multiple times to incorporate many different ncAAs have emerged: the tyrosyl-tRNA synthetase (TyrRS)-$tRNA^{Tyr}$ complex from *Methanocaldococcus jannaschii* [17] and the pyrrolysyl-tRNA synthetase (PylRS)-$tRNA^{Pyl}$ pairs from *Methanosarcinae* [70].

Engineered cells incorporating orthogonal aaRS-tRNA pairs are sometimes capable of generating recombinant ncAA-containing proteins at milligram yields per liter of culture [165], demonstrating that the systems can function very efficiently *in vivo*. Notwithstanding, it is generally recognized that the aspirations of synthetic biology, which include large scale rebuilding of the protein synthesis apparatus to accommodate “designer codes” [164], will require much better integration of the new aaRS-tRNA pairs into the translational apparatus. A central issue is that very high concentrations of ncAAs and overexpression of the new tRNAs are presently needed for recombinant protein expression, but these features may diminish cellular fitness by increasing the level of competition with endogenous aaRS for both amino acid and tRNA pools [162, 166]. Kinetic analysis of several purified PylRS variants that incorporate ncAAs revealed aminoacylation efficiencies reduced by several hundred-fold compared with that of wild-type PylRS [167], validating the notion that the directed evolution process does not generate optimally functioning aaRS.

A variety of strategies have been employed to increase recombinant ncAA-containing protein yields while maintaining (i) high levels of fidelity against other amino acids and (ii) low misacylation levels of the new tRNA by host aaRS and of host tRNAs by the evolved aaRS (the orthogonality requirement). For example, recent work to improve expression of noncanonical amino acids in insect and mammalian cells has focused on augmenting suppressor tRNA expression levels, with concomitant increases in yields of the ncAA-containing proteins [48, 168-169]. Use of a baculovirus-based delivery system to deliver both the engineered tRNA and aaRS components to mammalian cells has also been successful [50]. Another strategy has been to manipulate interactions with other components of the protein translation system, including release factors in bacterial and mammalian cells [168, 170], and the elongation factor Tu in bacteria [78, 171]. The orthogonality of *M. jannaschii* $tRNA^{Tyr}$ was improved by overexpression of prolyl-tRNA synthetase (ProRS), outcompeting an undesired interaction of engineered *M. jannaschii* TyrRS with *Escherichia coli* $tRNA^{Pro}$ [172]. This exemplifies the long-understood principle that optimal function of the translation system *in vivo* depends on the proper balance of aaRS and tRNA [164, 173]. Finally, directed evolution experiments targeted at the anticodon recognition interface of *M. jannaschii* TyrRS also led to improved incorporation efficiencies of some ncAAs [174].

As a contribution to these efforts, we focus here on improving recombinant ncAA-containing protein expression by examining the performance of an orthogonal aaRS:tRNA pair in detail. Recent other work along these lines has studied the PylRS:$tRNA^{Pyl}$ system for ncAA incorporation [167, 175]. Here, we examine modified *M. jannaschii* TyrRS enzymes that insert 3-nitrotyrosine (nitroTyr) and other ncAAs into recombinant proteins *in vivo* [19, 22]. To understand the role of oxidative stress-induced nitration, it is first necessary to express homogeneously nitrated proteins in *E. coli*, which requires an improved efficiency of nitroTyr incorporation [22-24]. Tyrosine nitration is extensive in human cells, is correlated with disease phenotypes, and has been shown to alter protein function *in vivo* [176-177]. Optimization of 3-nitrotyrosyl tRNA synthetases (nitroTyrRSs) will provide valuable research tools for studying the nitrated human proteome. In prior studies, we

established that modifying the experimental protocol for directed evolution, including alterations to the selection media and antibiotic concentrations, yielded new nitroTyrRS variants with markedly different efficiencies for incorporation of nitroTyr into the fluorescent reporter protein sfGFP [19]. Improved second-generation enzymes were able to incorporate nitroTyr at multiple sites in Hsp90 and apoA1 at efficiencies markedly superior to those of first-generation enzymes evolved using a more common directed evolution approach [23]. The best second-generation nitroTyrRS contains five substitutions, all located directly within the substrate amino acid binding pocket [19].

To understand and further improve the function of the nitroTyrRS derived from directed evolution, we measured the kinetic parameters of the best recombinant first- and second-generation nitroTyrRSs as a means of correlating *in vivo* performance in protein synthesis with *in vitro* enzymatic properties. We also examined the role of six nucleotides in *M. jannaschii* $tRNA^{Tyr}$ that were previously mutated to improve orthogonality and that have been incorporated into the tRNA used in all directed evolution experiments with this orthogonal pair [18]. The data reveal a clear correlation between *in vivo* protein synthesis efficiency and kinetic parameters for aminoacylation over a set of variant enzyme:tRNA pairs. We show that the identity of the nucleotide located immediately 3′ to the anticodon sequence plays a key role in modulating incorporation of four different ncAAs *in vivo* and *in vitro*, and that substitution of four other nucleotides in the $tRNA^{Tyr}$ core region is detrimental to protein expression. These findings should provide a basis for improving the performance of many directed evolution systems that employ the *M. jannaschii* TyrRS platform.

Experimental Procedures

Expression Plasmids for Aminoacyl-tRNA Synthetases

To construct *E. coli* expression vectors for *M. jannaschii* TyrRS variants, the DNA fragments containing the variant of interest were amplified by polymerase chain reaction (PCR) from the corresponding pBK plasmids and ligated into the NcoI/XhoI sites of expression vector pET28a(+) [19]. Primers were used to install an N-terminal six-histidine tag (forward primer, 5′-CGCGCGCCATGGACGAATTTGAAATG-3′;

reverse primer, 5′-GGGCGCTCGAGTAATCTCTTTCTAATTGGCTCTAAAATC-3′). The resulting pET-RS plasmid was transformed into DH10B cells and purified with a QIAprep spin mini kit.

Expression Plasmids for tRNAs

To introduce mutant tRNAs into the pALS plasmid, a DNA fragment containing the altered tRNA sequences was inserted via isothermal assembly [178]. The pALS plasmid was amplified by PCR using forward primer 5′-CCACTTATTTTGA TCGTTCGCTC-3′ and reverse primer 5′-CGTGACTGGGAAAACCCTGG-3′; a DpnI digest was performed on the resulting mixture and then purified with a GeneJET PCR purification kit (Thermo Scientific). A double-stranded DNA fragment or gBlock (Integrated DNA Technologies) with a front overlapping segment (5′-CCAGGGTTTTCCCAGTCACG-3′) and a rear overlapping segment (5′-CCACTTATTTTGATCGTTCGCTC-3′) was introduced into the previously amplified pALS plasmid as per the instructions for the NEB Gibson Assembly Master Mix (New England Biolabs). Chemically competent DH10B cells were transformed with 5 μL of the mix following assembly. The rescued cells were plated on LB agar plates containing 25 μg/mL tetracycline and allowed to grow for 28 h at 37 °C. The vectors were purified with a QIAprep spin mini kit (Qiagen), and the tRNA sequences were verified.

Expression and Purification of Aminoacyl-tRNA Synthetases

BL21-AI cells containing a pET-3NT8RS or pET-TyrRS gene were grown overnight at 37 °C in 5 mL of noninducing medium supplemented with 100 μg/mL kanamycin [179]. A 50 mL culture of arabinose autoinduction medium (Table 3.1) supplemented with 100 μg/mL kanamycin and 0.02% lactose was then inoculated with a 1:100 dilution of the starter culture [180]. After 24 h at 37 °C, cells were pelleted and stored at −80 °C [181].

Table 3.1. Components for autoinducing and non-inducing mediums, for final volume of 500 mL.

	A) Autoinducing Media[1]	B) Noninducing Media[1]
5% Aspartate, pH 7.5	25 ml	25 ml
10% Glycerol	25 ml	---
25 x 18 amino acid mix	20 ml	20 ml
25 x M-salts	20 ml	20 ml
Leucine (4 mg/ml), pH 7.5	5 ml	5 ml
20% Arabinose (w/v)	1.25 ml	---
1 M $MgSO_4$	1 ml	1 ml
40% Glucose	625 ul	6.25 ml
Trace Metals	100 ul	100 ul

The best performing first-generation nitroTyrRS and wild-type TyrRS were purified using methods similar to those previously described [182]. Briefly, cells were resuspended in approximately 10 mL of binding/wash buffer [20 mM sodium phosphate, 500 mM NaCl, and 20 mM imidazole (pH 7.4)], lysed once with a Microfluidics M-110P microfluidizer set at 18000 psi, and centrifuged at 20000 rcf for 25 min at 4 °C. The supernatant was filtered with an Acrodisc 32 mm syringe filter with a 0.45 Supor membrane before being applied to an ÄKTA Explorer FPLC system (GE Healthcare Life Sciences) fitted with a 1 mL HisTrap NiNTA column (GE). The column was washed with 20 mL of wash buffer and then eluted with a 0 to 100%, 30 mL linear gradient of elution buffer [20 mM sodium phosphate, 500 mM NaCl, and 500 mM imidazole (pH 7.4)]. Yields were approximately 15 mg/L of culture (Tyr-WT RS) and 180 mg/L of culture (nitroTyr-3NT8 RS). Fractions containing >95% pure nitroTyr-3NT8 and Tyr-WT RS as determined by sodium dodecyl sulfate–polyacrylamide gel electrophoresis were pooled, dialyzed overnight into storage buffer [20 mM Tris, 50 mM NaCl, and 10 mM β-mercaptoethanol (pH 8.5)], concentrated to 20 mg/mL, frozen in liquid nitrogen, and stored at −80 °C. The second-generation nitroTyrRS-5B was expressed and purified as previously described [19].

Plasmid and Medium Conditions for the Measurement of Efficiency, Fidelity, and Orthogonality

All measurements of efficiency, fidelity, and orthogonality *in vivo* were performed in DH10B E. coli cells with a superfolder GFP reporter [19]. For these measurements, the cells contained some combination of a pALS-sfGFP-WT or pALS-sfGFP-150TAG plasmid, expressing the sfGFP gene and the tRNA, and a pBK plasmid expressing the aaRS. The kanamycin (Kn) resistant pBK plasmid encodes the aminoacyl-tRNA synthetase of interest under control of the constitutive E. coli GlnRS promoter and terminator [183]. For efficiency measurements, cells containing both the pALS-sfGFP-150TAG and pBK plasmids were grown in media containing the ncAA of interest, with the level of GFP fluorescence reporting the efficiency of ncAA incorporation. Fidelity measurements were taken with cells containing the pALS-sfGFP-150TAG and pBK plasmids in media without the ncAA of interest. To assess the orthogonality of a particular tRNA sequence, cells containing the pALS-sfGFP-150TAG plasmid alone were grown in media without an ncAA.

Efficiency of NitroTyr Incorporation *In Vivo*

All protein expression was performed in DH10B cells containing either pALS-sfGFP or pALS-sfGFP-150TAG and a pBK vector to produce WT-sfGFP or nitroTyr-sfGFP. The arabinose autoinduction medium and protocol were used. Cultures were inoculated with 1:100 dilutions of noninducing cultures [179]. Expressions were performed in duplicate with 3 mL of autoinduction medium supplemented with 100 μg/mL kanamycin and 25 μg/mL tetracycline in 17 mm × 100 mm culture tubes being shaken at 250 rpm and 37 °C for 48 h. Error bars represent the standard deviation obtained from duplicate expressions. For the nitroTyr concentration-dependent sfGFP overexpression, nitroTyr was dissolved to a concentration of 10 mM in arabinose autoinduction medium, and 1 molar equiv of NaOH was added to help alleviate differences in cell growth due to media pH changes from the added amino acid. The nitroTyr stock was then serially diluted with medium to obtain the necessary concentrations of nitroTyr.

Fluorescence measurements of the cultures were collected 24 h after inoculation using a Synergy 2 Multi-Mode Reader (BioTEK). The emission and

excitation wavelengths were set to 528/20 nm and 485/20 nm, respectively. Samples were prepared by placing 200 μL of the cell suspension directly in Nunc MicroWell 96-well polypropylene plates (Sigma-Aldrich). The optical density of the cultures was determined at the same time by measuring the absorbance at 620 nm of a 1:10 dilution of the cells in Nunc MicroWell 96-well polystyrene clear flat bottom plates (Sigma-Aldrich). Cell fluorescence levels were normalized for the effects of OD and amino acids on fluorescence. To normalize for the effect of nitroTyr on sfGFP fluorescence, cells expressing WT sfGFP were grown in the presence of nitroTyr, normalized for OD, and the resulting fluorescence levels were normalized to each other. The resulting normalization factors were then applied to the remainder of the fluorescence data.

Efficiency of Incorporation of Various ncAAs with the C34/A37 Mutant tRNA

To determine the generality of the results for the C34/A37 mutant tRNA seen with nitroTyr, cells containing the pALS-sfGFP-150TAG plasmid with the C34/A37 mutant tRNA were cotransformed with pBK plasmids encoding genes for modified TyrRS enzymes selective for a variety of different ncAAs. The aaRS enzymes used were previously selected for incorporation of 4-benzoyl-L-phenylalanine (Bpa), 4-(trifluoromethyl)-L-phenylalanine (tfmF), 4-cyano-L-phenylalanine (pCNF), and acridon-2-ylalanine (Acd).(42-44) Each pALS/pBK pair was grown in autoinduction medium, in the presence of their respective ncAA at 0.25 mM (see Figure S3.2), for 48 h, with all other conditions and measurements as described above for nitroTyr. The ncAAs in this study were purchased from Peptech, Alfa Aesar, or Bachem or were synthesized as previously described [165].

Preparation and Labeling of tRNA Transcripts for Aminoacylation

The tRNA substrates for aminoacylation by TyrRS and nitroTyrRS were prepared by *in vitro* transcription [184]. Because tRNATyr and its variants begin with 5′-C1, which is unfavorable for transcription by T7 RNA polymerase, tRNAs were transcribed from DNA templates encoding a self-cleaving hammerhead ribozyme immediately upstream [185]. DNA templates were assembled from four synthetic oligonucleotides. Overlapping regions are underlined, and mutations were imposed at

positions indicated in boldface: (1) 5′-AATTCCTGCAGTAATACGACTC ACTATAGGGAGACCGGCTGATGAGTC-3′, (2) 5′-CCGGGACGGTACCGGGTA CCGTTTCGTCCTCACGGACTCATCAGCCGGTCTCCC-3′, (3) 5′-CCCGGTACC GTCCCGGCGGTAGTTCAGC**CT**GG**T**AGAACGGCGGACT**G**TA**G**-3′, and (4) 5′-TGGTCCGGCGGGCCGGATTTGAACCAGCGA**C**ATGCGGAT**CTAC**AGTCCGC CGTTCTACC-3′. Assembly was facilitated by the Vent polymerase [New England Biolabs (NEB)]. A 50 μL PCR was set up with 1× Thermopol Buffer (NEB), each oligonucleotide at 2 μM, each dNTP at 50 μM, and 1 μL of Vent polymerase (NEB). The reaction mixture was heated for 5 min at 94 °C and subjected to eight of the following PCR cycles: 94 °C for 1.5 min, 54 °C for 2 min, and 72 °C for 3 min. A fifth oligonucleotide was used, along with oligonucleotide 1, to amplify the assembled template: (5) 5′-[2′-OMe]U[2′-OMe]GGTCCGGCGGGCCGG-3′. The 2′-*O*-methyl modifications inhibit runover transcription by T7 RNA polymerase [186]. A 400 μL PCR was set up with 1× Taq buffer (Thermo), 2.5 mM MgCl2, each dNTP at 50 μM, each oligonucleotide at 1 μM (1 and 5), 4 μL of the Vent reaction mixture, and 0.031 unit/μL Taq polymerase (Thermo). The reaction mixture was heated at 95 °C for 3 min and then subjected to 40 of the following cycles: 95 °C for 0.5 min, 60 °C for 0.5 min, and 72 °C for 0.17 min. The template was purified using a GeneJET Purification Kit (Thermo) and diluted into a 2 mL transcription reaction mixture containing 40 mM Tris-HCl (pH 8.0), 25 mM $MgCl_2$, 2 μM spermidine, 0.01% Triton X-100, 40 mM DTT, each NTP at 4 mM, 0.001 unit/μL inorganic pyrophosphatase (Roche), and 0.04 mg/mL T7 RNA polymerase$_{\Delta 172–173}$, which was expressed and purified in the laboratory as described previously [187]. The reaction mixture was incubated at 37 °C for 16–24 h.

To promote cleavage of the hammerhead ribozyme, the reaction mixture was diluted 5-fold into a buffer containing 40 mM Tris-HCl (pH 8.0), 25 mM $MgCl_2$, 2 μM spermidine, 0.01% Triton X-100, and 40 mM DTT and incubated at 60 °C for 4–7 h. Cleaved RNAs were concentrated to 0.5 mL and washed with TE6 buffer [10 mM BisTris-HCl and 1 mM EDTA (pH 6.0)] using a centrifugal filtration device [Amicon; 10 kDa molecular weight cutoff (MWCO)]. After proteins had been removed by extraction with 1 volume of a 25:24:1 phenol/chloroform/isoamyl alcohol

mixture (pH 7.8) (Sigma), tRNA was purified away from uncleaved transcripts and free hammerhead ribozyme by electrophoresis through a 15 cm gel containing 15% polyacrylamide:bis(acrylamide) (29:1), 8 M urea, and 1× TBE. tRNA was visualized by UV shadowing and excised from the gel. tRNA was extracted from the gel band with 10 volumes of TE6, shaken for 16–24 h at room temperature. Insoluble gel debris were removed by centrifugation at 5000 rcf for 10 min. The supernatant was passed though a 0.45 μm filter and washed with TE6 buffer using a centrifugal filtration device (Amicon; 10 kDa MWCO) such that urea was diluted to a concentration of <1 μM.

The tRNA substrates for aminoacylation were radiolabeled at the 5′-phosphate of nucleotide A76 in accordance with established methods [188]. Labeling reactions (volume of 80 μL) were performed in siliconized conical microcentrifuge tubes in a solution containing 20 mM glycine (pH 9.0), 4 mM $MgCl_2$, 2.5 mM pyrophosphate, 0.2 unit of pyrophosphatase (Roche), 2.5 μM tRNA, ~50 μCi of [α-32P]ATP, and ~5 μM *E. coli* nucleotidyltransferase, purified in our laboratory as described previously [189]. Reactions were initiated by the addition of the nucleotidyltransferase and were allowed to proceed at 37 °C for 5 min. Prior to labeling, tRNA was denatured by being incubated for 10 min at 65 °C in ~50 μL of water and refolded by being slowly cooled to room temperature over the course of 1 h in the presence of glycine and $MgCl_2$. Labeled tRNA was purified by extraction with 1 volume of a 25:24:1 (pH 7.8) phenol/chloroform/isoamyl alcohol mixture (Sigma) and purified from unincorporated ATP by electrophoresis through a 15 cm gel containing 15% polyacrylamide:bis(acrylamide) (29:1) and 1× TBE. tRNA was visualized by phosphorimaging to facilitate excision from the gel. tRNA was extracted from the gel band with 2 volumes of TE6 buffer without shaking, in a 16–24 h incubation at ambient temperature.

Aminoacylation Reactions

Aminoacylation assays were conducted at 37 °C in siliconized conical tubes containing 20 μL of 50 mM HEPES-KOH (pH 7.5), 20 mM NaCl, 10 mM $MgCl_2$, 1 mM DTT, 2.5 mM MgATP, and various concentrations of amino acid, tRNA, and

enzyme as appropriate. Methods used were similar to those employed in our laboratory for the study of other tRNA synthetases [190-192]. Reactions were initiated by the addition of enzyme, which was diluted into the reaction mixture from a 10× stock. tRNAs were refolded prior to aminoacylation as follows. Labeled and unlabeled tRNAs were diluted into TE6 buffer to yield a 5× mixture, which was incubated at 65 °C for 10 min and then supplemented with 0.5 volume of 100 mM $MgCl_2$ that was prewarmed to 65 °C. The resulting tRNA/$MgCl_2$ mixture was then slowly cooled to room temperature over the course of 1 h. Time points were quenched by 1:3 dilution into a solution containing 200 mM NaOAc (pH 5.2) and 0.2% SDS and subsequently digested for 15 min at room temperature with Penicillium citrinum P1 nuclease (Sigma) at a concentration of 0.0125 unit/μL. Free nucleotides were separated by thin layer chromatography across 10 cm PEI cellulose sheets (Sigma) with a solvent containing 1 M ammonium acetate and 5% acetic acid. Spots corresponding to AMP and aminoacyl-AMP were visualized by phosphorimaging and quantified using imageJ [193].

For short-term (<2 months) storage at −20 °C as 10× stocks, enzymes were diluted into a buffer containing 20 mM Tris-HCl (pH 8.0), 50 mM NaCl, 1 mM DTT, and 50% glycerol.

Results

M. jannaschii Tyrosyl-tRNA Synthetase Efficiently Aminoacylates Unmodified Cognate tRNAs with Tyrosine

To establish an experimental system for measuring the detailed kinetic properties of TyrRS variants emerging from directed evolution, we first expressed and purified wild-type *M. jannaschii* TyrRS in *E. coli* and characterized its performance in the canonical two-step tyrosylation reaction using unmodified wild-type *M. jannaschii* $tRNA^{Tyr}$ (wt-tRNA) produced by *in vitro* transcription with T7 RNA polymerase. tRNA was labeled at the 3′-internucleotide linkage using tRNA nucleotidyltransferase and subjected to refolding prior to use [188]. After tRNA refolding parameters had been evaluated, including the magnesium ion concentration and maximal temperature (see Materials and Methods for details), the maximal aminoacylation capacity of the transcript reached 67% in reactions performed with a molar excess of enzyme (Figure

3.1). The failure to achieve complete aminoacylation is common in *in vitro* aminoacylation reactions and may be due to a subpopulation of tRNAs that is kinetically trapped in a nonfunctional conformation [194]. In our hands, plateau aminoacylation at this level yields reliable kinetic parameters in other aaRS systems [190].

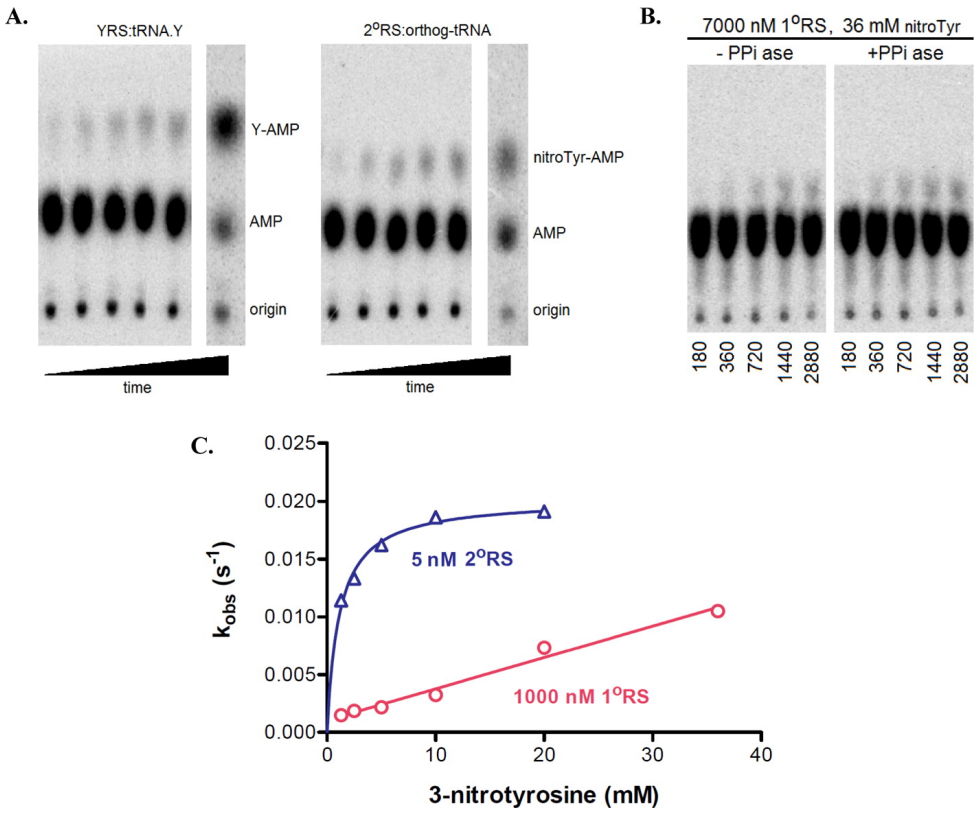

Figure 3.1. Representative *in vitro* aminoacylation reaction of Tyr- and NitroTyr-RSs. (A) Thin layer chromatograph (left) depicting results from an aminoacylation time course in which wild-type *M. jannaschii* TyrRS attaches tyrosine (Y) to a wild-type *M. jannaschii* $tRNA^{Tyr}$ transcript. The lane at the right shows plateau aminoacylation levels after 20 min, performed under conditions. Thin layer chromatograph (right) depicting results from an aminoacylation time course in which the second-generation nitroTyrRS attaches nitroTyr to orthog-tRNA (see the text for nomenclature). The lane at the right shows plateau aminoacylation levels after 20 min. Plateau levels are as follows: wild-type TyrRS:tRNATyr, 66%; wild-type TyrRS:orthog-tRNA, 50% (data not shown); second-generation nitroTyrRS:tRNATyr, 62% (data not shown); second-generation nitroTyrRS:tRNA-orthog, 45%. (B) Aminoacylation time courses for the first-generation enzyme at the aaRS and nitroTyr concentrations noted. The tRNA concentration was 5 nM. (C) Plot of the apparent rate constant k_{obs} for reactions of the first- and second-generation nitroTyrRS enzymes as a function of nitroTyr concentration. These experiments were conducted using wild-type

$tRNA^{Tyr}$. Note that the concentration of the first-generation enzyme is 200-fold greater than that of the second-generation enzyme. Only one of two replicates is shown for each enzyme.

Steady-state kinetics were then performed to determine k_{cat}, K_m(tRNA), and K_m(Tyr) (Table 3.2). The k_{cat} of 1.0 s^{-1} and the K_m(tRNA) of 1.4 μM indicate an efficiently performing cognate pair, suggesting that post-transcriptional modifications in the tRNA are unlikely to have strong effects on aminoacylation. Studies of bacterial tyrosylation also showed that modified nucleotides do not affect the kinetic efficiency in that system [195]. A K_m(Tyr) of 9.1 μM is very similar to the magnitude of the tyrosine equilibrium binding constant for bacterial TyrRS [196].

Table 3.2. Kinetic constants of TyrRS enzymes

	TyrRS:Tyr[a]				nitroTyrRS:nitroTyr			
tRNA	k_{cat} (s^{-1})	$K_{M,tRNA}$ (μM)	$k_{cat}/K_{M,tRNA}$ (s^{-1} μM^{-1})	$K_{M,aa}$ (μM)	k_{cat} (s^{-1})	$K_{M,tRNA}$ (μM)	$k_{cat}/K_{M,tRNA}$ (s^{-1} μM^{-1})	$K_{M,aa}$ (mM)
WT	1.0 ± 0.2	1.4 ± 0.1	0.7 ± 0.05	9.1 ± 0.5	0.26 ± 0.03	1.14 ± 0.13	0.23 ± 0.004	9.6 ± 6.1
G34C	0.05 ± 0.01	3.0 ± 1.3	0.02 ± 0.005	0.31 ± 0.01	<0.08[b]	>16	0.007 ± 0.001	2.3 ± 0.2
G34C/G37A	0.13 ± 0.04	4.8 ± 1.6	0.018 ± 0.009	0.33 ± 0.18	<0.2[b]	>16	0.01 ± 0.001	1.4 ± 0.2
orthog	0.52 ± 0.04	21.2 ± 2.0	0.02 ± 0.001	0.72 ± 0.04	0.31 ± 0.03	30.8 ± 3.6	0.01 ± 0.0003	0.56 ± 0.02

[a]Sample Michaelis–Menten plots for each reaction are provided in Figure S1. [b]Only the upper bound for k_{cat} is indicated, because tRNA could not be saturated (see the text).

The k_{cat} that we measure is 20-fold higher than previously reported for aminoacylation of the same unmodified *M. jannaschii* tRNATyr species (wt-tRNA), while K_m(tRNA) values are comparable [197]. The discrepancy is likely due to the use of just 11 μM tyrosine in the prior assays for K_m(tRNA) determination, a value almost identical to K_m(Tyr) and thus affording only partial enzyme saturation (Table 3.2). The prior study also used 10 mM ATP [197], a level that we have found to be inhibitory (data not shown; high concentrations of ATP may inhibit by competing for binding with the 3′-terminal A76 of tRNA) [198]. These finding emphasize the value of monitoring aminoacylation through the use of 32P-labeled tRNA. We used 48 μM tyrosine in the K_m(tRNA) determinations, 5-fold above K_m(Tyr) (Table 3.2). The ATP concentration of 2.5 mM was also confirmed to be saturating (data not shown). These measurements show that *M. jannaschii* TyrRS is an efficient aaRS and does not exhibit a slow k_{cat} as previously reported.

Correlating *In Vivo* Performance with Kinetic Measurements

We next compared the in vivo expression yields of nitroTyr-sfGFP by first- and second-generation nitroTyrRS enzymes, as a function of the concentration of nitroTyr included in the autoinduction expression medium (Figure 3.2). The first- and second-generation enzymes used in these experiments were the best performers among the isolates from those rounds of directed evolution [19, 22]. The crystal structure of the best-performing second-generation enyme is also available in apo and nitroTyr-bound states [19]. As previously demonstrated, the second-generation nitroTyrRS is substantially more efficient than the first-generation enzyme at all nitroTyr concentrations tested. This enzyme exhibits saturation at a nitroTyr concentration of approximately 0.2 mM, while the first-generation variant produces a weakly increasing level of nitroTyr-sfGFP up to the highest nitroTyr concentration tested (Figure 3.2). For reference, native sfGFP without an amber stop codon expresses at levels in autoinduction medium 5-fold higher than that of the second-generation nitroTyr aaRS under identical conditions supplemented with 1 mM nitroTyr [19].

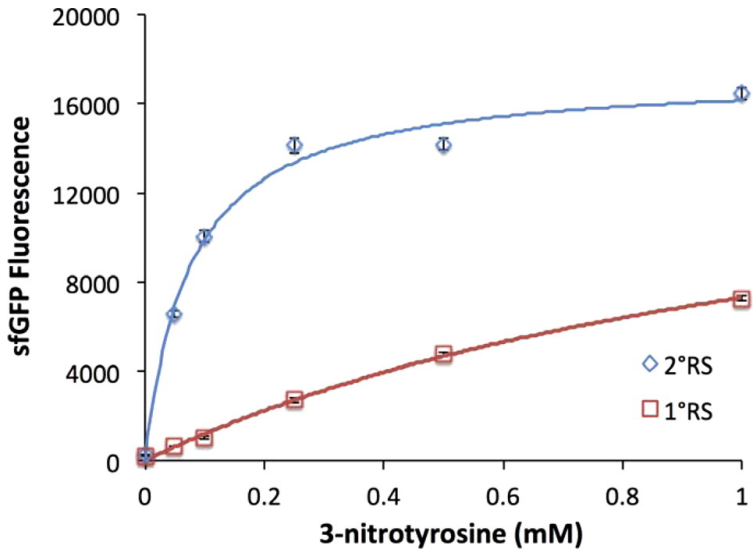

Figure 3.2. *In vivo* function of NitroTyr-RSs in *E. coli.*
In vivo fluorescent measurement of nitroTyr-150-sfGFP expression as a function of nitroTyr concentration in the medium using the first-generation (red) and second-generation (blue) nitroTyrRS enzymes. Values shown represent the mean of two experiments, and the error bars shown indicate the standard deviation of each measurement.

The determination of sfGFP yield *in vivo* at differing nitroTyr concentrations allows the possibility of a quantitative correlation with the catalytic performance of the enzymes *in vitro*. To examine this, we expressed and purified both first- and second-generation nitroTyrRS variants from *E. coli* and characterized aminoacylation by steady-state kinetics, as described above. The first-generation enzyme exhibits very weak nitrotyrosylation of wt-tRNA, with plateau levels of aminoacylated product much too low for determination of kinetic parameters (Figure 3.1). In contrast, the second-generation nitroTyrRS exhibits robust catalytic performance, with its K_m(tRNA) being identical to that of wild-type TyrRS and its k_{cat} diminished by only ~4-fold (Table 3.2). Comparative measurements under identical single-turnover conditions suggest that the first-generation enzyme performs approximately 1000-fold less efficiently, although precise estimates are difficult because we do not observe saturation for nitroTyr in that case (data not shown). These findings show that the much higher levels of nitroTyr incorporation by the second-generation enzyme are substantially based on direct catalytic improvement of the evolved nitroTyrRS.

Further measurements with the second-generation enzyme showed that a K_m(nitroTyr) of 10 mM is ~1000-fold higher than the K_m(Tyr) in WT-TyrRS (Table 3.2). However, the X-ray structure of the enzyme:nitroTyr complex offers no indication of weak binding, revealing instead a specific set of interactions with the nitroTyr substrate, including stacking interactions with the ring and several hydrogen bonds with the exocyclic nitro group [19]. Consistent with the high measured K_m value, nitroTyr was not observed in electron density maps when included at a concentration of 2 mM in crystallization drops but appeared only when the crystals were later soaked in solutions containing this ligand at a concentration of 100 mM [19]. A possible explanation for this apparent discrepancy is that the crystal structure was determined without tRNA, while K_m(nitroTyr) reflects the performance in its presence (see Discussion).

Next, we repeated kinetic measurements for tyrosylation by WT-TyrRS and nitrotyrosylation by the second-generation enzyme, this time using an *M. jannaschii* $tRNA^{Tyr}$ transcript corresponding to the "orthogonalized" species present in the cells

during both the directed evolution experiments and the measurements of sfGFP production [19]. This permits a more precise correlation of *in vivo* performance with *in vitro* aminoacylation efficiency. The orthogonalized tRNA (orthog-tRNA) was isolated using genetic selections when the *M. jannaschii* TyrRS:tRNA^{Tyr} system was first developed [18], and to the best of our knowledge, this particular species has been used in all subsequent directed evolution experiments with the *M. jannaschii* TyrRS scaffold. Orthog-tRNA possesses six nucleotide substitutions, comprising four replacements in the D and variable loop portions of the tertiary core (C17A/U17aG/U20G/U47G), and two replacements in the anticodon loop at the wobble position (G34C, as required to create the amber suppressor) and position 37 (G37A, located immediately 3′ to the anticodon sequence) (Figure 3.3).

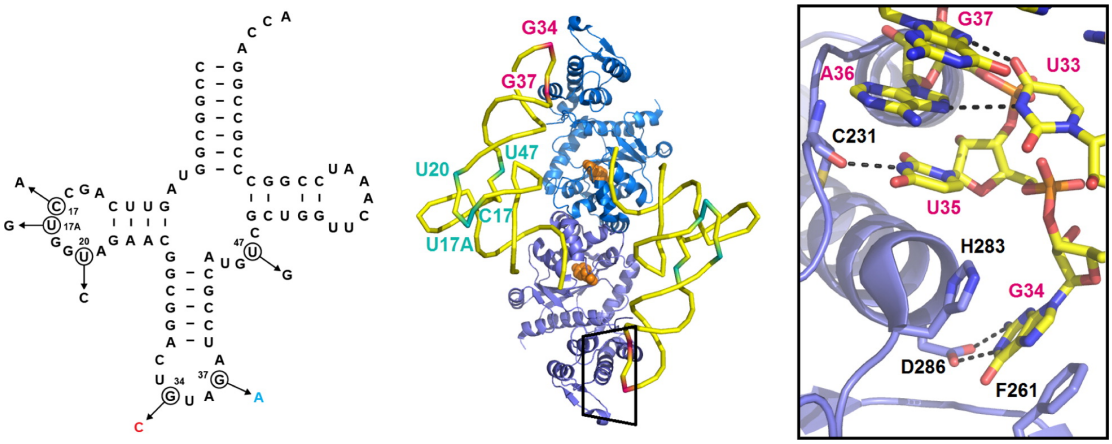

Figure 3.3. Structures of *M. jannaschii* tRNA^{Tyr} and TyrRS.
Cloverleaf depiction (left) of the sequence of wild-type *M. jannaschii* tRNA^{Tyr}. The six positions at which the tRNA sequence was altered to generate orthog-tRNA are circled, with the replaced nucleotide indicated. Crystal structure (middle) of *M. jannaschii* TyrRS bound to tRNA^{Tyr} and L-tyrosine (Protein Data Bank entry 1J1U). The two subunits of the dimeric enzyme are colored blue and purple. The tRNA anticodon is boxed at the bottom. Positions corresponding to substitutions in tRNA-orthog are indicated in one of the tRNAs. Detail (right) from the crystal structure of the TyrRS:tRNA^{Tyr}:L-tyrosine complex, showing hydrogen bonding and other contacts between TyrRS and the tRNA anticodon loop. Hydrogen bonds are depicted as dashed lines.

Orthog-tRNA elicits responses similar to those of a substrate for TyrRS and nitroTyrRS. k_{cat} is unchanged for nitroTyrRS and decreased ~2-fold for wild-type TyrRS, but K_m(tRNA) is very substantially elevated for both enzymes (by 16-fold for TyrRS and 27-fold for nitroTyrRS) (Table 3.2). Thus, orthog-tRNA exhibits reduced complementarity for both TyrRS and nitroTyrRS compared to that of wild-type $tRNA^{Tyr}$. Remarkably, both enzymes also show quantitatively similar decreases in K_m(amino acid) (13-fold for wild-type TyrRS with tyrosine and 17-fold for nitroTyrRS with nitroTyr) (Table 3.2), suggesting substantially improved complementarity with this substrate. Because the six substitutions in orthog-tRNA are located 15–40 Å from the amino acid binding pocket on each protein, these observations strongly suggest that long-distance intermolecular communication between the tRNA and amino acid binding sites is a key mechanistic feature of both enzymes. Because tRNA K_m values are so high with orthog-tRNA, saturation for tRNA could not be maintained in the experiments measuring K_m (amino acid). Thus, amino acid K_m values should be regarded as apparent values in these cases (Table 3.2).

Because nitroTyr-sfGFP synthesis *in vivo* depends on the function of nitroTyrRS, the nitroTyr concentration dependence of nitroTyr-sfGFP formation could bear some relation to the apparent K_m value for nitroTyr exhibited by the evolved enzyme (Figure 3.2). In fact, the nitroTyr concentration giving half-maximal nitroTyr-sfGFP production is slightly less than 0.1 mM, ~6-fold below the relevant apparent Km of 0.56 mM (Table 3.2). The quantitative relationship between these parameters will, of course, be influenced by differing ATP, tRNA, and ncAA concentrations in the two settings, and probably by other factors, as well (see Discussion).

Dissecting the Orthogonalized *M. jannaschii* $tRNA^{Tyr}$

The *M. jannaschii* $tRNA^{Tyr}$ identity is specified by the C1-G72 base pair in the acceptor stem, the single-stranded A73 nucleotide located adjacent to the 3′-CCA sequence, and the full anticodon triplet G34-U35-A36 (Figure 3.2) [197]. Introduction of these six identity nucleotides into a noncognate tRNA framework

conferred full tyrosylation capacity [197], showing that no other nucleotides are essential. Among these six nucleotides in wild-type $tRNA^{Tyr}$, the only one mutated in orthog-tRNA is G34, which must be substituted with C34 to create the amber suppressor. The necessity of this mutation at an identity position might be expected to diminish the quality of the *M. jannaschii* TyrRS:$tRNA^{Tyr}$ complex as an orthogonal pair for ncAA incorporation at amber codons. However, the kinetic measurements described above show that, while K_m(tRNA) is significantly elevated for the G34C tRNA with both TyrRS and nitroTyrRS, K_m(Tyr) and K_m(nitroTyr) are lowered by nearly the same magnitude in the respective enzymes (Table 3.2). Thus, the direct interaction of TyrRS with the $tRNA^{Tyr}$ anticodon, by which the G34 identity is expressed (Figure 3.3), may not be entirely detrimental (see Discussion).

The crystal structure of *M. jannaschii* TyrRS bound to $tRNA^{Tyr}$ and L-tyrosine shows that the core region of the tRNA does not interact with the enzyme, suggesting that the four orthog-tRNA mutations in the D and variable loops may not provide positive determinants for TyrRS aminoacylation. However, the base of G37 stacks between G38 and anticodon nucleotide U36 and makes steric contacts with a nearby protein element (Figure 3.3) [199]. While G37 was not identified as an identity nucleotide, these interactions and the proximity of the G34C and G37A substitutions in orthog-tRNA nonetheless suggest that the nucleotide at position 37 could influence tyrosylation and/or nitrotyrosylation efficiencies. To evaluate the importance of the replaced nucleotides in orthog-tRNA, we generated the G34C and G34C/G37A mutants in wt-tRNA and examined their abilities to efficiently synthesize nitroTyr-sfGFP in vivo. For G34C, the yields of nitroTyr-sfGFP are lower than for the fully orthogonalized suppressor at all nitroTyr concentrations tested (Figure 3.4A). However, G34C/G37A is significantly more efficient than orthog-tRNA, particularly at low concentrations of nitroTyr. Hence, for nitroTyr incorporation by the second-generation enzyme, the four additional mutations in the D and variable loops are deleterious to nitroTyr-sfGFP synthesis *in vivo*.

We next examined how G34C and G34C/G37A $tRNA^{Tyr}$ compare to wt-tRNA and orthog-tRNA as substrates for *in vitro* aminoacylation. As expected given the role of G34 as an identity determinant, G34C $tRNA^{Tyr}$ exhibits a 20-fold reduced k_{cat} with

TyrRS, while K_m(tRNA) is elevated by 2-fold (Table 3.2). Remarkably, however, K_m(Tyr) is sharply reduced by 30-fold. This large decrease in the amino acid K_m mirrors similar findings with orthog-tRNA and pinpoints the wobble base interactions as a key trigger for long-distance intramolecular communication to the amino acid binding pocket some 40 Å distant. Further, the small effect on K_m(tRNA) with this singly substituted species suggests that the altered wobble base contacts are not primarily responsible for the substantially weakened orthog-tRNA complementarity with TyrRS (Table 3.2). Because the G34C/G37A double mutant exhibits kinetic parameters with TyrRS that are very similar to those with G34C alone, it appears that the four substitutions in the D and variable loops are responsible for most of the weakened tRNA complementarity. However, k_{cat} for aminoacylation of orthog-tRNA by TyrRS is substantially higher than for G34C or G34C/G37A, so the four tRNA core region substitutions in orthog-tRNA do rescue this kinetic parameter (Table 3.2).

Although nitroTyrRS differs from TyrRS at just five residues in the amino acid substrate binding pocket, it does not respond similarly to substitutions at the anticodon loop wobble position. Most notably, K_m(nitroTyr) is decreased by only ~4-fold with G34C tRNA, substantially less than the 17-fold decrease in K_m(nitroTyr) observed with orthog-tRNA, and well below the 30-fold reduction in K_m(Tyr) by TyrRS with G34C tRNA (Table 3.2). Another very significant difference between TyrRS and nitroTyrRS is that K_m(tRNA) for the G34C tRNA with nitroTyrRS is greatly elevated: saturation could not be observed even at tRNA concentrations of >50 μM. This contrasts with the modest 2-fold increase in K_m(tRNA) for the G34C species with TyrRS. These distinctions in the enzymes' response to a single nucleotide substitution in the anticodon highlight the very strong interplay between amino acid and tRNA binding in this system, a characteristic that should influence the design of further directed evolution studies (see Discussion).

The kinetic measurements do not reveal large differences in steady-state nitrotyrosylation parameters between G34C and G34C/G37A tRNAs, although stronger effects may be present that are not revealed because of the technical limitation associated with weak tRNA binding. However, even without a precise determination, it is clear that k_{cat} for G34C/G37A is larger than for G34C, while

K_m(nitroTyr) is ~2-fold lower. These differences may explain the 5-fold lower ncAA concentration needed to reach half-maximal nitroTyr-GFP expression for G34C/G37A compared with that for G34C in vivo. The concentration of nitroTyr needed to reach half-maximal expression of nitroTyr-GFP is 3-fold lower for G34C/G37A than for the orthog-tRNA, although the basis for improved nitroTyr-sfGFP synthesis is not apparent from these kinetic measurements (see Figure 3.4A and Discussion).

Absolute Fidelity and Orthogonality of $tRNA^{Tyr}$ Suppressors *In Vivo*

To assess whether the variations among orthog-tRNA, G34C, and G34C/G37A affect the ability of nitroTyrRS to discriminate nitroTyr from other amino acids, we measured the sfGFP yields in vivo for each of these suppressors, both with and without the addition of nitroTyr to the culture medium. Because nitroTyr is not present in *E. coli*, any observed fluorescence from sfGFP must arise from aminoacylation of other amino acids by nitroTyrRS. The data reveal that all three strains permit a low level of sfGFP synthesis in the absence of nitroTyr, but the G34C and G34C/G37A suppressors are only 25% less selective for amino acids than orthog-tRNA (Figure 3.4B).

Next, we conducted similar experiments to measure yields of sfGFP with each of the three tRNAs, in the presence and absence of nitroTyrRS. All of these experiments were conducted in the absence of nitroTyr. Synthesis of sfGFP in the absence of nitroTyrRS indicates that readthrough of the amber codon occurs by misacylation of a $tRNA^{Tyr}$ suppressor with a canonical amino acid, by another aaRS in the cell. This measures the extent to which the engineered nitroTyrRS:$tRNA^{Tyr}$ pair is orthogonal to the endogenous aaRS:tRNA systems. Here we find that G34C $tRNA^{Tyr}$ exhibits a 4-fold increase in the level of misacylation compared to that of orthog-tRNA in the absence of the aaRS, but only a 2-fold increase when the aaRS is present (Figure 3.4C). However, both G34C/G37A and orthog-tRNA fully alleviate this effect, demonstrating that the four nucleotide substitutions in the D and variable loops of orthog-tRNA are not required to maintain orthogonality.

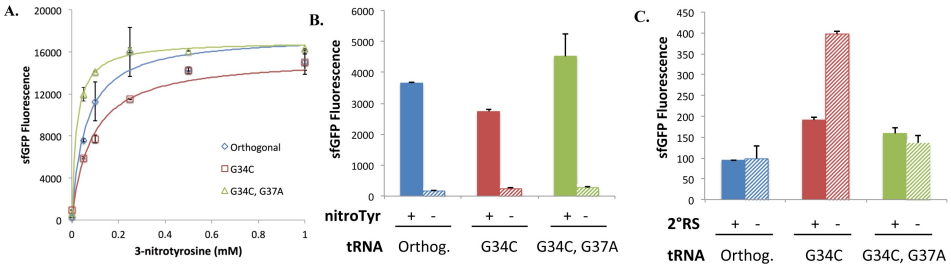

Figure 3.4. Effects of orthogonalized-tRNA^{Tyr} mutations in vivo.
(A) *In vivo* fluorescent measurement of nitroTyr-150-sfGFP expression using the second-generation nitroTyrRS with tRNA-orthog (blue), G34C tRNA (red), and G34C/G37A tRNA (green), as a function of nitroTyr concentration. (B) *In vivo* fluorescent measurement of nitroTyr-150-sfGFP expression for the respective suppressor tRNAs in the presence and absence of nitroTyr, in the presence of the second-generation nitroTyrRS. (C) *In vivo* fluorescent measurement of nitroTyr-150-sfGFP expression for the respective suppressor tRNAs in the presence and absence of the second-generation nitroTyrRS. Values shown represent the mean of two experiments, and the error bars shown indicate the standard deviation of each measurement.

Effect of Orthogonalized *M. jannaschii* tRNA^{Tyr} on Other ncAA tRNA/RS Pairs

To assess whether the superior performance of G34C/G37A tRNA for incorporation of nitroTyr can also be applied to the incorporation of other ncAAs, we measured ncAA-sfGFP synthesis in the presence of four other evolved *M. jannaschii* TyrRS enzymes. These aaRS enzymes were selected for 4-benzoyl-L-phenylalanine (Bpa), 4-(trifluoromethyl)-L-phenylalanine (tfmF), 4-cyano-L-phenylalanine (pCNF), and acridon-2-ylalanine (Acd) [19-20, 200]. To evaluate the pCNF-RS, we used 4-azido-L-phenylalanine because it is an extensively used cross-linker. In each case, we compared the performance of G34C/G37A with orthog-tRNA, in the presence and absence of 0.25 mM ncAA in the culture medium (Figure 3.5). This was chosen as the lowest concentration that can maximize incorporation of nitroTyr with G34C/G37A tRNA (Figure 3.4A). We find that evolved aaRSs specific for Bpa, tfmF, and pCNF each incorporate the ncAA more efficiently with G34C/G37A, with a particularly large improvement (340%) observed for Bpa (Figure 3.5). In contrast, the evolved AcdRS generated more than twice as much ncAA-sfGFP when paired with orthog-tRNA rather than G34C/G37A. Therefore, whether and the extent to which the G34C/G37A tRNA performs better than orthog-tRNA depend on which ncAA is incorporated. This provides yet another demonstration of the importance of

intramolecular signaling between the amino acid and tRNA binding sites of evolved TyrRS enzymes. Although the effects are weak, experiments in the absence of added ncAA suggest that the fidelity of amino acid incorporation is slightly compromised when G34C/G37A tRNA is substituted for orthog-tRNA, for all five ncAAs tested (Figure 3.5).

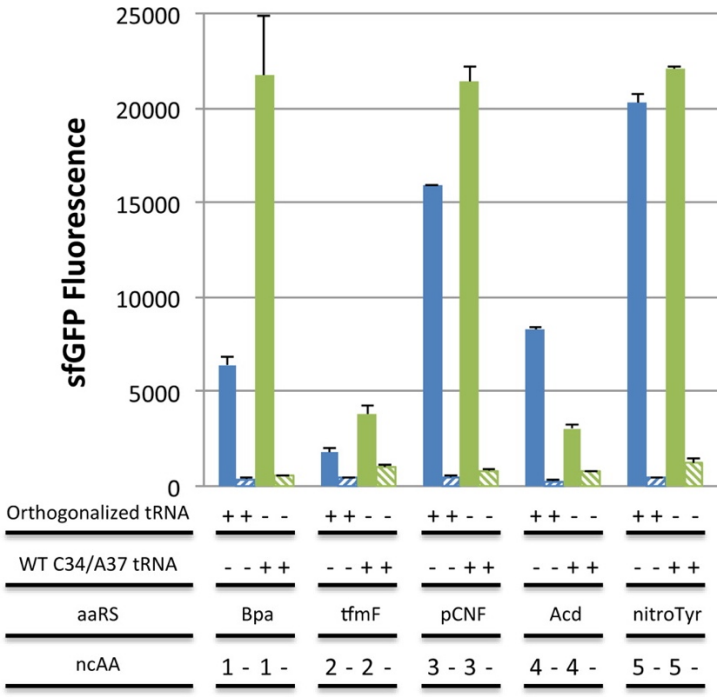

Figure 3.5 Effects of orthgonalized-tRNA^{Tyr} mutations on several different evolved ncAA-RSs *in vivo*.

In vivo fluorescent measurement of nitroTyr-150-sfGFP expression, using five ncAAs together with the five distinct aaRS obtained from prior directed evolution experiments. Each enzyme/ncAA pair is tested with orthog-tRNA and G34C/G37A tRNA. Each experiment was conducted in the presence and absence of the relevant ncAA to assess ncAA-GFP efficiency and fidelity. See Figure S3.2 for ncAA structures. Values shown represent the mean of two experiments, and the error bars shown indicate the standard deviation of each measurement.

Discussion

Our findings show that the efficiency of ncAA incorporation by evolved *M. jannaschii* TyrRS enzymes depends on nucleotide determinants in the cognate tRNA^{Tyr} suppressor. Four of five tRNA nucleotides previously identified by directed evolution are deleterious to the efficiency of ncAA-sfGFP production in *E. coli*, while the G37A substitution alone, when paired with the wobble mutation G34C,

substantially improves incorporation for four of the five tested ncAAs (Figure 3.5). We confirm the earlier conclusion that the single mutant G34C $tRNA^{Tyr}$ suppressor is not orthogonal in *E. coli* (Figure 3.4C) [18]. However, our findings additionally demonstrate that tRNAs selected from large libraries for purposes of improving orthogonality may possess other nucleotide substitutions that are deleterious for efficient protein synthesis. Clearly, negative tRNA determinants that block noncognate aaRS interactions *in vivo* might also affect the catalytic efficiency of the desired cognate reaction. As we have shown here, systematic testing of mutations found in evolved tRNAs can distinguish which new substitutions are useful and which are not. We expect that the new G34C/G37A *M. jannaschii* tRNATyr should improve ncAA incorporation for many, although not all, of the recombinant proteins that have been so far generated with orthog-tRNA in this system.

Steady-state measurements of aminoacylation kinetics are useful in characterizing evolved, orthogonal aaRS:tRNA pairs, as previously demonstrated for the PylRS system [167, 175]. Here, these measurements clearly show that a major improvement in the second-generation nitroTyrRS derives from improved aminoacylation efficiency (Figure 3.1). Kinetics also helps to pinpoint differences in catalytic function between wild-type and orthogonal components, to identify where further improvements might be made. The most remarkable finding is that, while Km for orthog-tRNA is elevated for both TyrRS and nitroTyrRS, Km for amino acid is sharply decreased by ~15-fold in both enzymes (Table 3.2). This demonstrates sizable structural coupling between amino acid and tRNA recognition in M. jannaschii TyrRS, of a magnitude substantially greater than that previously characterized in the well-studied bacterial glutaminyl-tRNA synthetase (GlnRS) system [201]. The unexpected improvement in amino acid binding engendered by tRNA mutation suggests that the enzyme–tRNA interface has evolved to maintain weak amino acid binding by the protein component of the complex.

This very weak amino acid binding could be an optimization reached on the basis of intracellular concentrations of all amino acids, tRNAs, and aaRS in *M. jannaschii*, as required to maintain the fidelity of protein synthesis, and perhaps influenced by the extreme environment that is inhabited by this hyperthermophilic

anaerobe. The interrelatedness of tRNA and amino acid binding also has implications for further design of TyrRS and $tRNA^{Tyr}$ to improve performance *in vivo*. It is important to note that no selections have yet been performed using the optimized G34C/G37A $tRNA^{Tyr}$; such experiments could yield novel and better-performing nitroTyrRS variants, and as mentioned, this new suppressor should also be of broad utility for other ncAAs. We also note that the major catalytic detriment in the system remains the very high K_m for tRNA. Thus, selections incorporating enzyme libraries that target the tRNA interface in regions spanning the anticodon to the active site could be fruitful, while maintaining the already evolved amino acid binding sites. This may build on the work of Guo and colleagues, who were able to improve incorporation of some ncAAs by *M. janaschii* TyrRS by manipulating protein residues at the anticodon interface of orthog-tRNA [16, 174]. It might also be possible to identify constellations of tRNA core region nucleotides that, rather than being detrimental as in orthog-tRNA, might instead improve tRNA binding through indirect modulation of the sugar–phosphate backbone conformation at the inner elbow portion of the tRNA L shape. Rationally engineered variants of *E. coli* GlnRS that incorporate noncognate glutamate manifested improved function when conserved $tRNA^{Glu}$ core region nucleotides were substituted into the GlnRS:tRNA ribonucleoprotein [202].

Our data also illustrate how measurement of aminoacylation kinetics is necessary but certainly not sufficient for a thorough understanding of how engineered orthogonal aaRS:tRNA complexes function in the cell. K_m(nitroTyr) is not a quantitative proxy for the efficiency of nitroTyr uptake and incorporation *in vivo* (Figure 3.2 and Table 3.1); the discrepancy between this parameter and the concentration of nitroTyr giving half-saturation may reflect other factors such as limitations in cellular uptake of nitroTyr or downstream aspects of protein synthesis. Characterization of EF-Tu binding kinetics and ribosomal performance may thus also be helpful in inspiring further improvement of TyrRS-based orthogonal systems. Ultimately, sophisticated applications in synthetic biology demand that the catalytic parameters of evolved aaRS should fully match those of endogenous aaRS in the host organism with respect to k_{cat}, K_m(tRNA), and K_m(amino acid). Thus, the 100-fold

lower k_{cat} of *Methanosarcina barkeri* PylRS compared to that of TyrRS [175], while not deleterious in the host cell due to the very small number of pyrrolysine codons, may be a disadvantage if the PylRS system is ultimately to provide a scaffold for extensive incorporation of ncAAs in genomically recoded microorganisms with alternate genetic codes [164]. In contrast, the perceived disadvantage of TyrRS in directly recognizing the anticodon, while still posing a challenge as shown by the high K_m(tRNA), is nonetheless mitigated by our findings that K_m(amino acid) is improved by tRNA mutation while k_{cat} is only modestly decreased (Table 3.2). Efforts in the synthetic biology of protein translation will doubtless also be promoted by the development of additional efficient aaRS scaffolds for ncAA incorporation [16, 78].

Acknowledgments

Research reported in this manuscript was funded by National Institutes of Health Grant RGM114653A (to R.A.M.).

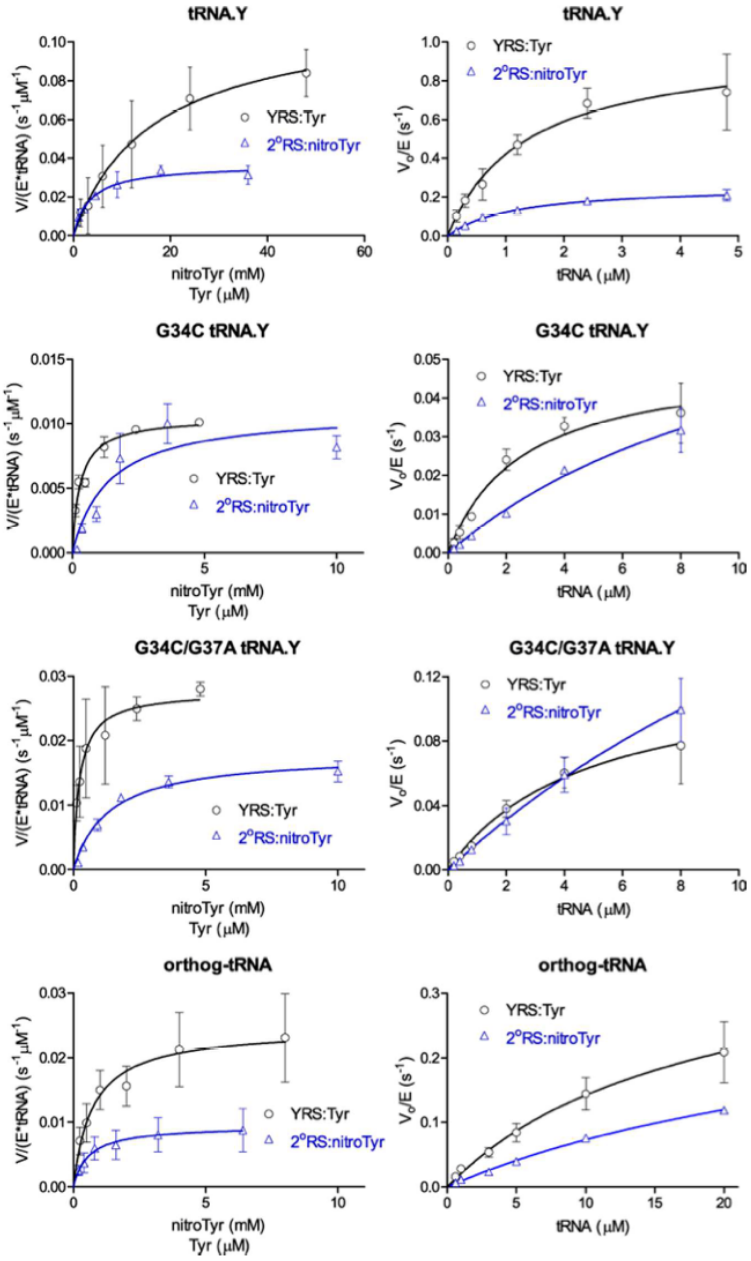

Figure S3.1. Michaelis-Menten plots depicting the dependence of aminoacyl-tRNA formation on either amino acid or tRNA concentration.

Ordinates are scaled by either the enzyme concentration or the product of enzyme and tRNA concentrations, enabling better comparison of the velocities for TyrRS (black circles) and nitroTyrRS (blue triangles) as a function of substrate concentration. Data points represent the mean values for all replicates, while error bars reflect the standard deviation. To generate values for Table 3.2 in the main text, data from each experimental replicate, shown pooled here, were fit individually to the Michaelis Menten function and subsequently averaged.

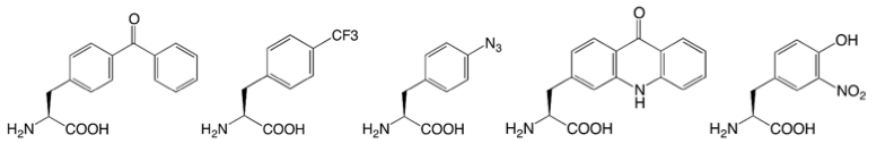

Figure S3.2. Structures of non-canonical amino acids tested with mutant tRNAs.

Chapter 4

Tyrosine Nitration on Calmodulin Regulates Calcium Sensing and Response

Joseph J. Porter, Hyo Sang Jang, Mohammad Mahfuzul Haque, Dennis J. Stuehr, and Ryan A. Mehl

Formatted for Publication in eLife

Abstract

The generation of reactive oxygen species called oxidative stress, results in a bewildering array of modifications to biological macromolecules including DNA, lipids, and proteins. The formation of 3-nitrotyrosine (nitroTyr) in proteins serves as the main biomarker for oxidative stress and is present in over 50 disease pathologies. In response to oxidative stress the calcium sensing protein calmodulin (CaM) has been shown to have both of its tyrosines nitrated in vivo. We applied genetic code expansion to site-specifically incorporate nitroTyr into CaM and assessed the functional alterations to calcium binding, and regulatory effects on binding and activation of a major target protein, endothelial nitric oxide synthase (eNOS). We found that the ability of nitroTyr-CaM to bind calcium alone is unaltered but when in the presence of eNOS nitroTyr-CaM retains affinity for eNOS in the absence of calcium signal. *In vitro* eNOS assays with CaM nitrated at tyrosine 99 results in less nitric oxide production and more eNOS decoupling than wild type CaM. In contrast, CaM nitrated at tyrosine 138 produces more nitric oxide and does it more efficiently than wild type CaM. These results indicate the importance of CaM tyrosine nitration as regulatory mechanism for target eNOS activity.

Introduction

Critical Calcium Regulation

Fundamental biological processes like cell proliferation, gene transcription, cell death, exocytosis, and metabolism are predicated on the tight regulation of cytosolic calcium (Ca^{2+}) concentration [25]. As a direct consequence of this, loss of Ca^{2+} regulation is implicated in a variety of neurodegenerative and debilitating diseases including amyotrophic lateral sclerosis, Alzheimer's disease, Parkinson's disease, cancer, diabetes, and cardiovascular disease [203-206]. At the heart of Ca^{2+} regulation is the Ca^{2+} sensing protein, calmodulin (CaM), which transduces intracellular Ca^{2+} signals into biological responses. CaM accomplishes this by serving as a Ca^{2+} binding regulatory subunit of a wide array of enzymes, structural proteins, and membrane transporters. Cellular CaM fluctuates between its Ca^{2+} bound form (Ca^{2+}-CaM) and Ca^{2+} and target protein bound forms (Ca^{2+}-CaM-target) depending on intracellular Ca^{2+} levels and target affinity. Cytosolic Ca^{2+} levels are tightly

regulated between ~0.1 μM under resting conditions to ~10 μM after stimulation [207]. CaM is an abundant protein with intracellular concentrations up to 10 μM, however due to the concentration of its many target proteins, CaM is the limiting agent in Ca^{2+} sensing [208-209]. Since CaM has many distinct target proteins, CaM post-translational modifications (PTMs) serve as an additional level of control over CaM activity necessary for the intracellular Ca^{2+} regulatory balance. These modifications range from phosphorylation of serine, threonine, and tyrosine to trimethylation of lysine and proteolytic cleavage [35, 210]. Tyrosine phosphorylation of CaM is a regulatory mechanism with the Tyr99/Tyr138 phosphorylation stoichiometries depending on the kinase involved [33]. The receptor tyrosine kinases insulin receptor and epidermal growth factor receptor along with the non-receptor kinases, Src family kinases, Janus kinase 2, and p38Syk are all capable of phosphorylating CaM. The impact of CaM phosphorylation on CaM activity is dependent both on the site of phosphorylation and CaM's associated target protein [208]. When purified, phosphoCaM-99 affinity for several different target protein binding domain peptides was tested. In general affinity was increased but the change was dependent on the target protein [34].

Abundant nitroTyr Ox-PTM on Calmodulin

CaM is susceptible to modification by reactive nitrogen and oxygen species (RNS) such as hydrogen peroxide (H_2O_2), nitric oxide ($NO^{\bullet}$), and peroxynitrite ($ONOO^-$) (Yan et al., 2006; Pacher et al., 2007; Smallwood et al., 2007). These RNS induce a variety of oxidative post-translational modifications (Ox-PTMs), but the most common are cysteine nitrosylation, methionine sulfoxidation, and tyrosine nitration [211]. Proteomic analysis on CaM has shown that these Ox-PTMs form on all of the methionine and tyrosine residues in vivo [26, 212-214]. It has been demonstrated that oxidation of methionines on CaM compromises target protein interactions and lowers target protein activity [37-38, 204, 212, 214]. While up to 30% of the cellular CaM pool is nitrated following macrophage activation on critical regulatory tyrosines residues [27], the effect of tyrosine nitration on CaM function has not been determined to date.

Critical Calmodulin Target – Nitric Oxide Synthase

Growing evidence supports that vascular misfunction and oxidative stress play a key role in cardiovascular diseases [215]. A key regulator of cardiovascular function dependent on Ca^{2+}-CaM activation is endothelial nitric oxide synthase (eNOS), a multi-domain enzyme that catalyzes the conversion of L-arginine to the biological signaling molecule nitric oxide ($NO^{\bullet}$), important for regulating vascular tone and angiogenesis. At maximal intracellular calcium levels, 25% of the Ca^{2+}-CaM pool in endothelial cells is associated with eNOS [40]. This amount of CaM bound by tight association with eNOS removes sufficient CaM from the intracellular pool to affect other target proteins as seen with the intracellular calcium regulatory channel plasma membrane Ca^{2+}-ATPase [40]. Under normal conditions eNOS transfers electrons from NADPH to oxygen and L-arginine to produce $NO^{\bullet}$, however under conditions of limiting substrate, electrons are instead shunted to oxygen resulting in the formation of the superoxide anion, a ROS involved in the formation of nitrotyrosine.

Targeting Ox-PTM with Genetic Code Expansion

To evaluate the impact of Ox-PTMs on CaM, standard site-directed mutagenesis was used to provide data on specific residues. This approach, while the best available at the time is problematic because altering amino acids to prevent Ox-PTM formation can have unknown effects at these regulatory hot-spots [26]. Genetic code expansion (GCE) provides the means to assess the effects of site-specific protein tyrosine nitration through co-translational installation of nitroTyr into the protein of interest. This methodology has been used recently to show that tyrosine nitration can cause a toxic gain-of-function for heat shock protein 90 (Hsp90) and apolipoprotein A-I (ApoAI) as well as a loss of function in manganese superoxide dismutase (MnSOD) [22-24].

Here, we use GCE to generate site-specifically modified nitroTyr-containing CaM and characterize the effect of this Ox-PTM on regulating CaM function. While we determined that nitration of CaM does not change Ca^{2+} affinity, we did find that tyrosine nitration increases the affinity of CaM for key target protein, eNOS, and

alters its ability to produce product, $NO^{\bullet}$, in a calcium-dependent manner. Based on the kinetics of the interaction between an eNOS peptide constituting the CaM binding domain, we determined that nitration at CaM-Tyr99 and Tyr138 bind eNOS more tightly than WT-CaM at subsaturating Ca^{2+} levels, and most strikingly that CaM nitrated at site 138 binds eNOS under resting physiological Ca^{2+} conditions. This constitutes a clear regulatory gain-of-function for nitroTyr-CaM as any subpopulation of CaM nitrated will activate eNOS in the absence of a Ca^{2+} signal. Moreover, when eNOS activity is monitored with nitroTyr-CaM-138 at saturating calcium levels, the efficiency and rate of $NO^{\bullet}$ production is significantly increased over that of WT-CaM. In addition, at lower calcium levels both nitroTyr-CaM species induce greater eNOS activity. In this study, we provide the first evidence that tyrosine nitration of CaM displays a regulatory gain-of-function to the Ca^{2+}-dependent activation of eNOS signaling and in so doing demonstrate that nitroTyr can serve as a regulatory PTM on proteins.

Results

CaM Tyrosine Residues are Targets for Nitration

Previous studies have indicated that nitration of CaM at tyrosine 99 is a biomarker of oxidative stress and that nitration of CaM at tyrosine 138 is subject to a denitrase activity in activated macrophages [26-27, 37]. We confirmed this result by monitoring the formation of nitroTyr-CaM in lipopolysaccharide-activated RAW 264.7 cells. Cell lysate when blotted for nitroTyr revealed significant bands at 15-17 kDa, which were also immunoreactive to anti-calmodulin antibody. These results confirm the presence of nitrated CaM in activated macrophages (Figure 4.1).

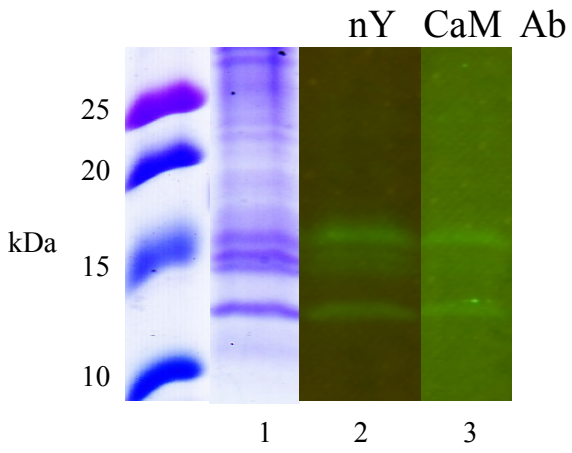

Figure 4.1. Calmodulin is nitrated *in vivo*.
Total lysate from Raw264.7 macrophages activated with LPS was separated on a 15% SDS-PAGE gel and coomassie stained (lane 1), or transferred to PVDF membrane and blotted for nitroTyr (lane 2) or CaM (lane 3). Bands co-localize on the nitroTyr and CaM blots, indicating endogenous nitration of CaM.

Production of Site-specific NitroTyr-CaM

We sought to characterize the functional effects of site-specifically nitrating the tyrosine residues on CaM because of nitroTyr-CaM abundance in cells. Genetic code expansion co-translationally installs site-specific oxidative modifications like nitroTyr and has recently been employed to effectively study oxidative stress because it generated homogeneously nitrated protein [22-23, 122, 137]. To generate homogeneous nitroTyr-CaM we co-transformed a plasmid expressing an *Mj* aminoacyl tRNA synthetase/$tRNA_{CUA}$ (aaRS/tRNA) pair engineered to efficiently incorporate nitroTyr (pDule-nitroTyr-5b) with human CaM constructs bearing an amber stop codon at either amino acid position 99 or position 138 (Figure 4.2A). NitroTyr-CaM was expressed in autoinduction medium supplemented with nitroTyr and purified using a C-terminal 6x-His tag. When nitroTyr was withheld from the media, no full-length protein was purified, indicating the fidelity of the engineered aaRS/tRNA pair for nitroTyr (Figure 4.2B). Yields of 320 and 305 mg (L of culture)$^{-1}$ were obtained for nitroTyr-CaM-99 and nitroTyr-CaM-138 respectively, compared to that of 364 mg (L of culture)$^{-1}$ for WT-CaM expression. The mass of the WT-CaM and nitroTyr-CaM species were also compared via mass spectrometry, with a mass increase of 44 Da corresponding to the addition of a single nitro group (Figure 4.3).

The presence of nitroTyr was further confirmed by anti-nitroTyr Western blot (Fig. 4.2C). These cumulative results validate the specific incorporation of nitroTyr into CaM.

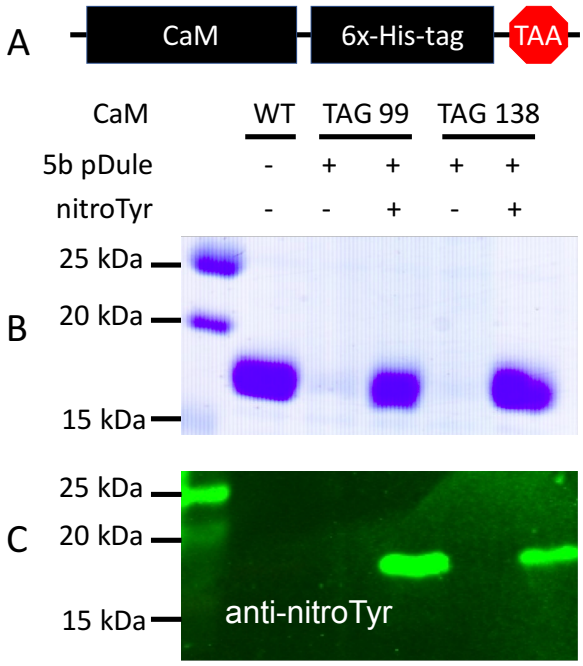

Figure 4.2. Incorporation of nitroTyr into CaM expressed in *E. coli*.
(A) CaM construct with C-terminal 6x-His-tag. (B) Expression of WT- and nitroTyr-CaM analyzed by 15% SDS-PAGE gel, both with and without pDule-nitroTyr-5b and 1 mM nitroTyr. (C) Western blot with primary antibody against nitroTyr.

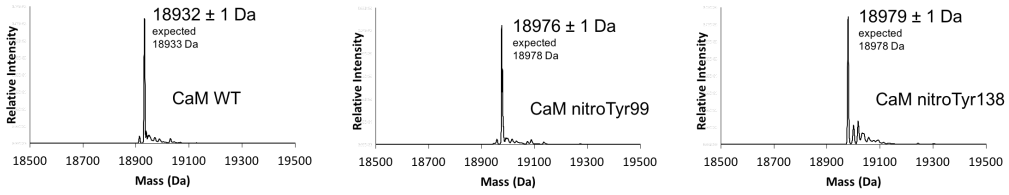

Figure 4.3. Mass spectrometric characterization of WT- and nitroTyr-CaM.
Electrospray ionization mass spectrometry confirms the quantitative incorporation of nitroTyr into CaM.

Nitration of CaM does not Impair Calcium Binding

As reversible Ca^{2+} binding is central to CaM function, it is essential to determine if CaM nitrated at tyrosine 99 or 138 shifts this equilibrium; increasing or decreasing Ca^{2+} binding affinity as compared to WT-CaM. CaM binds four Ca^{2+} leading to a structural shift and access to a central target protein binding domain, which can take place independently or in conjunction with target interactions. Isothermal titration calorimetry (ITC) provides a means to measure both the thermodynamic values associated with the Ca^{2+}-CaM interaction and the stoichiometry of this interaction. As is standard with CaM, ITC data were fit to a multiple site model (Figure 4.4) [216]. Values for the enthalpy changes (ΔH1 and ΔH2) and association constants (K_a1 and K_a2) are thus obtained for binding of Ca^{2+} to the higher affinity N-terminal lobe and lower affinity C-terminal lobe of CaM (Table 4.1) [217]. Our WT-human CaM produced in E. coli indicate affinities of K_a1 = 6.7±0.4 x 10^6 M and K_a2 = 1.1±0.1 x 10^5 M in close agreement with previous studies [218]. Affinities for both site-specific nitroTyr-CaM proteins binding to Ca^{2+} were similar for the high affinity sites (~0.2 μM) and slightly higher for the low affinity sites (~5 μM for nitroTyr-CaMs and ~10 μM for WT-CaM). The ITC results indicate that nitration of tyrosine 99 or 138 does not majorly affect CaM's affinity for Ca^{2+} binding (Table 4.1).

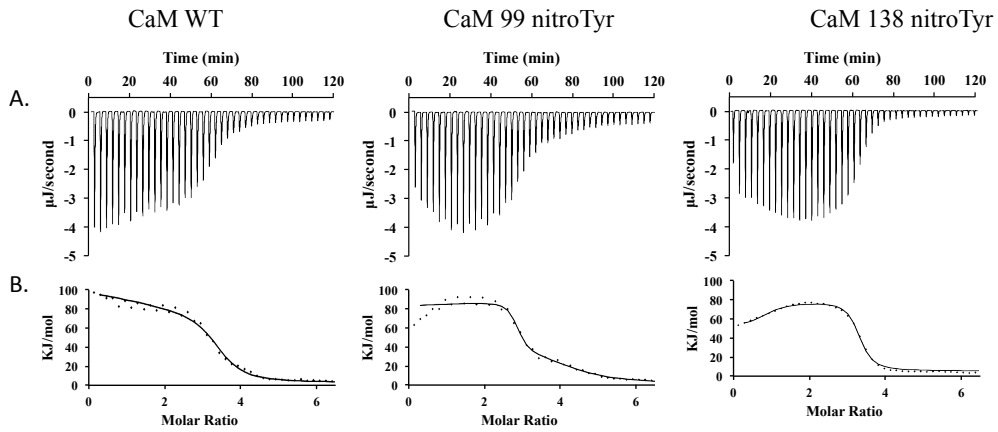

Figure 4.4. Sample ITC data for Ca^{2+} titration into WT-CaM and nitroTyr-CaMs.
(A) Representative thermograms for the interaction of $CaCl_2$ with WT- and nitroTyr-CaM. (B) Fits to binding isotherms.

Table 4.1. Thermodynamic constants derived from the calorimetry data of WT and nitroTyr CaM Ca^{2+} binding.

CaM	K_D 1 (µM)	K_D 2 (µM)	ΔH_1 (kJ mol^{-1})	ΔH_2 (kJ mol^{-1})	n_1	n_2
WT	0.15 ± 0.01	9.1 ± 0.08	22 ± 3	-4.0 ± 0.3	1.7 ± 0.2	1.8 ± 0.4
nitroTyr-99	0.22 ± 0.03	3.4 ± 0.9	3.5 ± 0.5	13 ± 2	1.8 ± 0.3	1.6 ± 0.3
nitroTyr-138	0.23 ± 0.04	5 ± 1	2.3 ± 0.5	12 ± 2	1.9 ± 0.1	1.9 ± 0.1

Dansylated CaM (dansyl-CaM) fluorescence has also been used for monitoring conformational changes in CaM as a result of interactions with Ca^{2+} [219-220]. In the presence of Ca^{2+}, the dansyl-CaMs fluorescence spectrum exhibits an enhancement and blue shift as the dansyl moiety is moved to a more hydrophobic environment [221]. To analyze the Ca^{2+} induced structural changes of the different dansyl-CaM species, we performed Ca^{2+} fluorescence titration experiments (Figure 4.4). Fitting the data (equation 4.2, materials and methods) gives the $EC_{50}(Ca^{2+})$, the free calcium concentration at which the dansyl-CaM is half saturated with Ca^{2+}, and n, the Hill cooperativity constant (Table 4.2). The $EC_{50}(Ca^{2+})$ values for all CaM forms were approximately 0.3 µM $[Ca^{2+}]_{free}$. This unaltered Ca^{2+} affinity for the WT- and nitroTyr-CaMs is in good agreement with the ITC data. The Ca^{2+} fluorescence titration did show a difference for the Hill cooperativity coefficient for the WT- as

compared to the nitroTyr-CaMs (Table 4.2). This indicates that there is slightly lower cooperativity for the nitroTyr-CaMs as compared to the WT-CaM. Taken together the Ca^{2+} ITC and fluorescence titration data confirm that nitration of tyrosine on CaM do not change its affinity for Ca^{2+}.

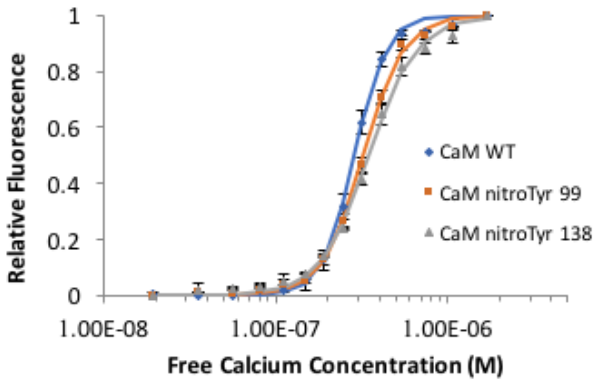

Figure 4.4. Dansyl-CaM fluorescence following titration with Ca^{2+}.
Ca^{2+} dependency of dansyl-CaM (WT, nitroTyr-99, and nitroTyr-138) fluorescence. The normalized fluorescence is shown for CaM under assay conditions described in Materials and Methods.

Table 4.2. Fit data from calcium titration of dansyl WT and nitroTyr-CaMs.

CaM	$EC(50)_{Ca2+}$ (μM)	Hill Coefficient
WT	0.3 ± 0.1	4.6 ± 0.1
nitroTyr-99	0.3 ± 0.1	3.7 ± 0.3
nitroTyr-138	0.3 ± 0.1	3.0 ± 0.3

NitroTyr-CaM Exhibits a Gain-of-Function Interaction with Target Protein eNOS

To determine if nitration of CaM changed its Ca^{2+}-dependent ability to bind target protein we employed the use of biolayer interferometry (BLI). This method allows for uniform attachment of a target protein-binding region to a BLI optical biosensor tip and measurement of CaM binding in different buffered concentrations of Ca^{2+}. To determine if CaM nitration alters its affinity for eNOS we used the synthesized 20 amino acid peptide CaM binding domain of eNOS with a C-terminal PEG-biotin to aid in solubility and surface attachment. BLI streptavidin biosensor tips were loaded with three different concentrations of biotin-eNOS peptide [222].

Biosensors with an immobilized eNOS peptide were then moved into a buffer containing either WT- or nitroTyr-CaM and varying concentrations of Ca^{2+} while the instrument monitors the CaM association, then moved to an analyte (CaM) free buffer to monitor dissociation. A Ca^{2+} buffer composed of a mixture of Ca^{2+} solution and Ca^{2+}-EGTA solution (see materials and methods) was used to precisely control a range of $[Ca^{2+}]_{free}$ (Figure 4.5). Fitting CaM association and dissociation to a kinetic model provides K_d under different Ca^{2+} concentrations (Table 4.3).

Consistent with values reported in the literature for WT-CaM, CaM binding of eNOS peptide affinity ranges from ~1 nM to undetectable levels as $[Ca^{2+}]_{free}$ is decreased from saturating levels (2 mM) to physiologically resting levels (20-50 nM) [223-225]. Both nitroTyr-CaM species exhibit similar eNOS-peptide binding affinity at saturating calcium levels. Strikingly they retain ~5 nM affinity at physiologically resting $[Ca^{2+}]_{free}$. Due to the retention of high affinity for eNOS at resting $[Ca^{2+}]_{free}$, nitroTyr-CaM has the potential to constitutively activate eNOS in the absence of calcium signal. A small intracellular population of constitutively active nitroTyr-CaM will dominate the rest of the CaM population in the absence of a Ca^{2+} signal, resulting in a gain-of-function alteration to eNOS signaling.

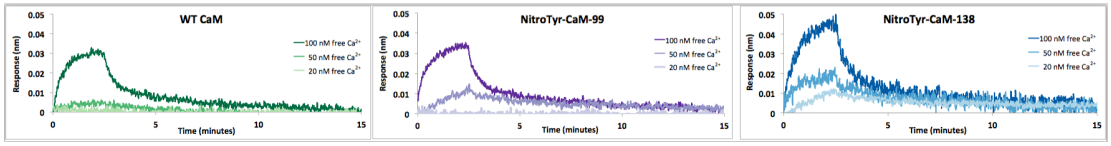

Figure 4.5. Representative BLI data of WT-CaM and nitroTyr-CaM binding to eNOS peptide.

Association and dissociation curves of WT-, nitroTyr-99, nitroTyr-138 CaMs with eNOS peptide at 100, 50, and 20 nM free calcium concentrations.

Table 4.3. Affinity constants derived from BLI data of WT- and nitroTyr-CaM binding to eNOS peptide.

Free [Ca^{2+}]	WT-CaM K_D (nM)	nitroTyr-CaM-99 K_D (nM)	nitroTyr-CaM-138 K_D (nM)
2 mM	0.65 ± 0.02	0.65 ± 0.02	0.64 ± 0.02
225 nM	3.84 ± 0.09	2.10 ± 0.06	2.75 ± 0.06
100 nM	5.1 ± 0.5	2.6 ± 0.3	3.8 ± 0.3
50 nM	360 ± 30	3.8 ± 0.1	4.94 ± 0.05
20 nM	>50,000	>50,000	7 ± 1

Data are means ± SD of at least 2 sets of 3 independent determinations.

NitroTyr-CaM Exhibits a Gain-of-Function Activation of eNOS Function

CaM nitration clearly causes eNOS binding at resting calcium concentrations but this change in affinity only has regulatory significance if nitration does not abolish full-length eNOS enzyme activity. Electron transfer between eNOS domains is dependent on the reversible binding of CaM, which is governed through changes in the intracellular Ca^{2+} concentration. To determine if the increased binding affinity of nitroTyr-CaM altered eNOS activity we measured the steady-state $NO^{\bullet}$ synthesis activities of eNOS in presence of WT-CaM and nitroTyr-CaMs (Table 4.4). The coincident rates of NADPH oxidation during the assays were also measured to determine the efficiency of $NO^{\bullet}$ production. Generally, these assays are conducted under saturating calcium levels (2 mM free Ca^{2+} concentration). At these Ca^{2+} concentrations, all CaM species bind eNOS with the same affinity (Table 4.3), so any differences in $NO^{\bullet}$ production seen are independent of CaM-eNOS affinity. It is not feasible to perform eNOS assays at very low Ca^{2+} concentrations due to slow eNOS turnover and detection limits of the oxyhemoglobin, NADPH, and cytochrome C assays. At saturating Ca^{2+} levels, the eNOS was ~1.3 times more active with nitroTyr-CaM-138 than eNOS with WT-CaM. NitroTyr-CaM-99 had an inhibitory effect and lowered $NO^{\bullet}$ synthesis by ~40 %. We also compared how these CaMs impact the NADPH oxidation rates of eNOS during $NO^{\bullet}$ synthesis. In general, the rate of NADPH oxidation followed the rate of $NO^{\bullet}$ synthesis, consistent with the coupling of these processes. Remarkably, the coupling in eNOS with nitroTyr-CaM-138 (3.0 NADPH per $NO^{\bullet}$) was more efficient than in eNOS with WT-CaM (4.4 NADPH per $NO^{\bullet}$). This means that that the eNOS works more efficiently with nitroTyr-CaM-138,

and enables greater NO• synthesis without an increased production of reactive oxygen species.

Table 4.4. Steady state rates (min^{-1}) of WT eNOS (Bovine) with different CaMs at 2 mM Free Ca^{2+}

Assays	WT CaM	nitroTyr-CaM-99	nitroTyr-CaM-138	Minus CaM
NO synth (+ L-Arg)	9.0 ± 0.8	5.5 ± 0.5	12 ± 1	0
NADPH Oxidation (+ L-Arg)	40 ± 2	27 ± 3	37 ± 3	6.0 ± 0.1
Cytochrome *c* reduction	490 ± 20	460 ± 20	540 ± 40	100 ± 9

The steady-state cytochrome c reductase activity is a useful way to measure the electron flux passing through the NOS FMN subdomain. Cytochrome c activity is suppressed in absence of CaM and cytochrome c activity increases in presence of CaM. A typical 5-fold increase in cytochrome C activity was induced by the binding of WT-CaM to WT-eNOS in our assays [45]. We found that nitroTyr-CaM-138 exhibits a 10% increase in activity as compared to WT-CaM and that nitroTyr-CaM-99 exhibits a 10% decrease in activity as compared to WT-CaM. Cytochrome c reductase activity data also indicate that the eNOS works more efficiently with nitroTyr-CaM-138. When supplemented with either of the nitroTyr-CaM species as opposed to WT-CaM, eNOS retained more activity at 225 nM $[Ca^{2+}]_{free}$ (Table 4.5). This indicates that the gain-of-function seen with nitroTyr-CaM-eNOS binding is conserved with the full-length protein.

Table 4.5. Steady state rates (min^{-1}) of WT eNOS (Bovine) with different CaMs at 225 nM Ca^{2+}_{free}

Assays	WT CaM	nitroTyr-CaM-99	nitroTyr-CaM-138	Minus CaM
NO synth (+ L-Arg)	7.0 ± 0.6	5.0 ± 0.2	11.0 ± 0.8	0
NADPH Oxidation (+ L-Arg)	34 ± 2	26 ± 3	41 ± 4	7.0 ± 0.1
Cytochrome *c* reduction	460 ± 30	440 ± 40	520 ± 30	105 ± 7
Coupling ratio	4.8:1	5.2:1	3.7:1	

NitroTyr-CaM interacts with and stimulates the function of eNOS in eNOS-expressing HEK293 cell lysate

In order to verify that nitroTyr-CaM interacts with eNOS while in the presence of WT-CaM and nitroTyr-CaM is not absorbed by other cellular CaM targets, we produced an HEK293 cell line stably expressing eNOS and using lysate from these cells showed that eNOS was co-immunoprecipitated via pulldown of the V5 tag on either WT- or nitroTyr-CaM (Figure 4.6). As eNOS was co-immunoprecipitated by both WT- and nitroTyr-CaM, this indicates that nitroTyr-CaM interacts with eNOS in the presence of other intracellular targets of CaM. Using lysate from eNOS producing HEK293 cells or EA.hy926 human endothelial cells we were able to control both the concentration of supplemented CaM and $[Ca^{2+}]_{free}$. We also verified that all CaM forms were able to stimulate eNOS activity in HEK293-eNOS lysate. As expected for eNOS we see a calcium concentration- (Figure 4.7) and time- (Figure 4.8) dependent increase in activity. This activity is responsive to the NOS inhibitor L-NAME (Figure 4.8) indicating that $NO^{\bullet}$ synthesis is a result of eNOS activity. Due to the presence of endogenous CaM there was a significant eNOS activity without the addition of exogenous CaM (Figure 4.7). As predicted from the increased affinity of nitroTyr-CaM-138 for eNOS at low calcium concentrations, the eNOS activity was stimulated to a significantly larger extent in lysate supplemented with nitroTyr-CaM-138 over WT-CaM (Figure 4.7), particularly at intermediate calcium levels (750-225 nM $[Ca^{2+}]_{free}$).

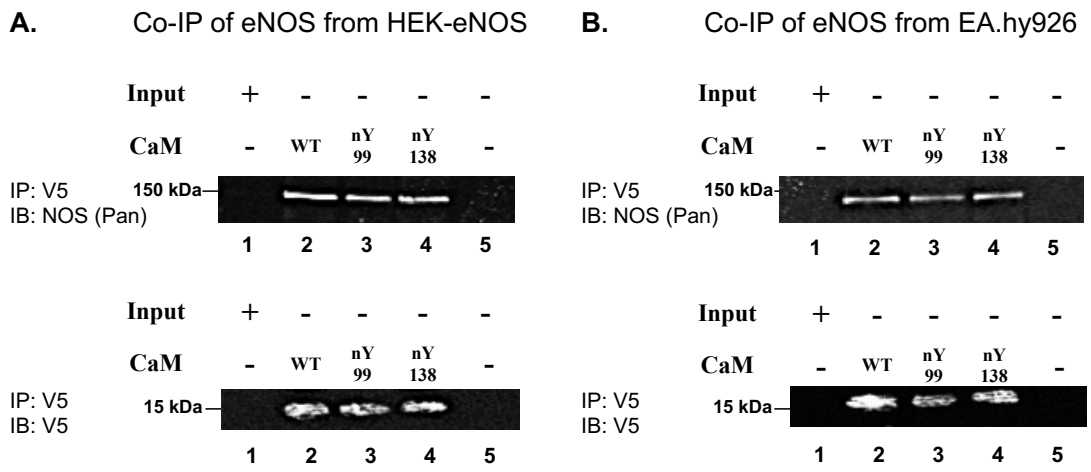

Figure 4.6. WT-CaM, CaM nitroTyr-99, and CaM nitroTyr-138 interact with eNOS protein from HEK293-eNOS and EA.hy926 cell lines.

Western blot analysis of immunoprecipitates of V5-tagged WT-, nitroTyr99-, and nitroTyr138-CaM from (A.) lysates of HEK293 cells stably expressing eNOS and (B.) EA.hy926 human endothelial cells show that WT- and nitroTyr-CaM interact with eNOS in the context of the cellular milieu containing other CaM target proteins.

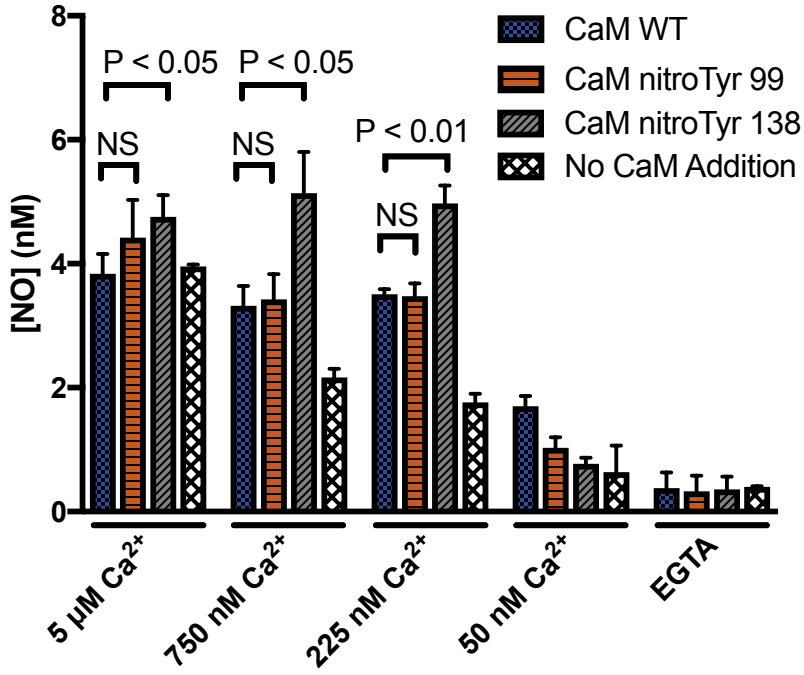

Figure 4.7. NitroTyr-CaM stimulates production of NO• by eNOS in HEK293-eNOS cell lysate.

HEK293-eNOS cell lysate was supplemented with WT- or nitroTyr-CaM and eNOS cofactors. The production of NO• was measured via NO• selective electrode.

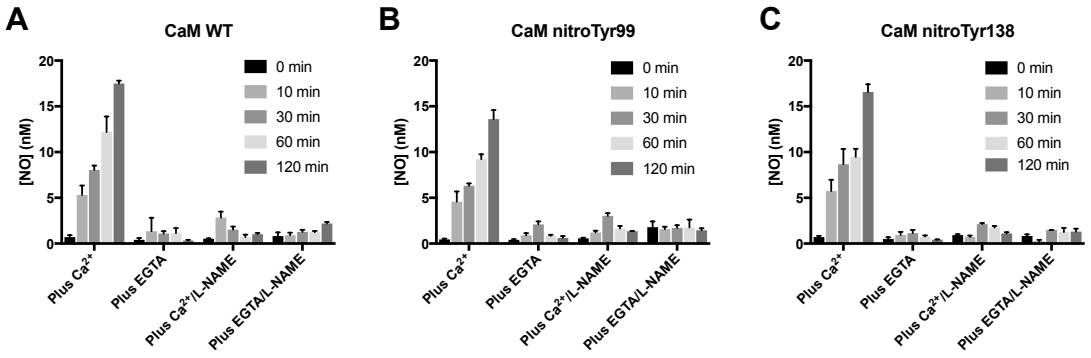

Figure 4.8. Timecourse of NO• production from lysate of eNOS expressing HEK cells. The production of NO• in eNOS-expressing HEK lysate supplemented with either (A) WT-CaM, (B) nitroTyr-CaM-99, (C) nitroTyr-CaM-138 displays time dependent NO• production and its dependence on EGTA, and NOS inhibitor L-NAME. The production of NO• was measured via NO• selective electrode.

Discussion

Here we sought to address a long standing question in the field of oxidative stress regarding if the nitroTyr PTM can regulate protein function [115]. The abundant literature on the strong connection between oxidative stress and calcium signaling dysregulation indicates that this Ox-PTM on CaM could be contributing to calcium dysregulation [226]. Nitrated CaM is seen in conditions of aging and inflammation but it was unclear whether nitration was simply protein damage or played a regulatory role due to the specific Ox-PTM. The perception that these modifications are solely damage has evolved and the concept of redox signaling is well established for a number of reactive oxygen and nitrogen species [2, 227]. Since nitroTyr can be incorporated site-specifically using GCE, it provides a method to evaluate if it can regulate protein function. CaMs central role in regulating calcium signaling, its abundant nitration of regulatory tyrosine residues, and the potential presence of a cellular denitrase [27] for nitrated CaM make it an ideal candidate for assessing the regulatory impact of tyrosine nitration.

For nitroTyr-CaM to serve a regulatory role, this Ox-PTM modification needs to provide a gain-of-function to CaM, since only a fraction of the cellular pool of CaM is likely nitrated, similar to other regulatory PTMs like phosphorylation [228].

There are three CaM equilibria that could shift and confer a gain-of-function to CaM signaling after nitroTyr modification. The first and most central potential alteration to CaM activity is a change in calcium binding. An increase in CaM's affinity for calcium would result in increase in activity of all Ca^{2+}-CaM dependent target proteins at lower calcium levels (Figure 4.9A). Second, is a shift in the equilibrium for binding target proteins such that nitroTyr-CaM binds a target protein at lower calcium concentrations, resulting in activation of target protein at lower calcium concentrations (Figure 4.9B). A third gain-of-function change from tyrosine nitration would result if nitroTyr-CaM-target protein complex increases client activity over that of WT-CaM-target protein complex (Figure 4.9C).

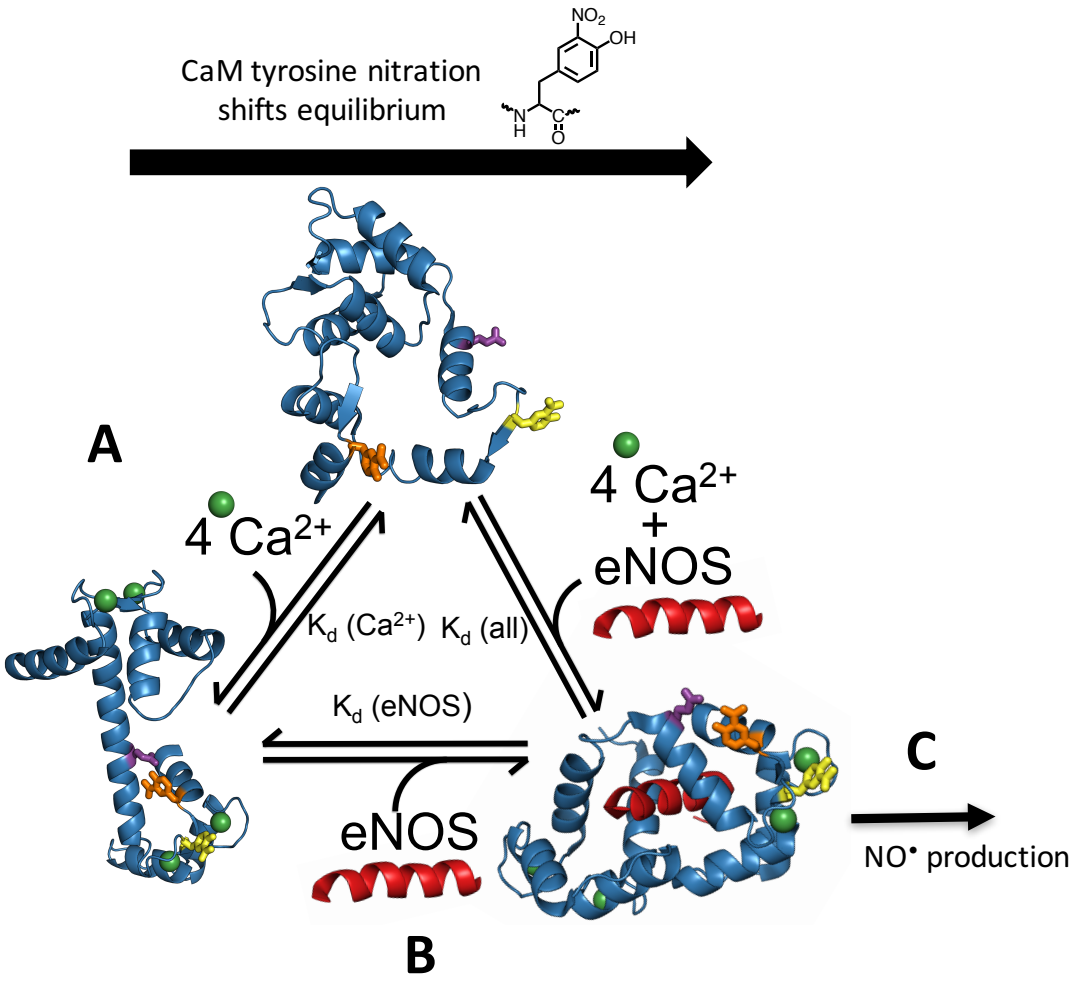

Figure 4.9. CaM function depends on several equilibria that may display a gain-of-function following tyrosine nitration here indicated as A, B, and C.
The two sites of physiological tyrosine nitration in calmodulin are shown, Tyr99 in yellow and Tyr138 in orange, and Ca^{2+} (shown as green spheres corresponding to the van der Waals radius). (A) A general gain-of-function occurs if apoCaM (PDB 1QX5) when nitrated possesses higher affinity for Ca^{2+} and shifts to the holoCaM (PDB 3CLN) at lower Ca^{2+} concentrations. (B) A gain-of-function may also occur if holoCaM binds to a target protein, like eNOS, with greater affinity (eNOS-CaM complex, PDB 1NIW). (C) Further, a gain-of-function could occur if nitroTyr-CaM binding induces increased target protein activity.

Reversible Ca^{2+} binding at the range of resting Ca^{2+} to saturating Ca^{2+} concentrations (0.1-10 μM) is at the core of CaM function, as it induces conformational changes resulting in exposure of hydrophobic patches and association with 100s of protein targets. If CaM tyrosine nitration alters Ca^{2+} affinity this will result in the most wide-reaching changes in CaM function. If Ca^{2+} affinity is increased, a general CaM gain-of-function occurs. Lower amplitude Ca^{2+} transients

would result in activation of target proteins. It has been reported that full oxidation of CaM methionines by hydrogen peroxide results in an unfolded apostate that binds 4 Ca^{2+} ions with equal lowered affinity resulting in a mild loss-of-function [229]. This is not the case for nitroTyr-CaM, as CaM retains its affinity for Ca^{2+} following tyrosine nitration resulting in neither a gain- nor loss-in-function. Tyr138 serves as a structural coupler between the N-terminal domain and the central linker of CaM through hydrogen bonding with Glu82 (Figure 4.10) [230-231]. In addition, an investigation via NMR into a phosphomimetic CaM mutant, Tyr99Glu, did show that residues involved in Ca^{2+} binding in the C-terminal lobe were affected by this mutation [32].

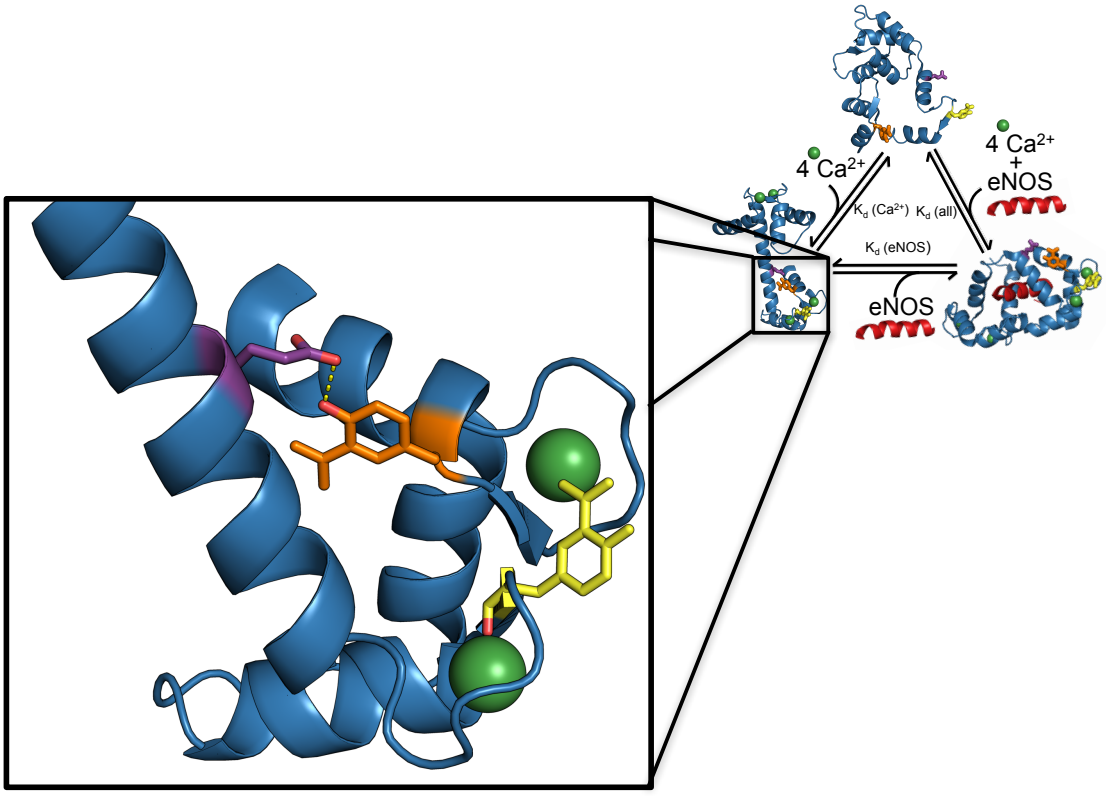

Figure 4.10. Interactions stabilizing holoCaM conformation.
Hydrogen bonding between glu 82 (purple) and tyr 138 (orange) is key to structural coupling between the N- and C-terminal lobes of CaM. Nitration of tyr 138 lowers the pKa of the residue resulting in a weakened hydrogen bond, lowering interlobe coupling. The carbonyl oxygen of Tyr 99 (yellow) involved in chelating Ca^{2+} in EF-hand III is also shown (ApoCaM structure, PDB 1QX5; Ca^{2+}-CaM structure, PDB 3CLN; Ca^{2+}-CaM-eNOS structure, PDB 1NIW).

Tyrosine phosphorylation of CaM has been shown to impact Ca^{2+}–dependent CaM signaling, including phosphoCaM-99 binding 4 times more tightly to neuronal NOS as compared to WT-CaM [34]. Given this its perhaps not surprising to think that CaM tyrosine nitration will alter CaM-eNOS affinity. Our data with WT-CaM show that under saturating 2 mM $[Ca^{2+}]_{free}$ WT-CaM exhibits sub-nanomolar affinity for eNOS peptide, that CaM begins dissociate from eNOS at 100 nM $[Ca^{2+}]_{free}$, and fully dissociates from eNOS at 20 nM $[Ca^{2+}]_{free}$. Both nitroTyr-CaM species bind with identical sub-nanomolar affinities as the WT-CaM under saturating $[Ca^{2+}]_{free}$, however they only exhibit a slight decrease in affinity at the resting $[Ca^{2+}]_{free}$ of 50 nM. Most strikingly, nitroTyr-CaM-138 remains bound even at 20 nM $[Ca^{2+}]_{free}$, indicating that eNOS in the presence of nitroTyr-CaM-138 is active even under resting conditions. A previous study with the eNOS CaM binding domain peptide showed no detectable interaction between CaM and the eNOS peptide at $[Ca^{2+}]_{free}$ <40 nM, and that eNOS was half maximally bound at a $[Ca^{2+}]_{free}$ of 228 nM [224]. Based on these conditions, eNOS is almost exclusively CaM-free under resting conditions but is half bound at roughly a quarter of maximum intracellular $[Ca^{2+}]_{free}$, meaning as expected, eNOS with WT-CaM is inactive under resting conditions but activated following influx of calcium. Previously, phosphorylation of eNOS at S1179 has shown a similar regulatory effect to the activation detected following CaM tyrosine nitration. Following eNOS phorphorylation by Akt or PKA, CaM is able to bind at lower $[Ca^{2+}]_{free}$ levels, effectively lowering the calcium signal required for eNOS activation [232]. In the same vein, nitration of CaM at tyrosine 138 provides a novel means of regulating CaM-target protein interactions and constitutively activating eNOS.

In order to study the catalytic activity of full-length eNOS, we employed several kinetic measurements. Monitoring $NO^{\bullet}$ production presents a direct measurement of the enzyme output, while monitoring NADPH oxidation provides information on the efficiency of the process in terms of substrate to product ratio, and monitoring cytochrome C reduction provides a means to assess correct electron transfer through the enzyme. Previous work with the phosphomimetic CaM mutation

Y99E showed a 40% decrease in NO• production, while the control mutation Y99Q only showed a 20% decrease in NO• production [32]. Due to issues with limits of sensitivity, eNOS assays are generally conducted under saturating $[Ca^{2+}]_{free}$ levels. At 2 mM $[Ca^{2+}]_{free}$, similar to the Y99E mutation, nitroTyr-CaM-99 resulted in a 40% decrease in NO• production and was less efficient with a 10% decrease in NADPH to NO• ratio as compared to WT-CaM. Strikingly, nitroTyr-CaM-138 was able to produce more NO• more efficiently than WT-CaM with a 33% increase in NO• output and a 62% efficiency increase. This increase in product output and increase in efficiency is comparable to what was seen for eNOS regulation by the phosphomimetic mutations S1179D or S617D [44-45]. As we do not expect the affinity of nitroTyr-CaM for eNOS to be altered at saturating $[Ca^{2+}]_{free}$ as compared to WT-CaM we may be able to ascribe the change in eNOS function to a shift in eNOS domain dynamics [233]. Under intermediate calcium conditions (225 nM $[Ca^{2+}]_{free}$) both nitroTyr-CaMs retained 10% more eNOS activity than the WT-CaM indicating that nitration will regulate CaM to increase NO• at low calcium levels.

NOS enzymes are homodimers of two peptide chains composed of an N-terminal oxygenase domain and C-terminal reductase domain with the two domains separated by a CaM-binding motif. During catalysis NADPH derived electrons are transferred into the FAD and FMN in each NOS subunit and then on to the ferric heme in the partner subunits of the homodimer. NOS electron transfer reactions are suppressed in the native state by several protein regulatory inserts including an auto-inhibitory insert in the FMN domain. CaM binding to NOS relieves suppression of the electron transfer process, activating NOS. Under conditions of limited arginine substrate NOS has also been observed to produce superoxide through electron transfer to molecular oxygen [234].

While *in vitro* eNOS assays give a detailed snapshot of CaM-eNOS regulation, we should remain cognizant of what occurs in the context of the intracellular environment. CaM regulates many proteins and nitroTyr-CaM pool may be biased towards target proteins other than eNOS. Regulation of eNOS is also multifaceted and is also dependent on interactions with proteins other than CaM and subcellular localization. In order to approach this problem we first assessed eNOS

function in HEK293-eNOS lysate. We saw that supplementation with nitroTyr-CaM, particularly at site 138, led to significantly more eNOS activity at intermediate calcium levels representing a gain-of-function even in the presence of other CaM target proteins and other eNOS regulatory interactions.

In summary, our results show that tyrosine nitration of CaM at sites 99 and 138 increase binding and activation of eNOS at lower Ca^{2+} concentrations than WT-CaM. While only a subset of cellular CaM will be nitrated on tyrosine 138 at any given time, due to its gain-of-function this subpopulation will activate eNOS with reduced influx of Ca^{2+}. The proper regulation of eNOS is important for healthy vascular function and the nitroTyr-CaM-eNOS gain-of-function clearly alters the regulatory function of CaM. What remains to be seen is whether this altered regulation is a component of of normal regulation in healthy intracellular function or dysregulation resulting in disease.

Materials and Methods

Immunoblotting

Western blot samples were separated on 15% SDS-PAGE gels, transferred to PVDF membrane, blocked with 5% nonfat milk in TBST, and probed with antinitrotyrosine (1:500) or anticalmodulin (1:1000) primary antibodies rocking for 16 hours at room temperature. After rinsing three times with TBST, the membranes were than incubated with Li-Cor IRDye 800CW Goat anti-Rabbit IgG (1:10,000) secondary antibody, rocking for 1 hour at room temperature, and washed three times for 5 minutes in TBST. The membrane was then scanned using a Li-Cor Odyssey 9120 Imaging System.

Recombinant expression of homogenous site-specifically modified nitroCaM

The human CaM sequence was codon optimized for expression in *E. coli* (GenScript USA) and cloned into a pBad/Myc-His_6 vector (Invitrogen). The protein was expressed via DH10B *E. coli* cells in autoinduction media in the presence of 100 μg/mL ampicillin for 24 hrs, at 37 °C, shaking at 250 rpm. Cells were pelleted at 5500 rcf then resuspended in approximately 10 mL binding/wash buffer (20 mM Tris, 500 mM NaCl, 20 mM imidazole, pH 7.4) at 4 °C and lysed once with a

Microfluidics M-110P microfluidizer set at 18,000 psi. Cell debris pelleted in oakridge tubes at 20,900 rcf for 25 min at 4 °C. Approximately 75 mL of supernatant was passed through an Acrodisc 32mm syringe filter with 0.45 um Supor membrane. The supernatant was loaded onto a 5mL HisTrap NiNTA column at 1ml/min, washed with 20 mL wash buffer, and eluted with 0-100%, 30 mL linear gradient of elution buffer (20 mM Tris, 500 mM NaCl, 500 mM imidazole, pH 7.4) using Amersham Pharmacia Biotech AKTA explorer. Peak elutions were between 30-40% elution buffer, corresponding to 150–200 mM imidazole. The pure protein fractions then had $CaCl_2$ added to a concentration of 5 mM and loaded on a 5 mL HiTrap phenyl sepharose column, washed with 20 mL of wash buffer (50 mM Tris-HCl, 1 mM $CaCl_2$, 500 mM NaCl, pH 7.5), and eluted with 0-100%, 30 mL linear gradient elution buffer (50 mM Tris-HCl, 1 mM EDTA, pH 7.5). Pure peak fractions determined via SDS-PAGE analysis were pooled and dialyzed for 4 hrs into ITC buffer (50 mM Tris-HCl, 100 mM NaCl, pH 7.5) twice, fresh ITC buffer was added for overnight dialysis. The purified CaM was concentrated via centricon tubes (3 kDa MWCO) to a concentration greater than 400 uM.

Expression and purification of CaM containing nitroTyr

E. coli DH10B was transformed with pBad-CaM-(99 or 138 TAG) and pDule-nitroTyr-5B (Addgene Plasmid #85498) [19]. Similar to WT-CaM, expression of nitroTyr-containing CaM was in autoinduction media containing 100 μg/mL ampicillin, 25 μg/mL tetracycline, and 1 mM nitroTyr. Purification of nitroTyr-containing CaM was identical to purification of WT-CaM.

Mass Spectromectry

Purified CaM samples were diluted to a concentration of 10 uM, desalted on Millipore C_4 zip tips, and analyzed using an FT LTQ mass spectrometer at the Oregon State University Mass Spectrometry Facility. Samples included WT-CaM and nitroTyr-containing CaM.

Isothermal Titration Calorimetry (ITC)

ITC recordings performed with a NanoITC Low Volume – 190 uL from TA Instruments' (New Castle, DE), with a stir speed of 250 rpm. The ITC conditions for CaM- Ca^{2+} binding were 50 mM Tris-HCl (pH 7.5) containing 100 mM NaCl at 25 °C. The concentration of CaM in the reaction cell was 350 μM with a volume of 300 μL added. A solution of 10 mM Ca^{2+} was loaded into the ITC syringe, with injections of 1.0 μL of solution at 3 minute [216]. In all cases injections of titrant into the corresponding buffer were used to account for the heat of mixing and dilutions.

Calmodulin dansylation and fluorescence measurements

Dansyl-CaM was prepared as previously described. CaM (1 mg/mL) was buffer exchanged into 10 mM $NaHCO_3$ and 1 mM EDTA (pH 10.0) at 4 °C. Thirty μL of 6 mM dansyl chloride (1.5 mol/mol of CaM) in acetone was added to 2 mL of CaM, while it was being stirred. After incubation for 12 h at 4 °C, the mixture was buffer exchanged into fluorescence buffer. Labeling yields were determined from absorbance spectra using an ε_{320} of 3400 M^{-1} cm^{-1} and were compared to actual protein concentrations determined using the Bradford method with wild-type CaM used as the protein standard.

Fluorescence emission spectra were recorded using a PTI (London, ON) QuantaMaster spectrofluorimeter. Fluorescence measurements were taken on 50 μL samples consisting of dansyl-CaM (2 μM) in 30 mM MOPS, 100 mM KCl, and 10 mM EGTA (pH 7.2) with an increasing concentration of free Ca^{2+}. The free Ca^{2+} concentration was controlled using the suggested protocol from the calcium calibration buffer kit from Invitrogen. The excitation wavelength for all of the dansyl-CaMs was set to 340 nm, and emission was monitored between 400 and 600 nm. Slit widths were set at 2 nm for excitation and 1 nm for emission. The relative fluorescence was calculated with the equation:

$$\text{Relative Fluorescence} = (F - F_0)/(F_{max} - F_0) \qquad (4.1)$$

where F is the measured intensity, F_{max} is the maximal intensity, and F_0 is the intensity without added Ca^{2+}. The Ca^{2+} sensitivities of the different dansyl-CaMs we

determined as the $EC_{50}(Ca^{2+})$ values, which were derived from fits of the relative fluorescence intensity increase upon addition of Ca^{2+} using the equation:

$$\text{Relative Fluorescence} = \frac{[Ca^{2+}]^{n}_{free}}{[Ca^{2+}]^{n}_{free}+[EC_{50}(Ca^{2+}]^{n}} \quad (4.2)$$

where relative fluorescence is obtained from equation 1; n is the Hill coefficient.

Octet Red96 Biolayer interferometry measurements

All BLI measurements were made on a fortéBIO (Menlo Park, CA) Octet Red96 system using streptavidin ('SA') sensors. Assays were performed in 96-well microplates at 37 °C. All sample volumes were 200 µL. The eNOS peptide was purchased from Genscript (Piscataway, NJ) homogeneously biotinylated at the N-terminus. After loading biotinylated eNOS peptide onto SA sensors, a baseline was established in buffer composed of 30 mM MOPS, 100 mM KCl (pH 7.2), and varying free calcium concentration. Free calcium was controlled by mixing two buffers containing 10 mM EGTA and 10 mM Ca^{2+}-EGTA in varying ratios. Free calcium concentration was calculated either from the ThermoFisher Scientific Calcium Calibration Kit #1 instructions or the Maxchelator program [235]. Association with the analyte CaM was then carried out in the same buffer for 90 seconds at CaM concentrations of 180 nM, 60 nM, and 20 nM. Dissociation was subsequently measured in buffer only over 1200 seconds.

Steady-state eNOS assays

$NO^{\bullet}$ synthesis and NADPH oxidation rates were determined using the oxyhemoglobin assay. The $NO^{\bullet}$ synthesis activity was determined by the conversion of oxyhemoglobin to methemoglobin using an extinction coefficient of 38 $mM^{-1}cm^{-1}$ at 401 nm. The NADPH oxidation rates were determined following the absorbance at 340 nm, using an extinction coefficient of 6.2 $mM^{-1}cm^{-1}$. Reaction mixtures (total volume 400 µl) contained 0.1 - 0.2 µM eNOS, 0.3 mM dithiotreitol, 4 µM FAD, 4 µM FMN, 10 µM H_4B, 2 mM L-Arg, 0.1 mg/ml bovine serum albumin, 2 mM $CaCl_2$, 0.2 mM EDTA, 2 - 5 µM CaM (WT or nitroTyr depending on the experiment), 100 units/ml catalase, 60 units/ml superoxide dismutase, 5 µM oxyhemoglobin and 150 mM NaCl in 40 mM EPPS buffer, pH 7.6. The reaction was initiated by adding

NADPH to a final concentration of 250 μM. In the assays without CaM, $CaCl_2$ was omitted and EDTA concentration was increased to 0.45 mM. Cytochrome *c* reductase activity was determined by following the absorbance change for the reduction of cytochrome *c* by eNOS at 550 nm using an extinction coefficient of 21 $mM^{-1}cm^{-1}$. Reaction mixtures (total volume 400 μl) contained ≤ 0.01 μM eNOS, 25 μM FAD, 25 μM FMN, 0.1 mg/ml bovine serum albumin, 2 mM $CaCl_2$, 0.2 mM EDTA, 1.0 - 4.0 μM CaM (WT or nitroTyr depending on the experiment), 100 units/ml catalase, 40 units/ml superoxide dismutase, 65 μM cytochrome *c* and 150 mM NaCl in 40 mM EPPS buffer, pH 7.6. The reaction was initiated by adding NADPH to a final concentration of 250 μM. In the assays without CaM, neither CaM nor $CaCl_2$ were added and EDTA concentration was 0.45 mM. All steady-state assays were carried out at 25 °C. Reported values are means ± SD of three or more determinations.

Production of the stable HEK293-eNOS line

The bovine eNOS sequence in a pcDNA3 vector and empty pcDNA3 vector were transfected into HEK293 cells (ATCC) using lipofectamine 2000 (Thermo Fischer Scientific) according to the manufacturer's protocol. Stable HEK293 cell populations were selected for using G418 250 μg/mL. Expression of eNOS was confirmed by western blot using pan-NOS antibody (Cell Signaling Technology).

Immunoprecipitation of V5-tagged WT-CaM and NitroTyr-CaM from HEK293-eNOS cells

ENOS was immunoprecipitated from cells (either HEK-eNOS expressing cells or EA.hy926 human endothelial cells) prepared in lysis buffer (50 mM Tris-HCl, pH 7.4, 150 mM NaCl, 1 mM EGTA, 1% Triton X-100, and 1x protease inhibitor cocktail). Recombinant WT- or nitroTyr-CaM was supplemented into the lysate at 20% of the endogenous CaM concentration in the lysate along with 5 mM $CaCl_2$. The lysate with recombinant CaM was incubated at 4°C overnight with 2 μl mouse anti-V5 antibody (Invitrogen). The mixture was further incubated with 20 μl of protein A/G magnetic beads for 6 hours at 4°C. The magnetic beads were washed four times with lysis buffer containing 5 mM $CaCl_2$, resuspended in 40 μl of Laemmli buffer, and incubated at 55 °C for 10 minutes. Western blot samples were separated on 4-

22% gradient SDS-PAGE gels, transferred to PVDF membrane, blocked with 5% nonfat milk in TBST, and probed with antiNOS (Pan) (1:1000) or antiV5 (1:5000) primary antibodies rocking for 16 hours at room temperature. After rinsing three times with TBST, the membranes were than incubated with Li-Cor IRDye 800CW Goat anti-Rabbit IgG (1:10,000) secondary antibody, rocking for 1 hour at room temperature, and washed three times for 5 minutes in TBST. The membrane was then scanned using a Li-Cor Odyssey 9120 Imaging System.

eNOS-lysate reaction conditions

Reactions to determine eNOS activity in eNOS expressing HEK293 cellular lysate were carried out. Lysate extracted as above was supplemented with 2 mM L-arginine, 1 mM NADPH, 20 nM BH4 in solution containing 3 mM dithiothreitol, and 500 nM WT- or nitroTyr-CaM. For those reactions containing Ca^{2+} or EGTA, they were supplemented with 10 mM of either, while those reactions supplemented with L-NAME to a concentration of 1 mM. The reaction was initiated by the addition of the NOS cofactors listed above and incubated for 30 minutes at 37 °C. The eNOS reactions were carried out at a 50 µL scale in triplicate and stopped via freezing in dry ice.

eNOS-activity assays

The amount of $NO^{\bullet}$ produced in lysate was measured amperometrically by an AmiNO700 $NO^{\bullet}$ selective electrode (Innovative Instruments, Inc.) as described previously [236]. In a cell lysate $NO^{\bullet}$ is autooxidized to its stable product nitrite.

Acknowledgements

This work was supported by grants from the National Institutes of Health Grant RGM114653A (to R.A.M.). We thank Dr. Colin Johnson for discussion and help with calcium binding properties of calmodulin and Dr. Sandra Loesgen for discussion and help with biolayer interferometry.

Chapter 5

Genetically Encoded Tyrosine Nitration in Mammalian Cells

Joseph J. Porter, Hyo Sang Jang, Duy P. Nguyen, Elise Van Fossen, Taylor S. Willi, and Ryan A. Mehl

Formatted for Publication

Abstract

Tyrosine nitration has served as a major biomarker for oxidative stress and is present in over 50 disease pathologies in humans. While data mounts on specific disease pathways from specific sites of tyrosine nitration, the role of these modifications is still largely unclear. Strategies for installing site-specific tyrosine nitration in target proteins in eukaryotic cells, through routes not dependent on oxidative stress, would provide a powerful method to address the consequences of tyrosine nitration. Developed here is a *Methanosarcina barkeri* aminoacyl-tRNA synthetase/tRNA pair that efficiently incorporates nitrotyrosine in mammalian cells. Demonstrating the utility of this approach, we produce site-specifically nitrated manganese superoxide dismutase (MnSOD) and 14-3-3 in eukaryotic cells with encoded nitroTyr at the sites identified to form under disease conditions.

Introduction

Tyrosine nitration is an oxidative post-translational modification (Ox-PTM) that has served as a biomarker of oxidative stress present in a variety of human diseases including neurodegeneration, atherosclerosis, and cancer [7]. Many proteins contain sites of nitration, however the consequences of most of these modifications of these sites remain unexplored. Progress in this field has been hampered because Ox-PTMs are installed differently than standard direct enzyme catalyzed PTM installation. Ox-PTMs like nitrotyrosine (nitroTyr) are installed through the reaction of protein with cellular reactive oxygen species (ROS) and reactive nitrogen species (RNS). The chemical methods to install Ox-PTMs on proteins results in modifications to many susceptible amino acids generating a complex mixture of proteins, which makes it not possible to understand the impact of a specific modification [211].

Genetic code expansion (GCE), using orthogonal aminoacyl-tRNA synthetase/$tRNA_{CUA}$ (aaRS/tRNA) pairs, allows for the direct co-translational installation of a diverse array of non-canonical amino acids (ncAAs) [14]. This method allows for the synthesis of recombinant proteins containing defined PTMs, providing insights into how these modifications regulate protein structure and function [237].

A GCE system has been developed for the incorporation of nitroTyr and used to show the functional consequences of this modification on proteins *in vitro* [19, 22]. This orthogonal pair based on a tyrosyl-RS/tRNA from the methanogenic archaeon *Methanocaldoccus janaschii* is orthogonal in *E. coli* and as such has been used to produce a number of site-specifically nitrated proteins for functional studies [22-24]. The ability to site-specifically install nitroTyr and structural analogues in mammalian cells would facilitate an understanding of the structural and functional consequences of this modification. Unlike approaches that manipulate levels of ROS and RNS, that modify many amino acids on many proteins, alternative methods like GCE directly address the consequences of site-specific nitration. The nitroTyr-RS/tRNA pair previously used to incorporate nitroTyr in *E. coli* is not orthogonal in eukaryotic cells necessitating a new system for studies in mammalian cells. The pyrrolysine RS/tRNA pair from several species of methanogenic archaea has emerged as a particularly useful platform for GCE as it allows for the evolution of new aaRSs in *E. coli* and application of the evolved aaRS/tRNA in bacterial and eukaryotic cells [160]. It is anticipated that a system to genetically encode nitroTyr in eukaryotic cells will be broadly applicable to the many different proteins nitrated *in vivo*.

The mitochondrial antioxidant enzyme manganese superoxide dismutase (MnSOD) is known to be nitrated in several chronic inflammatory diseases including chronic organ rejection, arthritis, and tumorigenesis [238]. Exposure of recombinant MnSOD to peroxynitrite resulted in a dose-dependent decrease in enzymatic activity and simultaneous increase in tyrosine nitration of MnSOD [239]. Expression of site-specifically nitrated MnSOD will allow us to determine the consequences of the production of specific nitroTyr-MnSOD species for mitochondria and cells.

14-3-3 proteins are a family of phospho-binding proteins that regulate many major cellular functions. The dynamics of the 14-3-3 interactome have been shown to be important as a stress-adaptive signaling hub in cancer. Regulation of 14-3-3 by PTMs is important for the adaptive mechanisms that orchestrate tumor cells' response to a variety of environmental conditions including hypoxia and chemotherapy [240]. Proteomic studies have uncovered the presence of nitroTyr on all seven members of

the 14-3-3 family both under normal conditions and under conditions of increased oxidative stress [241-243]. While the exact role tyrosine nitration for these processes is unknown, the ability to genetically encode tyrosine nitration allows us to directly observe the differences in the interactome of nitrated 14-3-3.

Here we develop a pyrrolysine aaRS/tRNA pair that can encode nitroTyr, and the structural analogue 3-nitrophenylalanine (3-nitroPhe). We characterize the efficiency and fidelity of this aaRS/tRNA pair using ncAA-sfGFP expressed in mammalian cells. We demonstrate the utility of this approach by producing the physiologically nitrated proteins, MnSOD and 14-3-3, in mammalian cells and verify the site-specific nitration *in vivo*. This technology opens up the ability to determine the impact of tyrosine nitration on protein interactomes *in vivo* and on transmembrane proteins only amenable to study in mammalian cells.

Results

Selection of an aminoacyl-tRNA synthetase specific for nitroTyrosine and 3-nitrophenylalanine.

To identify an orthogonal *Methanosarcina barkeri* pyrrolysyl tRNA synthetase/$tRNA_{CUA}$ pair (MbPylRS/tRNA) able to incorporate nitroTyr in response to an amber codon, we screened a library of MbPylRS variants in which five active-site residues were randomized to all 20 amino acids (L270, Y271, L274, N311, C313) [244]. After a single round of positive selection in the presence of nitroTyr or 3-nitroPhe and a round of negative selection against canonical amino acids, 48 colonies were assessed for their efficiency in suppressing an amber stop codon (TAG) interrupted sfGFP at amino acid site 150 (sfGFP-150TAG) in the presence of nitroTyr and 3-nitroPhe. Simultaneously, the ability of the selected synthetases to discriminate against canonical amino acids was assessed by expressing the sfGFP-150TAG in the absence of ncAA. The top 16 performing clones, as based on their efficiency and fidelity, were further evaluated a larger scale in the presence of 1 mM nitroTyr and 1 mM 3-nitroPhe. Sequencing of these 16 clones revealed 14 unique RS sequences (Supporting table S5.1). Of these clones, the selected mutant MbPylRS “F4” efficiently incorporated nitroTyr and showed remarkable permissivity for 3-nitroPhe compared to the other mutant MbPylRSs (Supporting Figure 5.1), and was chosen for

use in mammalian cells. While the F4 MbRS efficiently encoded nitroTyr in *E. coli*, when tested for incorporation of nitroTyr and 3-nitroPhe in HEK293T cells only 3-nitroPhe was efficiently incorporated (Supporting Figure 5.2). In order to select an MbRS that would efficiently incorporate nitroTyr in eukaryotic cells the entire pool of library members left after the first round of positive and negative selection were subjected to two more rounds each of positive and negative selections. The most efficient mutant MbPylRS from these rounds of selection "A7" incorporated nitroTyr in *E. coli* but was not permissive to 3-nitroPhe (Figure 5.1). The A7 MbRS/tRNA pair possesses comparable efficiency and fidelity for nitroTyr incorporation in *E. coli* as compared to the previously evolved *Methanocaldococcus jannaschii* tyrosyl-tRNA synthetase/tRNA pair (*Mj*-RS 5b) [19]. The MbPylRS/tRNA pair possesses the added utility of usage in eukaryotic cells [14, 245] potentially allowing the study of nitroTyr in its native cellular context. To that end we set out to apply this system to the first genetically encoded Ox-PTM in eukaryotic cells.

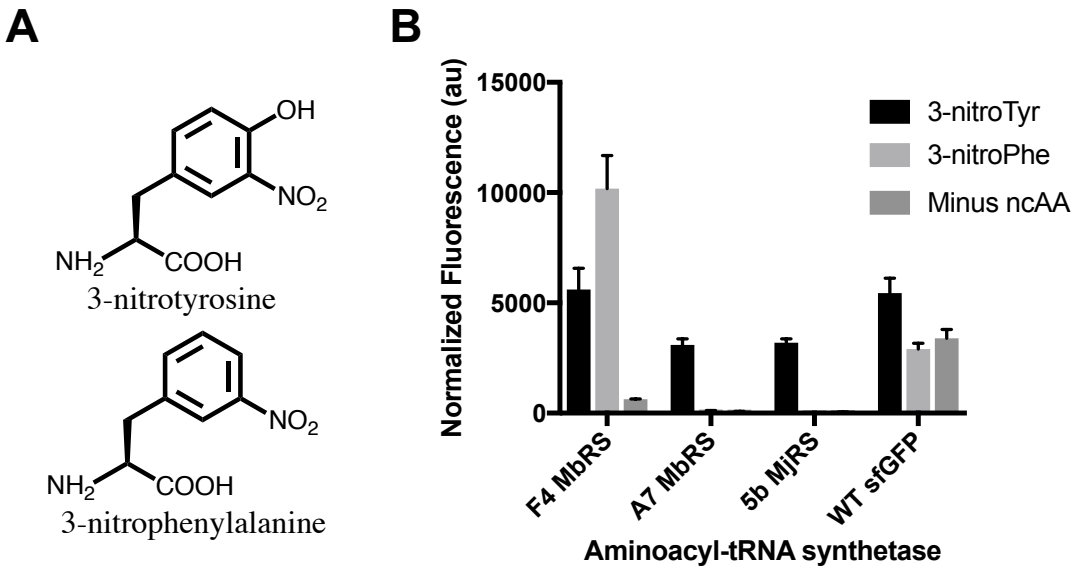

Figure 5.1**.** Noncanonical amino acids used in this study and characterization of synthetase hits from library selection.

(**A**) Structures of nitroTyr and the 3-nitroPhe incorporated via genetic code expansion in this study. (**B**) Assessment of fluorescence normalized to optical density at 600 nm for cells expressing the sfGFP150TAG gene along with each of the synthetase variants identified from the selection process. Cultures were expressed in the presence of 1 mM nitroTyr (black), 3-nitroPhe (light gray), in the absence of ncAA (dark grey). The two MbRSs characterized in this study were compared against the previously developed *Methanocaldococcus jannaschii* tyrosyl aminoacyl-tRNA/tRNA pair for nitroTyr (5b MjRS). In the case of the WT sfGFP sample the sfGFP-150TAG gene was replaced with a WT sfGFP gene.

Expression of site-specifically incorporated nitroTyr proteins in eukaryotic cells

As background mis-incorporation of structural analogues of canonical amino acids in translation can be toxic to cell growth, we determined the maximum allowable concentration of nitroTyr for HEK293T cell viability. We found that nitroTyr did not display significant toxicity at concentrations up to 0.3 mM at 48 hours after treatment, but cell viability was compromised when media was supplemented with 1 mM nitroTyr (Figure 5.2). Based on the toxicity profile for nitroTyr on HEK293T cells, future experiments were conducted using 0.3 mM nitroTyr in the media.

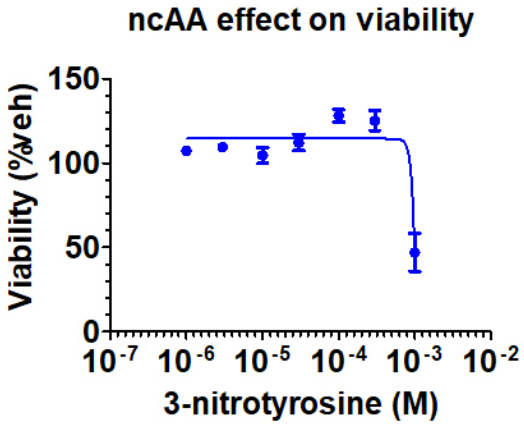

Figure 5.2. HEK293T cell viability assay with nitroTyr.
HEK293T cells were incubated for 48 h with nitroTyrosine and the cell viability was measured using CellTiter Glo assay kit (Promega). The data was normalized to vehicle control and fitted to a curve using non-linear regression method using GraphPad Prism 5. Based on these results the media in which HEK cells are grown can be supplemented up to 0.3 mM with nitroTyr without significant toxicity.

We hypothesized that we could take advantage of the highly efficient F4-MbRS/tRNA pair selected for incorporation of nitroTyr in *E. coli* and use it for incorporation of nitroTyr in mammalian cells. To test this, we cloned a human codon optimized version of the F4 synthetase and tRNA into a pAcBac1 mammalian expression vector and in a separate pAcBac1 vector we cloned a sfGFP-TAG150 (Supporting Figure 5.3). To our surprise, when transfected into HEK293T cells, the F4-MbRS and tRNA pair could only efficiently incorporate 3-nitroPhe but not nitroTyr (Supporting Figure 5.2). We reasoned that more stringent selection steps may yield nitroTyr-MbPylRS/tRNA pairs that can more efficiently incorporate nitroTyr at the lower concentrations needed in mammalian cells. After generation and characterization of the A7-MbRS, it was codon optimized for mammalian expression and incorporated into the the pAcBac1 plasmid. The A7-MbRS with lower efficiency but improved fidelity in *E. coli* did support robust incorporation of nitroTyr in mammalian cells only in the presence of 0.3 mM nitroTyr as shown by fluorescence microscopy and fluorescence of crude cell lysate (Figure 5.3).

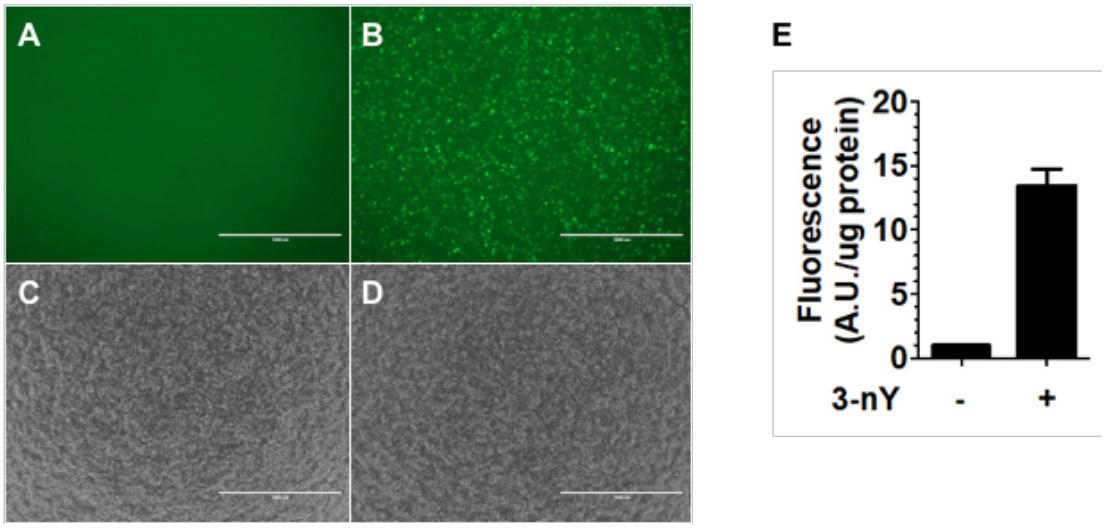

Figure 5.3. Expression of nitroTyr-containing sfGPF in HEK293T cells.
HEK293T cells were transfected for 48 h with A7 RS pAcBac1 and sfGFP-TAG-150 pAcBac1 using Lipofectamine 2000 (Thermofisher) in the presence (**B** and **D**) or absence (**A** and **C**) of 0.3 mM nitroTyrosine. Fluorescence images (**A** and **B**) and phase contrast images (**C** and **D**) were captured using EVOS FL cell imaging system (Thermofisher). Scale bar, 1 mm. (**E**) Cell lysates were prepared in modified RIPA buffer (20 mM Tris-HCl, pH 7.4, 150 mM NaCl, 0.1% SDS, 0.5% sodium deoxycholate, 1% NP-40, 1 mM EDTA, 1 mM EGTA, 2 mM sodium orthovanadate, 10% glycerol, 1x protease inhibitor cocktail), and fluorescence was measured using Synergy2 multi mode plate reader (Bio-Tek) using 485/20 nm excitation filter and 528/20 nm emission filter set.

Optimization of conditions for efficient incorporation of nitroTyrosine in mammalian cells

To perform efficiently the orthogonal translational components require maintenance at certain levels with respect to each other [246]. Our two vectors for co-transfection contain 4 copies of the Pyl tRNA and a CMV-driven sfGFP-150TAG on plasmid 1, and 4 copies of the Pyl tRNA and a CMV-driven MbRS on plasmid 2 (Figure 5.4A). We first sought to optimize the ratio of these two vectors by transfecting different ratios of plasmid 1 and 2 in HEK293T cells, assessing suppression efficiency in the presence and absence of 0.3 mM nitroTyr. Flow cytometry analysis of these cells indicates that a ratio of ~32:1 of the sfGFP-TAG150/MbRS is optimal for nitroTyr-containing sfGFP expression (Figure 5.4B, Supplementary Figure 5.4). After optimizing the ratio of the plasmids we next tested the utility of appending a strong nuclear export sequence (NES) to the N-terminus of the MbRS. Others previously identified a putative nuclear localization sequence (NLS), which improperly traffics the synthetase to the cell nucleus [247]. Addition of

a strong NES to the MbRS resulted in a significant enhancement of amber codon suppression efficiency in HEK cells [247]. In our hands appending this strong NES to our A7 MbRS resulted in a modest but significant 1.8-fold increase in amber codon suppression efficiency (Figure 5.4C).

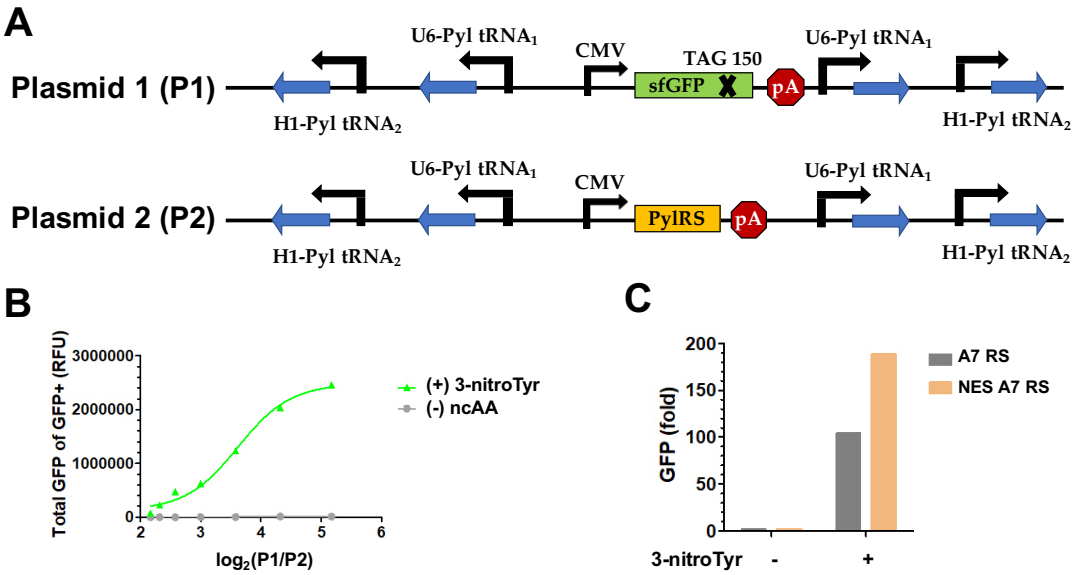

Figure 5.4. Optimization of the expression of nitroTyr-containing protein in HEK293T cells.

(**A**) Two plasmids were co-transfected for expression of nitroTyr-containing protein in HEK293T cells. The first plasmid (P1) contains 4 copies of the Pyl tRNA, downstream of either a U6 or H1 RNA pol. III promoter and sfGFP-150TAG, downstream of the CMV promoter. The second plasmid (P2) contains 4 copies of the Pyl tRNA, downstream of either a U6 or H1 RNA pol. III promoter and A7 Mb PylRS, downstream of the CMV promoter. (**B**) Assessment of production of nitroTyr-containing sfGFP based on the ratio of plasmid containing tRNA and sfGFP-150TAG (P1) to plasmid containing tRNA and A7 Mb RS (P2). Increasing the ratio of tRNA and sfGFP-150TAG to A7 Mb RS increases nitroTyr-containing sfGFP production shown here by flow cytometry. (**C**) Appending an N-terminal nuclear export sequence (NES) to the A7 Mb PylRS increases production of nitroTyr-containing sfGFP.

Characterization of nitroTyrosine-containing protein in mammalian cells

Using the optimized nitroTyr incorporation machinery, we sought to confirm stable incorporation of nitroTyr by mass spectrometry. We confirmed that the incorporated nitroTyr was not reduced to 3-aminotyrosine. HEK293T cells were co-transfected at the optimal ratio of 32:1 sGFP-150TAG pAcBac1 to NES-A7 MbRS pAcBac1 and grown for 48 hours in the presence of 0.3 mM nitroTyr. Following expression of nitroTyr-sfGFP, the cells were washed twice with PBS, lysed via

sonication in PBS containing protease inhibitor cocktail, and the sfGFP-150 nitroTyr was purified from the clarified cell lysate via TALON metal affinity chromatography. The mutant protein was characterized by ESI-q-TOF analysis, which revealed the correct mass (expected mass: 29232 ± 1 Da; measured mass: 29236 ± 1 Da) as compared to purified WT sfGFP (expected mass: 29141 ± 1 Da; measure mass: 29142 ± 1 Da) (Figure 5.5).

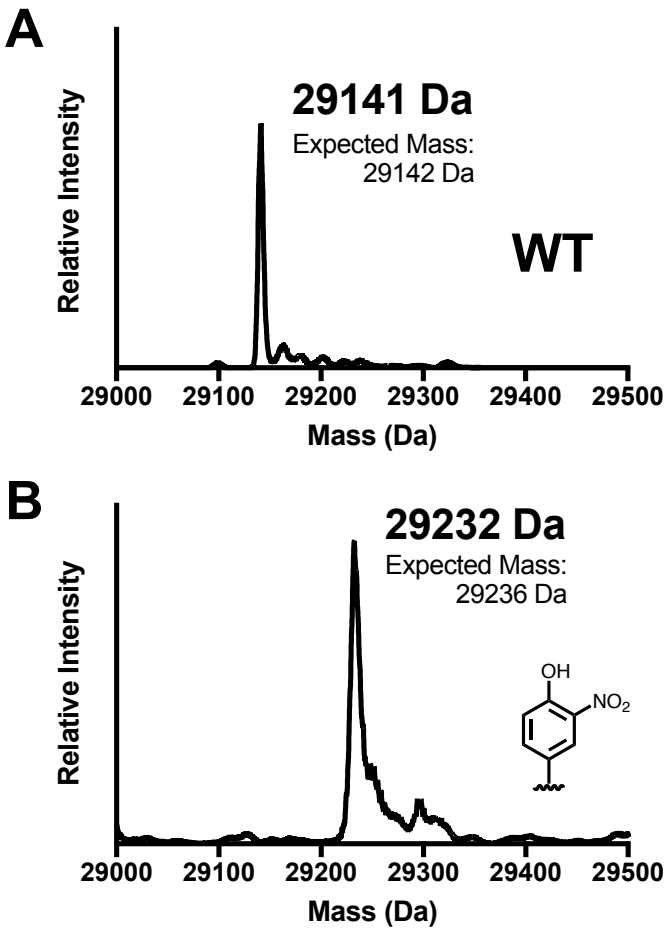

Figure 5.5. ESI-MS spectra of purified sfGFP expressed in HEK cells.
(A) ESI-MS spectra of GFP-wild-type and (B) ESI-MS spectra of sfGFP 150-nitroTyr.

Expression of site-specifically modified MnSOD and 14-3-3

To demonstrate the utility of our GCE for proteins known to be nitrated under physiological conditions we expressed site-specifically nitrated MnSOD and 14-3-3 in HEK293T cells. To do this we cloned MnSOD and 14-3-3 C-terminal monomeric-

EGFP fusion proteins into the pAcBac1 plasmid (Figure 5.6A). C-terminal EGFP fusions have been used for both MnSOD and 14-3-3 as a way to track intracellular expression and localization [248-250]. These plasmids were co-transfected into HEK293T cells with the NES-A7 MbRS pAcBac1 plasmid. The nitroTyr-dependent expression of TAG mutants of both MnSOD and 14-3-3 was demonstrated by flow cytometry using the C-terminal mEGFP tag (Figure 5.6B). In both cases, reserving nitroTyr from the media resulted in the same level of fluorescence as for the untransfected control cells. In the presence of 0.3 mM nitroTyr the TAG mutants of MnSOD and 14-3-3 expressed at 10-30% of the WT constructs, consistent with expression level of TAG-interrupted sfGFP. We further demonstrated that the GFP fluorescence was specific to the production of the proteins of interest by in gel fluorescence. A protein of the same size as the WT construct is only evident in the lysate of the sample supplemented with nitroTyr (Figure 5.6C).

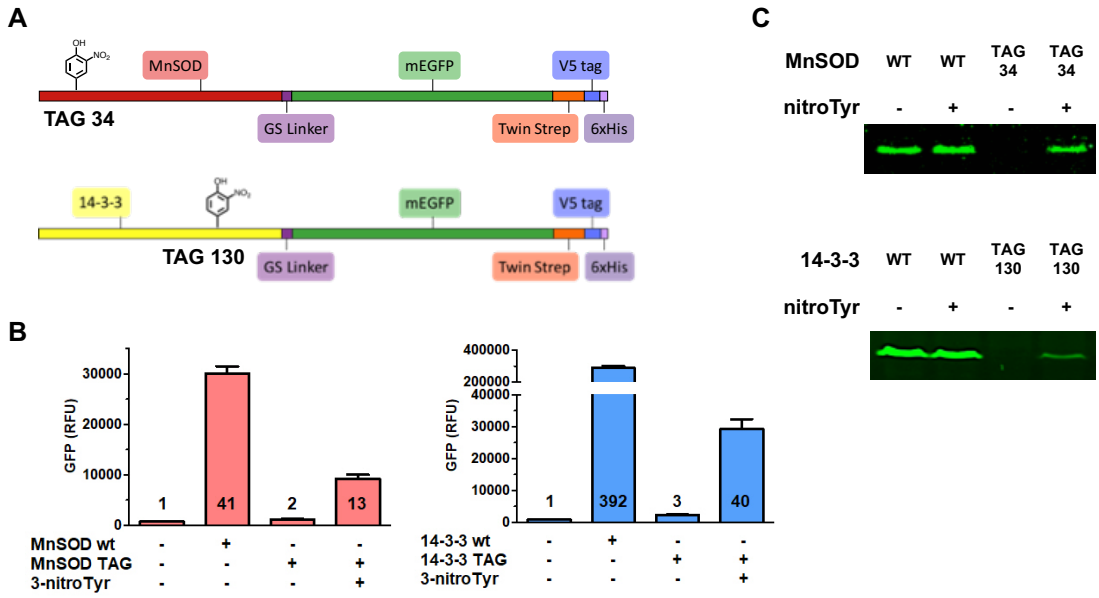

Figure 5.6. Expression of site-specifically nitrated MnSOD and 14-3-3 in HEK293T cells.

(A) MnSOD and 14-3-3 expression constructs. The gene of interest (either MnSOD or 14-3-3) was fused via a flexible gly-ser linker to monomeric enhanced green fluorescent protein containing a C-terminal twin strep, V5, and 6x His tags to aid in detection and purification. (B) Flow cytometry data of HEK cells transfected with either WT or TAG mutants of the MnSOD or 14-3-3 mEGFP fusion proteins. Fluorescence for the TAG mutants was detected

only in the presence of nitroTyr. The numbers on the bars represent fold-increase of fluorescence used to calculate the RFU. (C) In gel fluorescence of HEK cell lysate demonstrating the specific GFP signal resulting from the MnSOD and 14-3-3 mEGFP fusion proteins.

Discussion

Many reports have proposed the functional importance of tyrosine nitration on proteins involved in cell signaling, metabolism, and cellular structure but there is no effective way to evaluate which sites of tyrosine nitration have a cellular effect [251-256]. The standard approach to identify these modifications is to immunoblot for the nitroTyr modification and the site of modification is then pinpointed via mass spectrometry. Generally, the site(s) of tyrosine nitration are mutated to phenylalanine and the cells are exposed to the same conditions that caused the original modification. The comparison of activity between the tyrosine- and the phenylalanine-containing protein can show that removing a site of tyrosine nitration ablates the effect originally seen. This approach is not always feasible however, as conversion of tyrosine(s) to phenylalanine(s) may adversely affect protein function. A method to site-specifically install nitroTyr is necessary in order to unequivocally demonstrate the impact of a particular site of nitration on protein and cellular function. Genetic code expansion has been used previously to genetically encode nitroTyr into proteins expressed recombinantly in *E. coli* [22-24, 122]. Production of these site-specifically nitrated proteins allowed researchers to show for the first time that a single nitroTyr modification alters the activity of certain proteins *in vitro*. To enable studies of nitroTyr modifications on eukaryotic cellular function, we evolved a pyrrolysyl-aaRS/tRNA pair by performing selections for nitroTyr in *E. coli*. After validating the efficiency and fidelity of this pair in *E. coli*, we produced a human codon optimized version of the MbRS for mammalian cell studies. The nitroTyr-MbRS/tRNA pair was cloned into the pAcBac1 vector along with a TAG-interrupted sfGFP to demonstrate efficient, site-specific incorporation of nitroTyr in HEK293T cells.

The optimized eukaryotic nitroTyr-MbRS/tRNA was used to express site-specifically nitrated MnSOD and 14-3-3 in mammalian cell culture. MnSOD nitrated at tyrosine 34 is implicated in several chronic inflammatory disease. Previous work has indicated that nitrated MnSOD directly leads to the onset of these diseases. The

site-specific modification of this protein in mammalian cells provides the ability to investigate the impact of this modification on mitochondrial and cellular function, and will clarify the role of this modification in the onset of diseases.

It has been well established that the β isoform of human 14-3-3 is nitrated on tyrosine 130 *in vivo* [241-243]. While the impact of tyrosine nitration at this site is unknown, based on available structural data, our hypothesis is that nitration at site 130 will ablate 14-3-3-client interactions. Site-specific encoding of nitroTyr into 14-3-3, enabled here, can be used to test how nitration of 14-3-3 alters protein interactions via immunoprecipitation of nitroTyr-130- and WT-14-3-3 expressed in HEK293T cells. As this modification is genetically encoded we also have the ability to move the site of nitration around on the protein to provide controls to show the site-specific effect of this modification. In addition, we will be able to replace the modification with nitroPhe to contrast the effect from nitroTyr at this site. We expect that a similar pulldown method can be employed with other client-interacting proteins, like Hsp90, to show the nitroTyr-dependent alteration to interacting partners. The development of the eukaryotic nitroTyr-MbRS/tRNA system will also provide access to the investigation of the many reported nitrated membrane channel proteins, which are largely intractable to study in *E. coli*. We anticipate that extension of this approach will provide significantly increased clarity on the effect of the nitroTyr modification on proteins in mammalian cells.

Materials and Methods

Antibodies and Reagents

α-nitroTyrosine (Millipore (Upstate), Cat# 06-284). nitroTyrosine was purchased from Alfa Aesar (#A11018). 3-nitrophenylalanine was purchased from Peptech (#AL280).

nitroTyr tRNA-Synthetase Selection

The library of aminoacyl-tRNA synthetases was encoded on a kanamycin (Kn) resistant plasmid (pBK, 3000 bp) under control of the constitutive *Escherichia coli* GlnRS promoter and terminator. The aminoacyl synthetase library (D3-library) was randomized as follows: Leu270, Tyr271, Leu274, Asn311, and Cys313 were

randomized to all 20 natural amino acids. The library plasmid was moved between cells containing a positive selection plasmid (pREP-pylT) and cells containing a negative selection plasmid (pYOBB2-pylT).

The positive selection plasmid, pREP-pylT (3700 bp), encodes a mutant *Methanosarcina barkeri* pyrrolysyl-tRNA synthetase (MbPylRS), an amber codon-disrupted chloramphenicol acetyltransferase, an amber codon-disrupted T7 RNA polymerase that drives the production of green fluorescent protein, and the tetracycline (Tet) resistance marker. The negative selection plasmid, pYOBB2-pylT (7000 bp), encodes the mutant pyrrolysyl-$tRNA_{CUA}$, an amber codon-disrupted barnase gene under control of an arabinose promoter and rrnC terminator, and the chloramphenicol (Chlor) resistance marker. pREP-pylT electrocompetent cells and pYOBB2-pylT electrocompetent cells were made from DH10B cells carrying the respective plasmids and stored in 100 μL aliquots at −80 °C for future rounds of selection.

The synthetase library in D3-library (800 ng) was transformed by electroporation into 100 uL of DH10B cells containing the positive selection plasmid, pREP-pylT. To ensure complete coverage of the library, ten transformations were performed. All transformations were pooled and rescued for 75 minutes at 37°C and 250 RPM's. The resulting pREP-pylT/D3-Library-containing cells were used to inoculate 1 L of LB with 50 μg/mL Kn and 25 μg/mL Tet with shaking at 37 °C. The cells were grown for 18 hours to saturation, then 6 ml were drawn to inoculate 300 mL of LB. Once the culture reached an OD of 2.4, the cells were pelleted at 5000 RCF for 5 minutes, resuspended in 10 ml of 2xYT and 2.5 mL of 80% glycerol and stored at −80 °C in 1 mL aliquots for use in the first round of selections.

For the first positive selection, 2 mL of pREP-pylT/D3-Library cells were thawed on ice before addition to 1.2 L of room temperature 2×YT media containing 50 μg/mL Kn and 25 μg/mL Tet. After reaching saturation (18 h, 250 rpm, 37 °C), a 6 mL aliquot was used to inoculate 300 ml of LB. Once the culture reached an OD of 2.4, 200 μL aliquot of these cells were plated on eleven 15 cm LB-agar plates containing 25 μg/mL Kan, 12.5 μg/mL Tet, and 40 μg/mL chloramphenicol (Cm). The positive selection agar medium also contained 1 mM of nitroTyr. After spreading, the surface of the plates was allowed to dry completely before incubation (37 °C, 15 h). To harvest

the surviving library members from the plates, 10 mL of 2×YT was added to each plate. Colonies were scraped from the plate using a glass spreader. The resulting solution was incubated with shaking (60 min, 37 °C) to wash cells free of agar. The cells were then pelleted, and plasmid DNA was extracted. For the first positive selection a Qiagen midiprep kit was used to purify the plasmid DNA. For all other plasmid purification steps a Qiagen miniprep kit was used to purify the plasmid DNA. The smaller D3-Library plasmid was separated from the larger pREP-pylT plasmid by agarose gel electrophoresis and extracted from the gel using the Qiagen gel extraction kit.

The purified D3-Library was then transformed into pYOBB2-pylT -containing DH10B cells. A 100 µL sample of pYOBB2-pylT electrocompetent cells was transformed with ≈100 ng of purified D3-Library DNA. Cells were rescued in 1 mL of SOC for 90 minutes (37 °C, 250 rpm) and the entire 1 mL of rescue solution was plated on three 15 cm LB plates containing 40 µg/mL Chlor, 50 µg/mL Kan, and 0.2% L-arabinose. After 18 hours, cells were scraped from plates and D3-Library plasmid DNA was isolated in the same manner as described above for positive selections.

In order to evaluate the success of the selections based on variation in synthetase efficacy (as opposed to traditional survival/death results), the synthetases resulting from the selection rounds were tested with the pALS plasmid. This plasmid contains the sfGFP reporter with a TAG codon at residue 150 as well as pyrrolysyl-$tRNA_{CUA}$. When a Library plasmid with a functional synthetase is transformed with the pALS plasmid and the cells are grown in the presence of the appropriate amino acid on autoinduction agar, sfGFP is expressed and the colonies are visibly green.

Three microliters of each library resulting from the first negative round of selection was transformed with 100 µL of pALS-containing DH10B cells. The cells were rescued for 1.25 hr in 1 mL of SOC (37 °C, 250 rpm). 250 µL and 25 µL of cells from each library were plated on autoinducing minimal media with 50 µg/mL Kan, 25 µg/mL Tet, and 1 mM ncAA. Plates were grown at 37 °C for 24 hours and then allowed to maturate at room temperature for an additional 24 hours.

Autoinducing agar plates were prepared by combining the reagents in Supplementary table S5.3A with an autoclaved solution of 4.5 g of agarose in 400 mL water. Sterile water was added to a final volume of 500 mL. Antibiotics were added to

a final concentration of 25 μg/mL Tet and 50 μg/mL Kan. Plates were poured in duplicate for with/without 1 mM ncAA.

Visually green colonies were selected from the plates and used to innoculate a 96-well plate containing 0.5 mL per well non-inducing media (Supplementary table S5.3B, with sterile water added to a final volume of 500 mL) with 50 μg/mL Kan, 25 μg/mL Tet. 48 colonies were selected from plates containing 1 mM nitroTyr and 24 colonies were selected from plates containing 1 mM 3-nitroPhe. After 18 hours of growth (37 °C, 300 rpm), 10 μL of the 96 concentrated cell cultures were used to inoculate 0.45 ml expressions of autoinduction media (Supplementary table S5.3A, with sterile water added to a final volume of 500 mL) containing 50 μg/mL Kn, 25 μg/mL Tet. Four 96-well expressions (37°C, 300 RPM) were performed, containing either nitroTyr, 3-nitroPhe, or were not supplemented with ncAA. Fluorescence measurements of the cultures were collected 36 hours after inoculation using a BIOTEK® Synergy 2 Microplate Reader. The emission from 528 nm (20 nm bandwidth) was summed with excitation at 485 nm (20 nm bandwidth). Samples were prepared by diluting suspended cells directly from culture 4-fold with phosphate buffer saline (PBS). Results of fluorescence measurements are shown in Supplementary Figure 1.

Mass Spectrometry Analysis

Purified protein was diluted to 100 μM, desalted and concentrated using EMD Millipore C4 resin ZipTips, and analyzed using an FT LTQ mass spectrometer at the Mass Spectrometry Facility at Oregon State University.

Construction of pAcBac for Expression of Nitro-tyrosine-containing Proteins in Eukaryotic Cell Culture

The pAcBac1.tR4-MbPyl plasmid encoding 4 copies of Pyl tRNA and a CMV/BGH cassette for expression of an RS or protein of interest in human cells was a gift from Peter Schultz (Addgene plasmid # 50832) [50]. In order to generate a human codon optimized version of the A7 nitroTyr MbRS, the WT human codon optimized MbRS (a kind gift from Jason Chin) was amplified with primers (pJET1.2 for and P194T rev, for primer sequences see Supporting table S5.2), (P194T for and

L282 rev), (L282R for and N319G/C321N rev), and (N319G/C321N for and pylRS rev) in separate reactions. The purified PCR products from the above reactions were mixed at an equimolar ratio and PCR amplified with pJET1.2 for and pylRS rev to yield the entire A7 MbRS. In order to generate a human codon optimized version of the F4 nitroTyr MbRS, the WT human codon optimized MbRS was amplified with primers (JP1 and JP2), (JP3 and JP4), and (JP5 and JP6) in separate reactions. The resulting PCR pieces were assembled via PPY-based SLiCE reaction [257] into a CMV-BGH-cassette-containing pUC19 plasmid and the F4 MbRS was sequence verified. To construct the pAcBac1-sfGFP and pAcBac1-MbRS, WT or TAG 150 sfGFP was PCR amplified with primers (JP7 and JP8), the human codon optimized A7 or F4 MbRS was PCR amplified with primers (JP9 and JP10), and the resulting products were inserted downstream of the CMV promoter between the EcoRI and NheI restriction sites in pAcBac1.

Eukaryotic Cell culture and viability assessment

HEK293T cells were gift of Colin Johnson at Oregon State University. The cells were maintained in Dulbecco's modified Eagle's media (Corning) supplemented with 10% fetal bovine serum (VWR) and penicillin/streptomycin (Corning). Subculture of cells was done twice a week using trypsin/EDTA (Corning). HEK293T cells were plated in a white 96-well plate (Greiner) at a density of 3,000 cells per well and incubated for 48 h with 3-Cl-Tyr (ArkPharm AK-50086), 3-Br-Tyr (ArkPharm AK-82171), or vehicle at concentrations indicated in the figure. Cell viability was measured using CellTiter Glo assay kit (Promega) according to the manufacturer's protocol. The luminescence signal was recorded using TR717 microplate luminometer (Berthold) and WinGlow software (Berthold). The data was normalized to vehicle control and fitted to a curve using nonlinear regression method in GraphPad Prism 5 software (GraphPad Software).

Flow cytometry

HEK293T cells were dissociated into single cells by trypsin/EDTA and washed twice with PBS. Cells were resuspended in PBS and subjected to flow cytometry. Twenty thousand events were collected using CytoFlex (Beckman

Coulter) and CytExpert software (Beckman Coulter). Dead cells and cell aggregates were excluded from analysis by gating and doublet discrimination. The ratio and mean fluorescence intensity of GFP positive or negative populations were calculated using FlowJo v10 software (FlowJo).

Eukaryotic ncAA-protein mass spectrometry

HEK293T cells were transfected as described in transfection and imaging. Cells were washed twice with PBS and resuspended in PBS containing 1x protease inhibitor cocktail (Thermo Fisher Scientific). Cells were sonicated three times for 10 sec each time using Fisher dismembrator model 60 with microprobe. Lysed cells were centrifuged for 10 min at 21,000 x g at 4°C. The supernatant was used for purification of expressed sfGFP protein using TALON metal affinity chromatography. Purified protein was concentrated to 30 μL via spin concentrator, desalted and further concentrated using EMD Millipore C4 resin ZipTips, and analyzed using an FT LTQ mass spectrometer at the Mass Spectrometry Facility at Oregon State University.

In gel fluorescence

Lysate of HEK293T cells transfected with MnSOD or 14-3-3 mEGFP fusion in Laemmli buffer without heating was separated on a 12% SDS-PAGE gel. The gel was imaged using the UV transilluminator on a ChemiDoc XRS+ (Biorad).

Acknowledgments

This work was supported by grants from the National Institutes of Health Grant RGM114653A (to R.A.M.). We thank Yongwei Zhang (Albert Einstein College of Medicine) for the PPY strain used for SLiCE cloning.

Supporting Table S5.1. Sequences of *M. barkeri* 3-nitrotyrosine synthetase hits.

Mb Pyl RS hit	**Leu270**	**Tyr271**	**Leu274**	**Asn311**	**Cys313**	**Off Site**
D1	Leu	Tyr	Leu	Ser	Cys	I215V/I285V
B2	Leu	Tyr	Leu	Ser	Cys	
C2	Leu	Tyr	Leu	Ser	Ala	
B3	Phe	Tyr	Leu	Ser	Cys	E330G
E3	Leu	Tyr	Leu	Ser	Cys	N401T
H3	Leu	Tyr	Leu	Cys	Ala	
A4	Leu	Tyr	Leu	Ser	Ser	
D4	Leu	Tyr	Leu	Cys	Cys	
E4	Phe	Tyr	Leu	Cys	Cys	T269A
F4	Leu	Tyr	Leu	Ser	Ser	
G4	Leu	Tyr	Leu	Cys	Ser	
C5	Leu	Tyr	Leu	Gly	Ser	
B6	Gln	Tyr	Leu	Gly	Thr	
E6	Leu	Tyr	Leu	Gly	Thr	
A7	Leu	Tyr	Arg	Gly	Asn	P186T

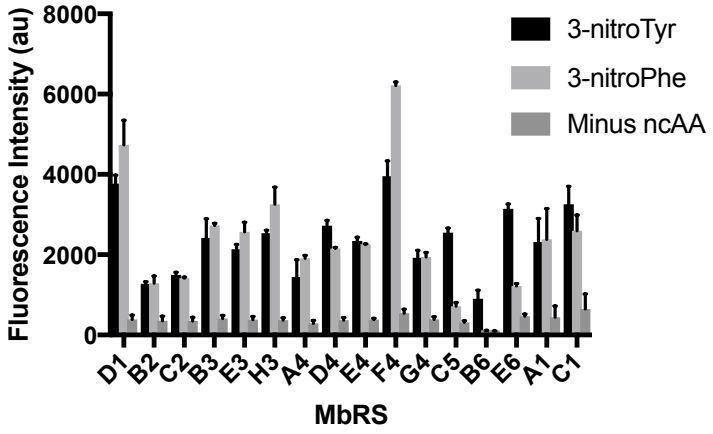

Supporting Figure 5.1. Results of initial screening of synthetase hits from library selection.

Assessment of fluorescence from culture expressing the sfGFP150TAG gene along with each of the 14 unique *M. barkeri* pyrrolysyl synthetase variants identified from the selection process. Cultures were expressed in the presence of 1 mM 3-nitroTyr (black), 1 mM 3-nitroPhe (light grey), or in the absence of ncAA (dark grey).

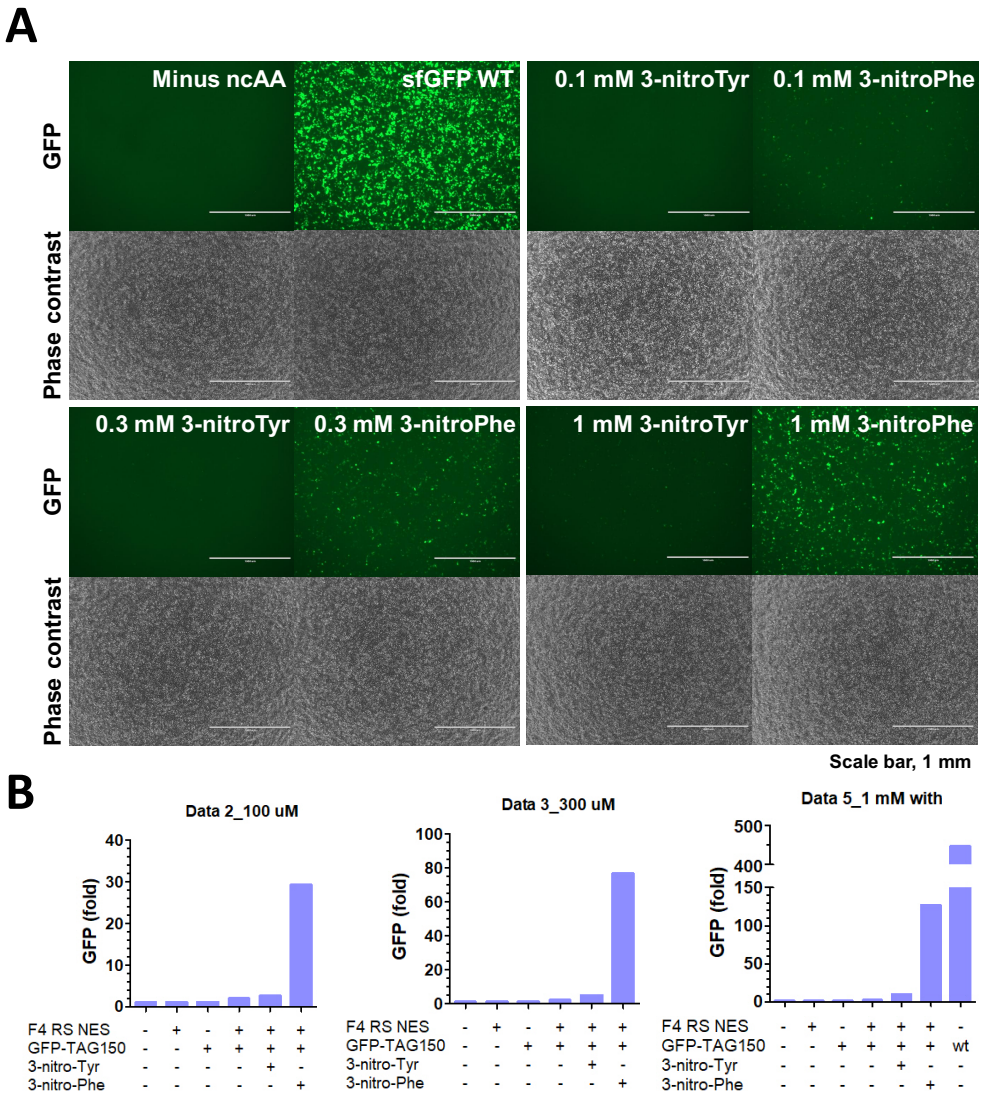

Supporting Figure 5.2. TAG suppression by the F4 synthetase/tRNA pair in HEK293T cells.

(**A**) HEK293T cells transfected for 48 hours with sfGFP-150TAG pAcBac1 and F4 synthetase/tRNA in media supplemented with the indicated amount of ncAA were imaged on an EVOS FL imaging system. In the panel labeled sfGFP WT, a pAcBac1 containing the WT sfGFP gene was used in place of the sfGFP-150TAG pAcBac1. (**B**) The relative level of sfGFP fluorescence at each concentration of ncAA is quantified based on flow cytometry data.

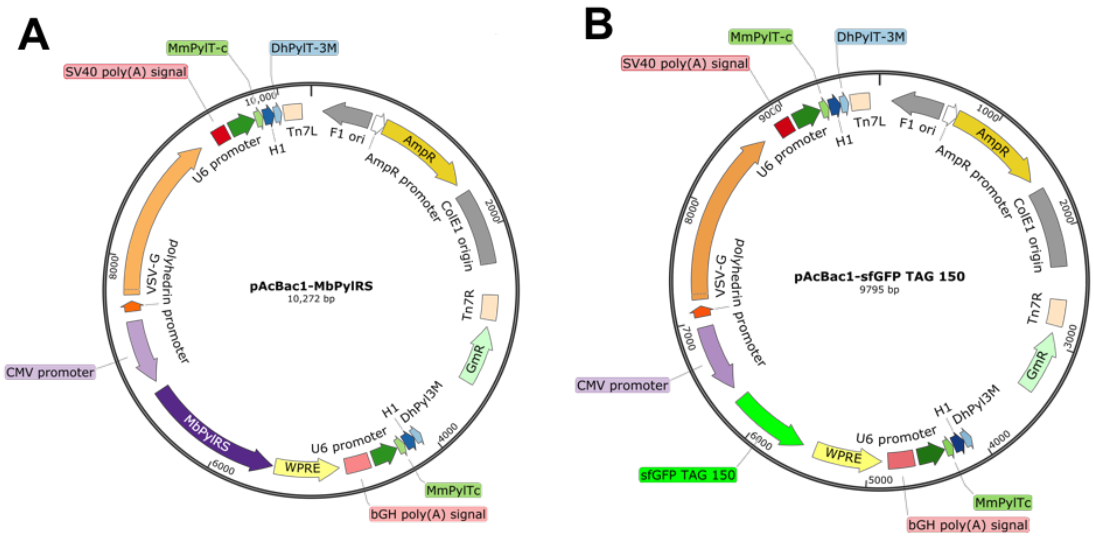

Supporting Figure 5.3. pAcBac1 expression vector maps.
(A) pAcBac1-MbPylRS. **(B)** pAcBac1-sfGFP TAG 150.

Supporting Table S5.2. DNA oligomers used to construct eukaryotic expression vectors.

	Primer Sequence
pJET1.2 for	5’ CGACTCACTATAGGGAGAGCGGC 3’
P194T for	5’ CGGGAGCTGGAAACCGAGCTGGTGA 3’
P194T rev	5’ TCACCAGCTCGGTTTCCAGCTCCCG 3’
L282R for	5' CTGTACAACTACAGGCGGAAACTGG 3'
L282R rev	5' CCAGTTTCCGCCTGTAGTTGTACAG 3'
N319G/C321N for	5’ GTTTACAATGGTGGGCTTTAACCAGATGGGCAGCGG 3’
N319G/C321N rev	5’ CCGCTGCCCATCTGGTTAAAGCCCACCATTGTAAAC 3’
pylRS rev	5’ GACTCGAGCGGCCGCCACTGTG 3’
JP1	5’-TAAACTTgctagcgccGCCACCATGGACTACAAGGACGACG ACGACAAGG ACAAGAAA-3’
JP2	5’-caggtagttgtaAAAGGCgggggccagc-3’
JP3	5’-gctggccccGCCTTTtacaactacctg-3’
JP4	5’-cccatctggcaaaaGCAcaccattgtaaactc-3’
JP5	5’-gagtttacaatggtgTGCttttgccagatggg-3’
JP6	5’-CAGCGGGTTTAAACGGGCCCTCTAGTCATCACAGGTTG GTGCTGATGC CGTTGTAGTAGC-3’
JP7	5’-CTGTGTGCTAGCgccgccaccATGGTTTCTAAAGGTGAAGA ACTTTTTACTGG-3’
JP8	5’-ctgcaaGAATTCTTAGTGGTGATGGTGGTGATGAGTAGAA TCCAGTCCC-3’
JP9	5’-TAAACTTgctagcGCCACCATGGCGTGTCCGGTTCCTTTGC AGTTGCCTCC-3’
JP10	5’-AGTggagaattcTCATCACAGGTTGGTGCTGATGCCGTTGTA GTAGCTCTCGC-3’

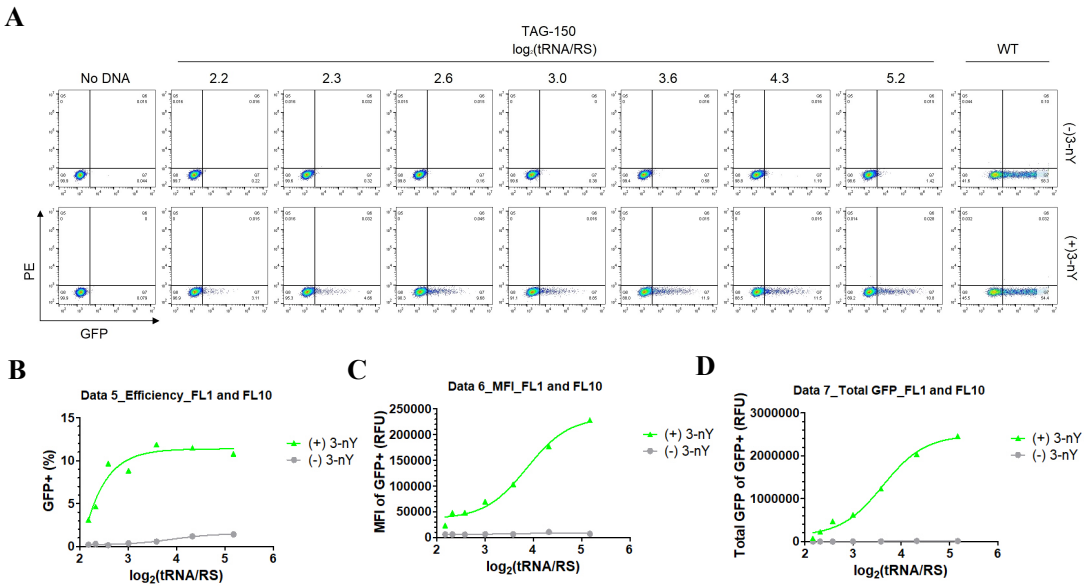

Supporting Figure 5.4. Flow cytometry analysis of TAG suppression in eukaryotic cells varying the ratio of tRNA to synthetase.

(**A**) HEK293T cells transfected with varying ratios of A7 synthetase/tRNA and sfGFP-150TAG pAcBac1 were analyzed by flow cytometry. The GFP axis shows GFP fluorescence and the PE axis shows PE fluorescence, a negative control. (**B**) The ratio of GFP positive population shows the fraction of cells expressing GFP at a level that is higher than the background. (**C**) The mean fluorescence intensity (MFI) of the cells is shown as a function the ratio of tRNA to MbRS. (**D**) The relative level of total GFP fluorescence was calculated by multiplying the ratio and MFI of each population.

Supporting Table S5.3. Media used in selections and expressions.

	A) Autoinducing Media	**B) Noninducing Media**
5% Aspartate, pH 7.5	25 ml	25 ml
10% Glycerol	25 ml	---
25 x 18 amino acid mix	20 ml	20 ml
25 x M-salts	20 ml	20 ml
Leucine (4 mg/ml), pH 7.5	5 ml	5 ml
20% Arabinose (w/v)	1.25 ml	---
1 M $MgSO_4$	1 ml	1 ml
40% Glucose	625 ul	6.25 ml
Trace Metals	100 ul	100 ul
	Fill to 500 mL with sterile water	

Chapter 6

Concluding Discussion and Outlook

Conclusion and Outlook

All of the studies presented in this dissertation highlight the use of GCE to address the role of the PTM, nitroTyr, in biological systems. Below, I detail the highlights and potential impacts of the work described here, both in terms of the specific alteration to CaM regulatory function resulting from tyrosine nitration and the application of GCE to studying tyrosine nitration in general. Then, I will suggest future directions that I feel are warranted based on the studies presented here and the existing body of literature on nitroTyr and GCE.

Impacts and Highlights of Reported Work

Reviewing the use of genetic code expansion for the study of oxidative post-translational modifications

A major roadblock to studying the effects of Ox-PTMs on protein function is the ability to generate pure site-specifically modified Ox-PTM protein. GCE has emerged as a way to study many of the regulatory PTMs like phosphorylation, acetylation, and ubiquitination [237]. Work in the Mehl lab previously has generated a system to genetically incorporate nitroTyr. Throughout this process it became clear that the development of GCE tools will rely both on those from the GCE field and the oxidative stress field. NitroTyr serves as a paradigm for the development of GCE tools to study Ox-PTMs – nitroTyr presence resulting from oxidative stresss was identified in biological samples, a GCE system was developed to incorporate this ncAA, the oxidative stress field embraced the use of this tool, and to address more challenging problems refinement of the GCE system was necessary. In our review we wanted to highlight this paradigm as well as the strengths and weaknesses of GCE for the study of Ox-PTMs so that those in the oxidative stress field have a clearer idea of what GCE requires and has to offer.

Improving the M. jannaschii tyrosyl-aaRS/tRNA pair by suppressor tRNA mutants

At its core, GCE requires the addition of orthogonal systems to translation. Largely these systems are aaRS/tRNA pairs that must be orthogonal to all of the cellular aaRS/tRNA pairs and must recognize an ncAA. In nature these three component systems co-evolve optimizing both orthgonality and efficiency

simultaneously. These systems have been selected such that the aaRS recognition of the amino acid is connected to tRNA recognition through long range allosteric modulators. This means that each time an active site is altered to accept a new ncAA the tRNA or the portions of the aaRS interacting with the tRNA need to be altered or the system will sacrifice orthogonality and efficiency. Over the course of its 15-year development the GCE field has relied on the original suppressor tRNA selected for incorporation of the first ncAA into recombinant protein in *E. coli*. It has become clear, based on production of ncAA-containing protein, that there are notable inefficiencies in the translational apparatus for incorporation of ncAAs. We were able to show that *in vitro* enzyme assays of aaRS/tRNA pair kinetics correlate to *in vivo* ncAA-containing protein expression. This allowed us to show that some of the mutations made to the *M. jannaschii* $tRNA^{Tyr}$ in order to make it orthogonal in *E. coli* are not required for orthogonality and deleterious to function. While we were studying this in the context of the incorporation of nitroTyr, these insights are generalizable. There are *M. jannaschii* GCE systems for incorporating a diverse range of chemical functionality like bioorthogonal reactive handles, photocrosslinkers, or PTMs into proteins, all of which can be incorporated more efficiently employing our novel tRNA uncovered in this work.

Tyrosine Nitration on Calmodulin Regulates Calcium Sensing and Response

A major question in the oxidative stress field is whether tyrosine nitration can regulate protein function? The calcium regulatory protein CaM is known to be nitrated on both tyrosines *in vivo*. Here I have shown that nitration of either of these tyrosines results in altered Ca^{2+}-dependent regulation of eNOS function. Nitration of CaM at tyrosine 99 results in increased binding to eNOS at low physiological Ca^{2+} levels and lower production of $NO^{\bullet}$, while CaM nitrated at tyrosine 138 exhibits a similar increased affinity for eNOS at low Ca^{2+} levels but it stimulates eNOS to produce more $NO^{\bullet}$ than WT CaM. I recapitulated these results for nitro-CaM-138 in HEK-eNOS cell lysate, indicating that the pool of nitrated CaM can activated eNOS at low Ca^{2+} levels in the cell. This constitutes a clear gain-of-function alteration to Ca^{2+}-dependent activation of eNOS signaling by the installation of nitroTyr on CaM.

Genetically encoded tyrosine nitration in mammalian cells

A clear need to study Ox-PTMs in the context of an entire cell exists in the oxidative stress field. To that end, I developed the first eukaryotic cell compatible methods for site-specific installation of nitroTyr into proteins. This involved evolving an orthogonal nitrotyrosyl-PylRS/tRNA pair in *E. coli*, producing a human codon optimized version in a eukaryotic expression vector, and transfecting it into human cells. This system was validated using sfGFP and shown to contain the native Ox-PTM, nitroTyr, using mass spectrometry. To demonstrate the generality of the nitroTyr-MbRS/tRNA pair, I applied this system to the expression of the physiologically nitrated proteins MnSOD and 14-3-3.

Directions of Future Research

While we have developed several tools for probing the effect of tyrosine nitration on protein structure and regulation of protein interactions, there are still refinements to be made and new areas to be explored. In particular we have outlined new Ox-PTMs that may be addressed in the future by GCE, pinpointed inadequacies in the *M. jannaschii* GCE system that need to be addressed, and uncovered features associated with CaM nitration that require further investigation. There are many directions that this research can be taken, here I describe several that are of particular interest.

New GCE systems for incorporating Ox-PTMs

If we look at the majority of the Ox-PTMs previously encoded via GCE, they are almost all tyrosine derviatives, likely because of the early adoption of the *M. jannaschii* tyrosyl-aaRS-tRNA pair, which was amenable to evolution for incorporating tyrosine derivative ncAAs. An exciting development in the past few years is the development of designer aaRS-tRNA pairs, specifically 'liberated' *E. coli* trypotophanyl- and tyrosyl-aaRS-tRNA pairs, which can be evolved in *E. coli* and applied in eukaryotes [71, 258]. These systems function by importing either a tryptophanyl- or tyrosyl- aaRS-tRNA pair from yeast into *E. coli*, thus liberating the *E. coli* aaRS-tRNA pair for evolution. One tryptophan Ox-PTM has been incorporated via the liberated tryptophanyl-aaRS-tRNA pair [71] and likely this

system can be further evolved to incorporate many of the other tryptophan Ox-PTMs. Given the interest in cysteine and methionine Ox-PTMs, similar systems for incorporating these families of Ox-PTMs could be generated in an analogous fashion in the future.

Many Ox-PTMs are inherently unstable and difficult to isolate and handle. GCE presents ways to address these problems through genetically encoding chemically-caged or photocaged stable Ox-PTM precursors.

Evolving the *M. jannaschii* tyrosyl-tRNA^{Tyr} for more efficient GCE

Our work characterizing the *in vitro* kinetics of the evolved *M. jannaschii* tyrosyl-aaRS-tRNA variants has clearly shown that affinity of the aaRS for the tRNA is compromised in the evolution process [259]. Likely this is because natural aaRS/tRNA/aa systems co-evolve, while GCE systems have been evolved piecemeal. In order to match the levels of efficiency displayed by natural translation we will need to address this. We will likely need to create libraries of both tRNA and aaRS mutants at sites predicted to influence aaRS-tRNA interactions and select mutants with increased efficiency. Successive rounds of selection using either the aaRS or tRNA library punctuated by assessment by *in vitro* assays will allow us to further pinpoint the inefficiencies of this system. If this method of development proves successful for the *M. jannaschii* system it will likely be amenable to application to the pyrrolysyl-aaRS-tRNA pair and the other designer orthogonal systems mentioned above.

The impact of calmodulin tyrosine nitration

While it is clear that CaM is nitrated *in vivo*, it remains challenging to assess the cellular- and tissue-level localization of this modification and under what conditions it forms. A major challenge for the detection of nitroTyr-CaM is the poor sensitivity of the commercially available nitroTyr antibodies for this Ox-PTM protein. Using pure nitroTyr-CaM produced using GCE, between 200 and 500 ng are required in order to detect this Ox-PTM on a western blot with the best-performing (for nitroTyr-CaM) commercial nitroTyr antibody. A good antibody for detecting this Ox-PTM-protein would be able to detect on the order of 10-100 pg nitroTyr-CaM. The current commercial nitroTyr antibody sensitivity is not amenable for detection of

nitroTyr-CaM in endogenous tissue samples. Elise Van Fossen in the Mehl lab is working to overcome this limitation by generating new recombinant antibodies [260] and camelid nanobodies [261] for nitroTyr CaM in collaboration with the Jim Wells and the Recombinant Antibody Network, and the OSU College of Veterinary Medicine. The generation of recombinant antibodies or nanobodies specific for nitrated CaM would open up many avenues for tracking the production and localization of this Ox-PTM modified protein *in vivo* both *in situ* and via western blot from specific tissues.

While it is striking that eNOS produces both of the chemical species, $O_2^{\bullet-}$ and $^{\bullet}NO$ needed to generate $ONOO^-$, which nitrates CaM, the specifics of how much nitration actually occurs are unknown. As calcium alters the conformation adopted by CaM, I would predict that the presence of calcium may affect the stoichiometry of Tyr99 and Tyr138 nitration. Further, the interaction of CaM with eNOS may influence this stoichiometry as well. As the sites of nitration differentially regulate eNOS function it will be important to determine in more detail these stoichiometries either by assaying CaM following *in vitro* eNOS reactions or isolating CaM associated with eNOS *in vivo* via mass spectrometry.

In collaboration with Kelsey Kean in the Karplus lab at OSU we have preliminary structural data on both WT- and nitroTyr-CaM-138 in complex with the eNOS CaM binding domain peptide. These structural characterizations do not particularly illuminate the differences in regulation seen from the Ox-PTM. As the dynamics of the CaM-eNOS interaction are particularly important for protein function, likely methods to characterize this interaction in more dynamic environments will yield more information. In the past both NMR [32, 220] and cryo EM [233] have been employed to characterize the interaction. In particular cryo EM has provided significant insights into the effect of CaM on full length eNOS sampling different conformations and have helped describe how mutations in NOS affect protein function [233].

We are also seeking to extend our findings with nitroTyr-CaM and eNOS, and investigate the phenotype in tissue or a whole organism. Genetic code expansion has been shown to work in several different tissues and organisms [262]. The Mehl lab

has been working to employ GCE in zebrafish, which will prove useful as a model system to investigate the phenotype of the nitroTyr-CaM-eNOS interaction *in vivo*. This will also allow us to investigate the global effect of CaM tyrosine nitration in the organism. While this system is still in development, GCE in zebrafish has been shown to work by others and this will likely play a key part in determining the regulatory effect of tyrosine nitration in the future.

Genetically encoding nitroTyr in mammalian cell culture

While we have demonstrated that specific incorporation of nitroTyr into proteins in HEK cells, we would like to have access to other cell types and tighter control over ncAA-protein protein in mammalian cell culture. Several methods have been developed to address these issues in mammalian cell culture, and even for application in isolated tissues. These methods include viral delivery of GCE machinery [50, 246] and methods for generating stable cell lines [263]. We are exploring these possibilities as a way to investigate tyrosine nitration in more challenging proteins like transmembrane proteins and more challenging cell lines like neuronal cell types, which will be key for the application of GCE in mammalian cell culture.

Concluding remarks

In this dissertation I have presented a series of research projects surrounding the effect of the Ox-PTM, nitroTyr. I described the development of GCE systems with which to study this modification and how we can employ these systems to begin to address the role of this modification in regulation. These studies contribute not only to the understanding how tyrosine nitration alters the regulation of a particular protein (e.g. CaM) but also that we should be cognizant of the role of tyrosine nitration may play in regulating other cellular functions. It is my hope that the reader can appreciate not only the difficulty inherent in studying Ox-PTMs but also the power of GCE to overcome some major hurdles for determining the role of modifications like nitroTyr in biology.

Bibliography

1. Sies, H., Oxidative stress: a concept in redox biology and medicine. *Redox Biol* **2015,** *4*, 180-3.
2. Spickett, C. M.; Pitt, A. R., Protein oxidation: role in signalling and detection by mass spectrometry. *Amino acids* **2012,** *42* (1), 5-21.
3. Krebs, E. G.; Fischer, E. H., Phosphorylase activity of skeletal muscle extracts. *The Journal of biological chemistry* **1955,** *216* (1), 113-20.
4. Sies H., J. D., Oxidative Stress. In *Encyclopedia of Stress*, 2nd ed.; G., F., Ed. Elsevier: Amsterdam, 2007; Vol. 3, pp 45-48.
5. Uttara, B.; Singh, A. V.; Zamboni, P.; Mahajan, R. T., Oxidative stress and neurodegenerative diseases: a review of upstream and downstream antioxidant therapeutic options. *Curr Neuropharmacol* **2009,** *7* (1), 65-74.
6. Huie, R. E.; Padmaja, S., The reaction of no with superoxide. *Free Radic Res Commun* **1993,** *18* (4), 195-9.
7. Pacher, P.; Beckman, J. S.; Liaudet, L., Nitric oxide and peroxynitrite in health and disease. *Physiol Rev* **2007,** *87* (1), 315-424.
8. Radi, R.; Beckman, J. S.; Bush, K. M.; Freeman, B. A., Peroxynitrite oxidation of sulfhydryls. The cytotoxic potential of superoxide and nitric oxide. *The Journal of biological chemistry* **1991,** *266* (7), 4244-50.
9. Castro, L.; Rodriguez, M.; Radi, R., Aconitase is readily inactivated by peroxynitrite, but not by its precursor, nitric oxide. *The Journal of biological chemistry* **1994,** *269* (47), 29409-15.
10. Tsai, J.-H. M.; Harrison, J. G.; Martin, J. C.; Hamilton, T. P.; van der Woerd, M.; Jablonsky, M. J.; Beckman, J. S., Role of Conformation of Peroxynitrite Anion (ONOO-) with Its Stability and Toxicity. *Journal of the American Chemical Society* **1994,** *116* (9), 4115-4116.
11. Radi, R., Nitric oxide, oxidants, and protein tyrosine nitration. *Proc Natl Acad Sci U S A* **2004,** *101* (12), 4003-8.
12. Haddad, I. Y.; Pataki, G.; Hu, P.; Galliani, C.; Beckman, J. S.; Matalon, S., Quantitation of nitrotyrosine levels in lung sections of patients and animals with acute lung injury. *The Journal of clinical investigation* **1994,** *94* (6), 2407-13.
13. Ye, Y. Z.; Strong, M.; Huang, Z. Q.; Beckman, J. S., Antibodies that recognize nitrotyrosine. *Methods in enzymology* **1996,** *269*, 201-9.
14. Chin, J. W., Expanding and reprogramming the genetic code. *Nature* **2017,** *550* (7674), 53-60.
15. Dumas, A.; Lercher, L.; Spicer, C. D.; Davis, B. G., Designing logical codon reassignment - Expanding the chemistry in biology. *Chemical science* **2015,** *6* (1), 50-69.
16. Wang, L.; Xie, J.; Schultz, P. G., Expanding the genetic code. *Annual review of biophysics and biomolecular structure* **2006,** *35*, 225-49.
17. Wang, L.; Brock, A.; Herberich, B.; Schultz, P. G., Expanding the genetic code of Escherichia coli. *Science (New York, N.Y.)* **2001,** *292* (5516), 498-500.

18. Wang, L.; Schultz, P. G., A general approach for the generation of orthogonal tRNAs. *Chemistry & biology* **2001,** *8* (9), 883-90.
19. Cooley, R. B.; Feldman, J. L.; Driggers, C. M.; Bundy, T. A.; Stokes, A. L.; Karplus, P. A.; Mehl, R. A., Structural basis of improved second-generation 3-nitro-tyrosine tRNA synthetases. *Biochemistry* **2014,** *53* (12), 1916-24.
20. Miyake-Stoner, S. J.; Miller, A. M.; Hammill, J. T.; Peeler, J. C.; Hess, K. R.; Mehl, R. A.; Brewer, S. H., Probing protein folding using site-specifically encoded unnatural amino acids as FRET donors with tryptophan. *Biochemistry* **2009,** *48* (25), 5953-62.
21. Cooley, R. B.; Karplus, P. A.; Mehl, R. A., Gleaning unexpected fruits from hard-won synthetases: probing principles of permissivity in non-canonical amino acid-tRNA synthetases. *Chembiochem : a European journal of chemical biology* **2014,** *15* (12), 1810-9.
22. Neumann, H.; Hazen, J. L.; Weinstein, J.; Mehl, R. A.; Chin, J. W., Genetically encoding protein oxidative damage. *J Am Chem Soc* **2008,** *130* (12), 4028-33.
23. Franco, M. C.; Ye, Y.; Refakis, C. A.; Feldman, J. L.; Stokes, A. L.; Basso, M.; Melero Fernandez de Mera, R. M.; Sparrow, N. A.; Calingasan, N. Y.; Kiaei, M.; Rhoads, T. W.; Ma, T. C.; Grumet, M.; Barnes, S.; Beal, M. F.; Beckman, J. S.; Mehl, R.; Estevez, A. G., Nitration of Hsp90 induces cell death. *Proc Natl Acad Sci U S A* **2013,** *110* (12), E1102-11.
24. DiDonato, J. A.; Aulak, K.; Huang, Y.; Wagner, M.; Gerstenecker, G.; Topbas, C.; Gogonea, V.; DiDonato, A. J.; Tang, W. H.; Mehl, R. A.; Fox, P. L.; Plow, E. F.; Smith, J. D.; Fisher, E. A.; Hazen, S. L., Site-specific nitration of apolipoprotein A-I at tyrosine 166 is both abundant within human atherosclerotic plaque and dysfunctional. *The Journal of biological chemistry* **2014,** *289* (15), 10276-92.
25. Berridge, M. J.; Bootman, M. D.; Roderick, H. L., Calcium signalling: dynamics, homeostasis and remodelling. *Nature reviews. Molecular cell biology* **2003,** *4* (7), 517-29.
26. Smallwood, H. S.; Galeva, N. A.; Bartlett, R. K.; Urbauer, R. J.; Williams, T. D.; Urbauer, J. L.; Squier, T. C., Selective nitration of Tyr99 in calmodulin as a marker of cellular conditions of oxidative stress. *Chemical research in toxicology* **2003,** *16* (1), 95-102.
27. Smallwood, H. S.; Lourette, N. M.; Boschek, C. B.; Bigelow, D. J.; Smith, R. D.; Pasa-Tolic, L.; Squier, T. C., Identification of a denitrase activity against calmodulin in activated macrophages using high-field liquid chromatography--FTICR mass spectrometry. *Biochemistry* **2007,** *46* (37), 10498-505.
28. Kretsinger, R. H.; Nockolds, C. E., Carp muscle calcium-binding protein. II. Structure determination and general description. *The Journal of biological chemistry* **1973,** *248* (9), 3313-26.
29. Nakayama, S.; Moncrief, N. D.; Kretsinger, R. H., Evolution of EF-hand calcium-modulated proteins. II. Domains of several subfamilies have diverse evolutionary histories. *Journal of molecular evolution* **1992,** *34* (5), 416-48.
30. Carafoli, E.; Krebs, J., Why Calcium? How Calcium Became the Best Communicator. *The Journal of biological chemistry* **2016,** *291* (40), 20849-20857.

31. Marshall, C. B.; Nishikawa, T.; Osawa, M.; Stathopulos, P. B.; Ikura, M., Calmodulin and STIM proteins: Two major calcium sensors in the cytoplasm and endoplasmic reticulum. *Biochemical and biophysical research communications* **2015,** *460* (1), 5-21.
32. Piazza, M.; Futrega, K.; Spratt, D. E.; Dieckmann, T.; Guillemette, J. G., Structure and dynamics of calmodulin (CaM) bound to nitric oxide synthase peptides: effects of a phosphomimetic CaM mutation. *Biochemistry* **2012,** *51* (17), 3651-61.
33. Salas, V.; Sanchez-Torres, J.; Cusido-Hita, D. M.; Garcia-Marchan, Y.; Sojo, F.; Benaim, G.; Villalobo, A., Characterisation of tyrosine-phosphorylation-defective calmodulin mutants. *Protein expression and purification* **2005,** *41* (2), 384-92.
34. Corti, C.; Leclerc L'Hostis, E.; Quadroni, M.; Schmid, H.; Durussel, I.; Cox, J.; Dainese Hatt, P.; James, P.; Carafoli, E., Tyrosine phosphorylation modulates the interaction of calmodulin with its target proteins. *European journal of biochemistry* **1999,** *262* (3), 790-802.
35. Panina, S.; Stephan, A.; la Cour, J. M.; Jacobsen, K.; Kallerup, L. K.; Bumbuleviciute, R.; Knudsen, K. V.; Sanchez-Gonzalez, P.; Villalobo, A.; Olesen, U. H.; Berchtold, M. W., Significance of calcium binding, tyrosine phosphorylation, and lysine trimethylation for the essential function of calmodulin in vertebrate cells analyzed in a novel gene replacement system. *The Journal of biological chemistry* **2012,** *287* (22), 18173-81.
36. Gao, J.; Yin, D.; Yao, Y.; Williams, T. D.; Squier, T. C., Progressive decline in the ability of calmodulin isolated from aged brain to activate the plasma membrane Ca-ATPase. *Biochemistry* **1998,** *37* (26), 9536-48.
37. Gao, J.; Yao, Y.; Squier, T. C., Oxidatively modified calmodulin binds to the plasma membrane Ca-ATPase in a nonproductive and conformationally disordered complex. *Biophysical journal* **2001,** *80* (4), 1791-801.
38. Montgomery, H. J.; Bartlett, R.; Perdicakis, B.; Jervis, E.; Squier, T. C.; Guillemette, J. G., Activation of constitutive nitric oxide synthases by oxidized calmodulin mutants. *Biochemistry* **2003,** *42* (25), 7759-68.
39. Lee, D. Y.; Wauquier, F.; Eid, A. A.; Roman, L. J.; Ghosh-Choudhury, G.; Khazim, K.; Block, K.; Gorin, Y., Nox4 NADPH oxidase mediates peroxynitrite-dependent uncoupling of endothelial nitric-oxide synthase and fibronectin expression in response to angiotensin II: role of mitochondrial reactive oxygen species. *The Journal of biological chemistry* **2013,** *288* (40), 28668-86.
40. Tran, Q. K.; Black, D. J.; Persechini, A., Intracellular coupling via limiting calmodulin. *The Journal of biological chemistry* **2003,** *278* (27), 24247-50.
41. Quillon, A.; Fromy, B.; Debret, R., Endothelium microenvironment sensing leading to nitric oxide mediated vasodilation: a review of nervous and biomechanical signals. *Nitric oxide : biology and chemistry* **2015,** *45*, 20-6.
42. Dudzinski, D. M.; Michel, T., Life history of eNOS: partners and pathways. *Cardiovascular research* **2007,** *75* (2), 247-60.
43. Tran, J.; Magenau, A.; Rodriguez, M.; Rentero, C.; Royo, T.; Enrich, C.; Thomas, S. R.; Grewal, T.; Gaus, K., Activation of Endothelial Nitric Oxide

(eNOS) Occurs through Different Membrane Domains in Endothelial Cells. *PloS one* **2016,** *11* (3), e0151556.

44. Tran, Q. K.; Leonard, J.; Black, D. J.; Nadeau, O. W.; Boulatnikov, I. G.; Persechini, A., Effects of combined phosphorylation at Ser-617 and Ser-1179 in endothelial nitric-oxide synthase on EC50(Ca2+) values for calmodulin binding and enzyme activation. *The Journal of biological chemistry* **2009,** *284* (18), 11892-9.
45. Haque, M. M.; Ray, S. S.; Stuehr, D. J., Phosphorylation Controls Endothelial Nitric-oxide Synthase by Regulating Its Conformational Dynamics. *The Journal of biological chemistry* **2016,** *291* (44), 23047-23057.
46. Srinivasan, G.; James, C. M.; Krzycki, J. A., Pyrrolysine encoded by UAG in Archaea: charging of a UAG-decoding specialized tRNA. *Science (New York, N.Y.)* **2002,** *296* (5572), 1459-62.
47. Wan, W.; Tharp, J. M.; Liu, W. R., Pyrrolysyl-tRNA synthetase: an ordinary enzyme but an outstanding genetic code expansion tool. *Biochimica et biophysica acta* **2014,** *1844* (6), 1059-70.
48. Mukai, T.; Kobayashi, T.; Hino, N.; Yanagisawa, T.; Sakamoto, K.; Yokoyama, S., Adding l-lysine derivatives to the genetic code of mammalian cells with engineered pyrrolysyl-tRNA synthetases. *Biochemical and biophysical research communications* **2008,** *371* (4), 818-22.
49. Hancock, S. M.; Uprety, R.; Deiters, A.; Chin, J. W., Expanding the genetic code of yeast for incorporation of diverse unnatural amino acids via a pyrrolysyl-tRNA synthetase/tRNA pair. *J Am Chem Soc* **2010,** *132* (42), 14819-24.
50. Chatterjee, A.; Xiao, H.; Bollong, M.; Ai, H. W.; Schultz, P. G., Efficient viral delivery system for unnatural amino acid mutagenesis in mammalian cells. *Proc Natl Acad Sci U S A* **2013,** *110* (29), 11803-8.
51. Xia, X. G.; Zhou, H.; Ding, H.; Affar el, B.; Shi, Y.; Xu, Z., An enhanced U6 promoter for synthesis of short hairpin RNA. *Nucleic acids research* **2003,** *31* (17), e100.
52. Maquat, L. E.; Kinniburgh, A. J.; Rachmilewitz, E. A.; Ross, J., Unstable beta-globin mRNA in mRNA-deficient beta o thalassemia. *Cell* **1981,** *27* (3 Pt 2), 543-53.
53. Baker, K. E.; Parker, R., Nonsense-mediated mRNA decay: terminating erroneous gene expression. *Current opinion in cell biology* **2004,** *16* (3), 293-9.
54. Murphy, M. P.; Holmgren, A.; Larsson, N. G.; Halliwell, B.; Chang, C. J.; Kalyanaraman, B.; Rhee, S. G.; Thornalley, P. J.; Partridge, L.; Gems, D.; Nystrom, T.; Belousov, V.; Schumacker, P. T.; Winterbourn, C. C., Unraveling the biological roles of reactive oxygen species. *Cell Metab* **2011,** *13* (4), 361-366.
55. Reddie, K. G.; Carroll, K. S., Expanding the functional diversity of proteins through cysteine oxidation. *Curr Opin Chem Biol* **2008,** *12* (6), 746-54.
56. Stadtman, E. R., Role of oxidized amino acids in protein breakdown and stability. *Methods in enzymology* **1995,** *258*, 379-93.

57. Drazic, A.; Winter, J., The physiological role of reversible methionine oxidation. *Biochimica et biophysica acta* **2014,** *1844* (8), 1367-82.
58. Feeney, M. B.; Schöneich, C., Tyrosine Modifications in Aging. *Antioxidants & Redox Signaling* **2012,** *17* (11), 1571-1579.
59. Nuriel, T.; Hansler, A.; Gross, S. S., Protein Nitrotryptophan: Formation, Significance and Identification. *Journal of proteomics* **2011,** *74* (11), 2300-2312.
60. Uchida, K., Histidine and lysine as targets of oxidative modification. *Amino acids* **2003,** *25* (3-4), 249-57.
61. Davies, M. J., The oxidative environment and protein damage. *Biochimica et biophysica acta* **2005,** *1703* (2), 93-109.
62. Tsikas, D.; Duncan, M. W., Mass spectrometry and 3-nitrotyrosine: strategies, controversies, and our current perspective. *Mass Spectrom Rev* **2014,** *33* (4), 237-76.
63. Batthyany, C.; Bartesaghi, S.; Mastrogiovanni, M.; Lima, A.; Demicheli, V.; Radi, R., Tyrosine-Nitrated Proteins: Proteomic and Bioanalytical Aspects. *Antioxid Redox Signal* **2017,** *26* (7), 313-328.
64. Bachi, A.; Dalle-Donne, I.; Scaloni, A., Redox proteomics: chemical principles, methodological approaches and biological/biomedical promises. *Chem Rev* **2013,** *113* (1), 596-698.
65. Dumas, A.; Lercher, L.; Spicer, C. D.; Davis, B. G., Designing logical codon reassignment - Expanding the chemistry in biology. *Chemical Science* **2015,** *6* (1), 50-69.
66. Quast, R. B.; Mrusek, D.; Hoffmeister, C.; Sonnabend, A.; Kubick, S., Cotranslational incorporation of non-standard amino acids using cell-free protein synthesis. *FEBS Lett* **2015,** *589* (15), 1703-12.
67. Wang, L.; Brock, A.; Herberich, B.; Schultz, P. G., Expanding the Genetic Code of *Escherichia coli*. *Science* **2001,** *292* (5516), 498.
68. Wu, N.; Deiters, A.; Cropp, T. A.; King, D.; Schultz, P. G., A Genetically Encoded Photocaged Amino Acid. *J. Am. Chem. Soc.* **2004,** *126* (44), 14306-14307.
69. Chin, J. W.; Cropp, T. A.; Anderson, J. C.; Mukherji, M.; Zhang, Z.; Schultz, P. G., An expanded eukaryotic genetic code. *Science (New York, N.Y.)* **2003,** *301* (5635), 964-7.
70. Neumann, H.; Peak-Chew, S. Y.; Chin, J. W., Genetically encoding N(epsilon)-acetyllysine in recombinant proteins. *Nat Chem Biol* **2008,** *4* (4), 232-4.
71. Italia, J. S.; Addy, P. S.; Wrobel, C. J.; Crawford, L. A.; Lajoie, M. J.; Zheng, Y.; Chatterjee, A., An orthogonalized platform for genetic code expansion in both bacteria and eukaryotes. *Nat. Chem. Biol.* **2017,** *13* (4), 446-450.
72. Parrish, A. R.; She, X.; Xiang, Z.; Coin, I.; Shen, Z.; Briggs, S. P.; Dillin, A.; Wang, L., Expanding the genetic code of Caenorhabditis elegans using bacterial aminoacyl-tRNA synthetase/tRNA pairs. *ACS Chem Biol* **2012,** *7* (7), 1292-302.
73. Luo, X.; Fu, G.; Wang, R. E.; Zhu, X.; Zambaldo, C.; Liu, R.; Liu, T.; Lyu, X.; Du, J.; Xuan, W.; Yao, A.; Reed, S. A.; Kang, M.; Zhang, Y.; Guo, H.; Huang, C.; Yang, P. Y.; Wilson, I. A.; Schultz, P. G.; Wang, F., Genetically encoding

phosphotyrosine and its nonhydrolyzable analog in bacteria. *Nat Chem Biol* **2017,** *13* (8), 845-849.
74. Mehl, R. A.; Anderson, J. C.; Santoro, S. W.; Wang, L.; Martin, A. B.; King, D. S.; Horn, D. M.; Schultz, P. G., Generation of a bacterium with a 21 amino acid genetic code. *J Am Chem Soc* **2003,** *125* (4), 935-9.
75. Zhang, M. S.; Brunner, S. F.; Huguenin-Dezot, N.; Liang, A. D.; Schmied, W. H.; Rogerson, D. T.; Chin, J. W., Biosynthesis and genetic encoding of phosphothreonine through parallel selection and deep sequencing. *Nat Methods* **2017,** *14* (7), 729-736.
76. Hoppmann, C.; Wong, A.; Yang, B.; Li, S.; Hunter, T.; Shokat, K. M.; Wang, L., Site-specific incorporation of phosphotyrosine using an expanded genetic code. *Nat Chem Biol* **2017,** *13* (8), 842-844.
77. Rogerson, D. T.; Sachdeva, A.; Wang, K.; Haq, T.; Kazlauskaite, A.; Hancock, S. M.; Huguenin-Dezot, N.; Muqit, M. M.; Fry, A. M.; Bayliss, R.; Chin, J. W., Efficient genetic encoding of phosphoserine and its nonhydrolyzable analog. *Nat Chem Biol* **2015,** *11* (7), 496-503.
78. Park, H. S.; Hohn, M. J.; Umehara, T.; Guo, L. T.; Osborne, E. M.; Benner, J.; Noren, C. J.; Rinehart, J.; Soll, D., Expanding the genetic code of Escherichia coli with phosphoserine. *Science (New York, N.Y.)* **2011,** *333* (6046), 1151-4.
79. Muir, T. W., Semisynthesis of proteins by expressed protein ligation. *Annu Rev Biochem* **2003,** *72*, 249-89.
80. Holt, M.; Muir, T., Application of the Protein Semisynthesis Strategy to the Generation of Modified Chromatin. *Annu. Rev. Biochem.* **2015,** *84* (1), 265-290.
81. Muralidharan, V.; Muir, T. W., Protein ligation: an enabling technology for the biophysical analysis of proteins. *Nat Methods* **2006,** *3* (6), 429-38.
82. Burai, R.; Ait-Bouziad, N.; Chiki, A.; Lashuel, H. A., Elucidating the Role of Site-Specific Nitration of α-Synuclein in the Pathogenesis of Parkinson's Disease via Protein Semisynthesis and Mutagenesis. *J. Am. Chem. Soc.* **2015,** *137* (15), 5041-5052.
83. Lo Conte, M.; Carroll, K. S., The redox biochemistry of protein sulfenylation and sulfinylation. *The Journal of biological chemistry* **2013,** *288* (37), 26480-8.
84. Chen, K.; Kirber, M. T.; Xiao, H.; Yang, Y.; Keaney, J. F., Jr., Regulation of ROS signal transduction by NADPH oxidase 4 localization. *J Cell Biol* **2008,** *181* (7), 1129-39.
85. Paulsen, C. E.; Truong, T. H.; Garcia, F. J.; Homann, A.; Gupta, V.; Leonard, S. E.; Carroll, K. S., Peroxide-dependent sulfenylation of the EGFR catalytic site enhances kinase activity. *Nat Chem Biol* **2011,** *8* (1), 57-64.
86. Wilson, M. A., The Role of Cysteine Oxidation in DJ-1 Function and Dysfunction. *Antioxidants & Redox Signaling* **2011,** *15* (1), 111-122.
87. Salsbury, F. R., Jr.; Knutson, S. T.; Poole, L. B.; Fetrow, J. S., Functional site profiling and electrostatic analysis of cysteines modifiable to cysteine sulfenic acid. *Protein Sci* **2008,** *17* (2), 299-312.

88. Hamann, M.; Zhang, T.; Hendrich, S.; Thomas, J. A., Quantitation of protein sulfinic and sulfonic acid, irreversibly oxidized protein cysteine sites in cellular proteins. *Methods in enzymology* **2002,** *348*, 146-56.
89. Jacob, C.; Holme, A. L.; Fry, F. H., The sulfinic acid switch in proteins. *Org Biomol Chem* **2004,** *2* (14), 1953-6.
90. Lee, S. R.; Yang, K. S.; Kwon, J.; Lee, C.; Jeong, W.; Rhee, S. G., Reversible inactivation of the tumor suppressor PTEN by H2O2. *The Journal of biological chemistry* **2002,** *277* (23), 20336-42.
91. Salmeen, A.; Andersen, J. N.; Myers, M. P.; Meng, T. C.; Hinks, J. A.; Tonks, N. K.; Barford, D., Redox regulation of protein tyrosine phosphatase 1B involves a sulphenyl-amide intermediate. *Nature* **2003,** *423* (6941), 769-73.
92. Leonard, S. E.; Carroll, K. S., Chemical 'omics' approaches for understanding protein cysteine oxidation in biology. *Curr Opin Chem Biol* **2011,** *15* (1), 88-102.
93. Tanner, J. J.; Parsons, Z. D.; Cummings, A. H.; Zhou, H.; Gates, K. S., Redox regulation of protein tyrosine phosphatases: structural and chemical aspects. *Antioxid Redox Signal* **2011,** *15* (1), 77-97.
94. Giannoni, E.; Buricchi, F.; Raugei, G.; Ramponi, G.; Chiarugi, P., Intracellular reactive oxygen species activate Src tyrosine kinase during cell adhesion and anchorage-dependent cell growth. *Mol Cell Biol* **2005,** *25* (15), 6391-403.
95. Smith, J. K.; Patil, C. N.; Patlolla, S.; Gunter, B. W.; Booz, G. W.; Duhe, R. J., Identification of a redox-sensitive switch within the JAK2 catalytic domain. *Free Radic Biol Med* **2012,** *52* (6), 1101-10.
96. Song, M. Y.; Makino, A.; Yuan, J. X., Role of reactive oxygen species and redox in regulating the function of transient receptor potential channels. *Antioxid Redox Signal* **2011,** *15* (6), 1549-65.
97. Rhee, S. G., Overview on Peroxiredoxin. *Mol Cells* **2016,** *39* (1), 1-5.
98. Stamler, J. S.; Simon, D. I.; Osborne, J. A.; Mullins, M. E.; Jaraki, O.; Michel, T.; Singel, D. J.; Loscalzo, J., S-nitrosylation of proteins with nitric oxide: synthesis and characterization of biologically active compounds. *Proceedings of the National Academy of Sciences of the United States of America* **1992,** *89* (1), 444-8.
99. Hess, D. T.; Matsumoto, A.; Kim, S. O.; Marshall, H. E.; Stamler, J. S., Protein S-nitrosylation: purview and parameters. *Nature reviews. Molecular cell biology* **2005,** *6* (2), 150-66.
100. Stamler, J. S.; Lamas, S.; Fang, F. C., Nitrosylation. the prototypic redox-based signaling mechanism. *Cell* **2001,** *106* (6), 675-83.
101. Kornberg, M. D.; Sen, N.; Hara, M. R.; Juluri, K. R.; Nguyen, J. V.; Snowman, A. M.; Law, L.; Hester, L. D.; Snyder, S. H., GAPDH mediates nitrosylation of nuclear proteins. *Nat Cell Biol* **2010,** *12* (11), 1094-100.
102. Foster, M. W.; McMahon, T. J.; Stamler, J. S., S-nitrosylation in health and disease. *Trends Mol Med* **2003,** *9* (4), 160-8.
103. Gaston, B.; Reilly, J.; Drazen, J. M.; Fackler, J.; Ramdev, P.; Arnelle, D.; Mullins, M. E.; Sugarbaker, D. J.; Chee, C.; Singel, D. J.; et al., Endogenous nitrogen oxides and bronchodilator S-nitrosothiols in human airways.

Proceedings of the National Academy of Sciences of the United States of America **1993,** *90* (23), 10957-61.
104. Schoneich, C., Methionine oxidation by reactive oxygen species: reaction mechanisms and relevance to Alzheimer's disease. *Biochimica et biophysica acta* **2005,** *1703* (2), 111-9.
105. Nauser, T.; Pelling, J.; Schoneich, C., Thiyl radical reaction with amino acid side chains: rate constants for hydrogen transfer and relevance for posttranslational protein modification. *Chemical research in toxicology* **2004,** *17* (10), 1323-8.
106. Ghesquiere, B.; Jonckheere, V.; Colaert, N.; Van Durme, J.; Timmerman, E.; Goethals, M.; Schymkowitz, J.; Rousseau, F.; Vandekerckhove, J.; Gevaert, K., Redox proteomics of protein-bound methionine oxidation. *Mol. Cell. Proteomics* **2011,** *10* (5), M110.006866.
107. Weissbach, H.; Resnick, L.; Brot, N., Methionine sulfoxide reductases: history and cellular role in protecting against oxidative damage. *Biochimica et biophysica acta* **2005,** *1703* (2), 203-12.
108. Lowther, W. T.; Weissbach, H.; Etienne, F.; Brot, N.; Matthews, B. W., The mirrored methionine sulfoxide reductases of Neisseria gonorrhoeae pilB. *Nat Struct Biol* **2002,** *9* (5), 348-52.
109. Kwak, G. H.; Kim, T. H.; Kim, H. Y., Down-regulation of MsrB3 induces cancer cell apoptosis through reactive oxygen species production and intrinsic mitochondrial pathway activation. *Biochemical and biophysical research communications* **2017,** *483* (1), 468-474.
110. Zhang, L.; Peng, S.; Sun, J.; Yao, J.; Kang, J.; Hu, Y.; Fang, J., A specific fluorescent probe reveals compromised activity of methionine sulfoxide reductases in Parkinson's disease. *Chemical science* **2017,** *8* (4), 2966-2972.
111. Drazic, A.; Miura, H.; Peschek, J.; Le, Y.; Bach, N. C.; Kriehuber, T.; Winter, J., Methionine oxidation activates a transcription factor in response to oxidative stress. *Proc Natl Acad Sci U S A* **2013,** *110* (23), 9493-8.
112. Erickson, J. R.; Joiner, M. L.; Guan, X.; Kutschke, W.; Yang, J.; Oddis, C. V.; Bartlett, R. K.; Lowe, J. S.; O'Donnell, S. E.; Aykin-Burns, N.; Zimmerman, M. C.; Zimmerman, K.; Ham, A. J.; Weiss, R. M.; Spitz, D. R.; Shea, M. A.; Colbran, R. J.; Mohler, P. J.; Anderson, M. E., A dynamic pathway for calcium-independent activation of CaMKII by methionine oxidation. *Cell* **2008,** *133* (3), 462-74.
113. Lee, B. C.; Peterfi, Z.; Hoffmann, F. W.; Moore, R. E.; Kaya, A.; Avanesov, A.; Tarrago, L.; Zhou, Y.; Weerapana, E.; Fomenko, D. E.; Hoffmann, P. R.; Gladyshev, V. N., MsrB1 and MICALs regulate actin assembly and macrophage function via reversible stereoselective methionine oxidation. *Mol Cell* **2013,** *51* (3), 397-404.
114. Pan, J.; Carroll, K. S., Light-Mediated Sulfenic Acid Generation from Photocaged Cysteine Sulfoxide. *Org Lett* **2015,** *17* (24), 6014-7.
115. Radi, R., Protein tyrosine nitration: biochemical mechanisms and structural basis of functional effects. *Acc Chem Res* **2013,** *46* (2), 550-9.

116. Aulak, K. S.; Miyagi, M.; Yan, L.; West, K. A.; Massillon, D.; Crabb, J. W.; Stuehr, D. J., Proteomic method identifies proteins nitrated in vivo during inflammatory challenge. *Proc Natl Acad Sci U S A* **2001,** *98* (21), 12056-61.
117. Gow, A. J.; Farkouh, C. R.; Munson, D. A.; Posencheg, M. A.; Ischiropoulos, H., Biological significance of nitric oxide-mediated protein modifications. *Am J Physiol Lung Cell Mol Physiol* **2004,** *287* (2), L262-8.
118. Kanski, J.; Behring, A.; Pelling, J.; Schoneich, C., Proteomic identification of 3-nitrotyrosine-containing rat cardiac proteins: effects of biological aging. *Am J Physiol Heart Circ Physiol* **2005,** *288* (1), H371-81.
119. Kanski, J.; Hong, S. J.; Schoneich, C., Proteomic analysis of protein nitration in aging skeletal muscle and identification of nitrotyrosine-containing sequences in vivo by nanoelectrospray ionization tandem mass spectrometry. *J. Biol. Chem.* **2005,** *280* (25), 24261-6.
120. Heinecke, J. W., Mechanisms of oxidative damage by myeloperoxidase in atherosclerosis and other inflammatory disorders. *J Lab Clin Med* **1999,** *133* (4), 321-5.
121. Heinecke, J. W., Mass spectrometric quantification of amino acid oxidation products in proteins: insights into pathways that promote LDL oxidation in the human artery wall. *FASEB J* **1999,** *13* (10), 1113-20.
122. Franco, M. C.; Ricart, K. C.; Gonzalez, A. S.; Dennys, C. N.; Nelson, P. A.; Janes, M. S.; Mehl, R. A.; Landar, A.; Estevez, A. G., Nitration of Hsp90 on Tyrosine 33 Regulates Mitochondrial Metabolism. *The Journal of biological chemistry* **2015,** *290* (31), 19055-66.
123. Nicholls, S. J.; Shen, Z.; Fu, X.; Levison, B. S.; Hazen, S. L., Quantification of 3-Nitrotyrosine Levels Using a Benchtop Ion Trap Mass Spectrometry Method. In *Methods Enzymol.*, Academic Press: 2005; Vol. 396, pp 245-266.
124. Brennan, M. L.; Wu, W.; Fu, X.; Shen, Z.; Song, W.; Frost, H.; Vadseth, C.; Narine, L.; Lenkiewicz, E.; Borchers, M. T.; Lusis, A. J.; Lee, J. J.; Lee, N. A.; Abu-Soud, H. M.; Ischiropoulos, H.; Hazen, S. L., A tale of two controversies: defining both the role of peroxidases in nitrotyrosine formation in vivo using eosinophil peroxidase and myeloperoxidase-deficient mice, and the nature of peroxidase-generated reactive nitrogen species. *The Journal of biological chemistry* **2002,** *277* (20), 17415-27.
125. Souza, J. M.; Choi, I.; Chen, Q.; Weisse, M.; Daikhin, E.; Yudkoff, M.; Obin, M.; Ara, J.; Horwitz, J.; Ischiropoulos, H., Proteolytic degradation of tyrosine nitrated proteins. *Arch Biochem Biophys* **2000,** *380* (2), 360-6.
126. Kamisaki, Y.; Wada, K.; Bian, K.; Balabanli, B.; Davis, K.; Martin, E.; Behbod, F.; Lee, Y. C.; Murad, F., An activity in rat tissues that modifies nitrotyrosine-containing proteins. *Proc Natl Acad Sci U S A* **1998,** *95* (20), 11584-9.
127. Aulak, K. S.; Koeck, T.; Crabb, J. W.; Stuehr, D. J., Dynamics of protein nitration in cells and mitochondria. *Am J Physiol Heart Circ Physiol* **2004,** *286* (1), H30-8.
128. Deeb, R. S.; Nuriel, T.; Cheung, C.; Summers, B.; Lamon, B. D.; Gross, S. S.; Hajjar, D. P., Characterization of a cellular denitrase activity that reverses nitration of cyclooxygenase. *Am J Physiol Heart Circ Physiol* **2013,** *305* (5), H687-98.

129. Gochman, E.; Mahajna, J.; Shenzer, P.; Dahan, A.; Blatt, A.; Elyakim, R.; Reznick, A. Z., The expression of iNOS and nitrotyrosine in colitis and colon cancer in humans. *Acta Histochem* **2012,** *114* (8), 827-35.
130. Souza, J. M.; Peluffo, G.; Radi, R., Protein tyrosine nitration--functional alteration or just a biomarker? *Free Radic Biol Med* **2008,** *45* (4), 357-66.
131. Shao, B.; Oda, M. N.; Oram, J. F.; Heinecke, J. W., Myeloperoxidase: An Oxidative Pathway for Generating Dysfunctional High-Density Lipoprotein. *Chem. Res. Toxicol.* **2010,** *23* (3), 447-454.
132. Pattison, D. I.; Davies, M. J., Kinetic Analysis of the Reactions of Hypobromous Acid with Protein Components: Implications for Cellular Damage and Use of 3-Bromotyrosine as a Marker of Oxidative Stress. *Biochemistry* **2004,** *43* (16), 4799-4809.
133. Thomson, E.; Brennan, S.; Senthilmohan, R.; Gangell, C. L.; Chapman, A. L.; Sly, P. D.; Kettle, A. J., Identifying peroxidases and their oxidants in the early pathology of cystic fibrosis. *Free Radical Biol. Med.* **2010,** *49* (9), 1354-1360.
134. Strzepa, A.; Pritchard, K. A.; Dittel, B. N., Myeloperoxidase: A new player in autoimmunity. *Cell Immunol* **2017,** *317*, 1-8.
135. Wang, J.; Slungaard, A., Role of eosinophil peroxidase in host defense and disease pathology. *Arch Biochem Biophys* **2006,** *445* (2), 256-60.
136. Hazen, S. L.; Heinecke, J. W., 3-Chlorotyrosine, a specific marker of myeloperoxidase-catalyzed oxidation, is markedly elevated in low density lipoprotein isolated from human atherosclerotic intima. *The Journal of clinical investigation* **1997,** *99* (9), 2075-81.
137. Huang, Y.; DiDonato, J. A.; Levison, B. S.; Schmitt, D.; Li, L.; Wu, Y.; Buffa, J.; Kim, T.; Gerstenecker, G. S.; Gu, X.; Kadiyala, C. S.; Wang, Z.; Culley, M. K.; Hazen, J. E.; DiDonato, A. J.; Fu, X.; Berisha, S. Z.; Peng, D.; Nguyen, T. T.; Liang, S.; Chuang, C.-C.; Cho, L.; Plow, E. F.; Fox, P. L.; Gogonea, V.; Tang, W. H. W.; Parks, J. S.; Fisher, E. A.; Smith, J. D.; Hazen, S. L., An abundant dysfunctional apolipoprotein A1 in human atheroma. *Nature Medicine* **2014,** *20*, 193.
138. Ishii, Y.; Ogara, A.; Katsumata, T.; Umemura, T.; Nishikawa, A.; Iwasaki, Y.; Ito, R.; Saito, K.; Hirose, M.; Nakazawa, H., Quantification of nitrated tryptophan in proteins and tissues by high-performance liquid chromatography with electrospray ionization tandem mass spectrometry. *J Pharm Biomed Anal* **2007,** *44* (1), 150-9.
139. Kawasaki, H.; Shigenaga, A.; Uda, M.; Baba, T.; Ogawa, H.; Takamori, K.; Yamakura, F., Nitration of tryptophan in ribosomal proteins is a novel post-translational modification of differentiated and naive PC12 cells. *Nitric oxide : biology and chemistry* **2011,** *25* (2), 176-82.
140. Bogan, A. A.; Thorn, K. S., Anatomy of hot spots in protein interfaces. *J Mol Biol* **1998,** *280* (1), 1-9.
141. Ikeda, K.; Yukihiro Hiraoka, B.; Iwai, H.; Matsumoto, T.; Mineki, R.; Taka, H.; Takamori, K.; Ogawa, H.; Yamakura, F., Detection of 6-nitrotryptophan in proteins by Western blot analysis and its application for peroxynitrite-treated PC12 cells. *Nitric oxide : biology and chemistry* **2007,** *16* (1), 18-28.

142. Rebrin, I.; Bregere, C.; Kamzalov, S.; Gallaher, T. K.; Sohal, R. S., Nitration of tryptophan 372 in succinyl-CoA:3-ketoacid CoA transferase during aging in rat heart mitochondria. *Biochemistry* **2007,** *46* (35), 10130-44.
143. Zhao, F.; Ghezzo-Schoneich, E.; Aced, G. I.; Hong, J.; Milby, T.; Schoneich, C., Metal-catalyzed oxidation of histidine in human growth hormone. Mechanism, isotope effects, and inhibition by a mild denaturing alcohol. *The Journal of biological chemistry* **1997,** *272* (14), 9019-29.
144. Alvarez, B.; Demicheli, V.; Duran, R.; Trujillo, M.; Cervenansky, C.; Freeman, B. A.; Radi, R., Inactivation of human Cu,Zn superoxide dismutase by peroxynitrite and formation of histidinyl radical. *Free Radic Biol Med* **2004,** *37* (6), 813-22.
145. Alvarez, B.; Radi, R., Peroxynitrite reactivity with amino acids and proteins. *Amino acids* **2003,** *25* (3-4), 295-311.
146. Xiao, H.; Peters, F. B.; Yang, P. Y.; Reed, S.; Chittuluru, J. R.; Schultz, P. G., Genetic incorporation of histidine derivatives using an engineered pyrrolysyl-tRNA synthetase. *ACS Chem Biol* **2014,** *9* (5), 1092-6.
147. Traoré, D. A. K.; Ghazouani, A. E.; Jacquamet, L.; Borel, F.; Ferrer, J.-L.; Lascoux, D.; Ravanat, J.-L.; Jaquinod, M.; Blondin, G.; Caux-Thang, C.; Duarte, V.; Latour, J.-M., Structural and functional characterization of 2-oxo-histidine in oxidized PerR protein. *Nat. Chem. Biol.* **2008,** *5*, 53.
148. Alfonta, L.; Zhang, Z.; Uryu, S.; Loo, J. A.; Schultz, P. G., Site-specific incorporation of a redox-active amino acid into proteins. *J Am Chem Soc* **2003,** *125* (48), 14662-3.
149. Hauf, M.; Richter, F.; Schneider, T.; Faidt, T.; Martins, B. M.; Baumann, T.; Durkin, P.; Dobbek, H.; Jacobs, K.; Moglich, A.; Budisa, N., Photoactivatable Mussel-Based Underwater Adhesive Proteins by an Expanded Genetic Code. *Chembiochem : a European journal of chemical biology* **2017,** *18* (18), 1819-1823.
150. Furth, A. J.; Hope, D. B., Studies on the chemical modification of the tyrosine residue in bovine neurophysin-II. *Biochem J* **1970,** *116* (4), 545-53.
151. Beeckmans, S.; Kanarek, L., The modification with tetranitromethane of an essential tyrosine in the active site of pig fumarase. *Biochimica et biophysica acta* **1983,** *743* (3), 370-8.
152. Beckmann, J. S.; Ye, Y. Z.; Anderson, P. G.; Chen, J.; Accavitti, M. A.; Tarpey, M. M.; White, C. R., Extensive nitration of protein tyrosines in human atherosclerosis detected by immunohistochemistry. *Biol Chem Hoppe Seyler* **1994,** *375* (2), 81-8.
153. Frijhoff, J.; Winyard, P. G.; Zarkovic, N.; Davies, S. S.; Stocker, R.; Cheng, D.; Knight, A. R.; Taylor, E. L.; Oettrich, J.; Ruskovska, T.; Gasparovic, A. C.; Cuadrado, A.; Weber, D.; Poulsen, H. E.; Grune, T.; Schmidt, H. H.; Ghezzi, P., Clinical Relevance of Biomarkers of Oxidative Stress. *Antioxid Redox Signal* **2015,** *23* (14), 1144-70.
154. Nuriel, T.; Deeb, R. S.; Hajjar, D. P.; Gross, S. S., Protein 3-nitrotyrosine in complex biological samples: quantification by high-pressure liquid chromatography/electrochemical detection and emergence of proteomic

approaches for unbiased identification of modification sites. *Methods in enzymology* **2008,** *441*, 1-17.
155. Buuh, Z. Y.; Lyu, Z.; Wang, R. E., Interrogating the Roles of Post-Translational Modifications of Non-Histone Proteins. *J. Med. Chem.* **2017**.
156. Davis, L.; Chin, J. W., Designer proteins: applications of genetic code expansion in cell biology. *Nature reviews. Molecular cell biology* **2012,** *13* (3), 168-82.
157. Neumann, H., Rewiring translation - Genetic code expansion and its applications. *FEBS Lett* **2012,** *586* (15), 2057-64.
158. Lemke, E. A., The exploding genetic code. *Chembiochem : a European journal of chemical biology* **2014,** *15* (12), 1691-4.
159. Cheng, A. A.; Lu, T. K., Synthetic biology: an emerging engineering discipline. *Annu Rev Biomed Eng* **2012,** *14*, 155-78.
160. Chin, J. W., Expanding and reprogramming the genetic code of cells and animals. *Annu Rev Biochem* **2014,** *83*, 379-408.
161. Liu, C. C.; Schultz, P. G., Adding new chemistries to the genetic code. *Annu Rev Biochem* **2010,** *79*, 413-44.
162. O'Donoghue, P.; Ling, J.; Wang, Y. S.; Soll, D., Upgrading protein synthesis for synthetic biology. *Nat Chem Biol* **2013,** *9* (10), 594-8.
163. Neumann, H.; Wang, K.; Davis, L.; Garcia-Alai, M.; Chin, J. W., Encoding multiple unnatural amino acids via evolution of a quadruplet-decoding ribosome. *Nature* **2010,** *464* (7287), 441-4.
164. Lajoie, M. J.; Soll, D.; Church, G. M., Overcoming Challenges in Engineering the Genetic Code. *J Mol Biol* **2016,** *428* (5 Pt B), 1004-21.
165. Speight, L. C.; Muthusamy, A. K.; Goldberg, J. M.; Warner, J. B.; Wissner, R. F.; Willi, T. S.; Woodman, B. F.; Mehl, R. A.; Petersson, E. J., Efficient synthesis and in vivo incorporation of acridon-2-ylalanine, a fluorescent amino acid for lifetime and Forster resonance energy transfer/luminescence resonance energy transfer studies. *J Am Chem Soc* **2013,** *135* (50), 18806-14.
166. Fan, C.; Ho, J. M. L.; Chirathivat, N.; Soll, D.; Wang, Y. S., Exploring the substrate range of wild-type aminoacyl-tRNA synthetases. *Chembiochem : a European journal of chemical biology* **2014,** *15* (12), 1805-1809.
167. Guo, L. T.; Wang, Y. S.; Nakamura, A.; Eiler, D.; Kavran, J. M.; Wong, M.; Kiessling, L. L.; Steitz, T. A.; O'Donoghue, P.; Soll, D., Polyspecific pyrrolysyl-tRNA synthetases from directed evolution. *Proc Natl Acad Sci U S A* **2014,** *111* (47), 16724-9.
168. Schmied, W. H.; Elsasser, S. J.; Uttamapinant, C.; Chin, J. W., Efficient multisite unnatural amino acid incorporation in mammalian cells via optimized pyrrolysyl tRNA synthetase/tRNA expression and engineered eRF1. *J Am Chem Soc* **2014,** *136* (44), 15577-83.
169. Mukai, T.; Wakiyama, M.; Sakamoto, K.; Yokoyama, S., Genetic encoding of non-natural amino acids in Drosophila melanogaster Schneider 2 cells. *Protein Sci* **2010,** *19* (3), 440-8.
170. Johnson, D. B.; Xu, J.; Shen, Z.; Takimoto, J. K.; Schultz, M. D.; Schmitz, R. J.; Xiang, Z.; Ecker, J. R.; Briggs, S. P.; Wang, L., RF1 knockout allows

ribosomal incorporation of unnatural amino acids at multiple sites. *Nat Chem Biol* **2011,** *7* (11), 779-86.
171. Guo, J.; Melancon, C. E., 3rd; Lee, H. S.; Groff, D.; Schultz, P. G., Evolution of amber suppressor tRNAs for efficient bacterial production of proteins containing nonnatural amino acids. *Angew Chem Int Ed Engl* **2009,** *48* (48), 9148-51.
172. Javahishvili, T.; Manibusan, A.; Srinagesh, S.; Lee, D.; Ensari, S.; Shimazu, M.; Schultz, P. G., Role of tRNA orthogonality in an expanded genetic code. *ACS Chem Biol* **2014,** *9* (4), 874-9.
173. Swanson, R.; Hoben, P.; Sumner-Smith, M.; Uemura, H.; Watson, L.; Soll, D., Accuracy of in vivo aminoacylation requires proper balance of tRNA and aminoacyl-tRNA synthetase. *Science (New York, N.Y.)* **1988,** *242* (4885), 1548-51.
174. Wang, N.; Ju, T.; Niu, W.; Guo, J., Fine-tuning interaction between aminoacyl-tRNA synthetase and tRNA for efficient synthesis of proteins containing unnatural amino acids. *ACS Synth Biol* **2015,** *4* (3), 207-12.
175. Fan, C.; Xiong, H.; Reynolds, N. M.; Soll, D., Rationally evolving tRNAPyl for efficient incorporation of noncanonical amino acids. *Nucleic acids research* **2015,** *43* (22), e156.
176. Abello, N.; Kerstjens, H. A.; Postma, D. S.; Bischoff, R., Protein tyrosine nitration: selectivity, physicochemical and biological consequences, denitration, and proteomics methods for the identification of tyrosine-nitrated proteins. *J Proteome Res* **2009,** *8* (7), 3222-38.
177. Ng, J. Y.; Boelen, L.; Wong, J. W., Bioinformatics analysis reveals biophysical and evolutionary insights into the 3-nitrotyrosine post-translational modification in the human proteome. *Open Biol* **2013,** *3* (2), 120148.
178. Stokes, A. L.; Miyake-Stoner, S. J.; Peeler, J. C.; Nguyen, D. P.; Hammer, R. P.; Mehl, R. A., Enhancing the utility of unnatural amino acid synthetases by manipulating broad substrate specificity. *Mol Biosyst* **2009,** *5* (9), 1032-8.
179. Hammill, J. T.; Miyake-Stoner, S.; Hazen, J. L.; Jackson, J. C.; Mehl, R. A., Preparation of site-specifically labeled fluorinated proteins for 19F-NMR structural characterization. *Nat Protoc* **2007,** *2* (10), 2601-7.
180. Studier, F. W., Protein production by auto-induction in high density shaking cultures. *Protein expression and purification* **2005,** *41* (1), 207-34.
181. Horowitz, S.; Adhikari, U.; Dirk, L. M.; Del Rizzo, P. A.; Mehl, R. A.; Houtz, R. L.; Al-Hashimi, H. M.; Scheiner, S.; Trievel, R. C., Manipulating unconventional CH-based hydrogen bonding in a methyltransferase via noncanonical amino acid mutagenesis. *ACS Chem Biol* **2014,** *9* (8), 1692-7.
182. Turner, J. M.; Graziano, J.; Spraggon, G.; Schultz, P. G., Structural plasticity of an aminoacyl-tRNA synthetase active site. *Proc Natl Acad Sci U S A* **2006,** *103* (17), 6483-8.
183. Wang, L.; Zhang, Z.; Brock, A.; Schultz, P. G., Addition of the keto functional group to the genetic code of Escherichia coli. *Proc Natl Acad Sci U S A* **2003,** *100* (1), 56-61.

184. Sherlin, L. D.; Bullock, T. L.; Nissan, T. A.; Perona, J. J.; Lariviere, F. J.; Uhlenbeck, O. C.; Scaringe, S. A., Chemical and enzymatic synthesis of tRNAs for high-throughput crystallization. *RNA* **2001,** *7* (11), 1671-8.
185. Price, S. R.; Ito, N.; Oubridge, C.; Avis, J. M.; Nagai, K., Crystallization of RNA-protein complexes. I. Methods for the large-scale preparation of RNA suitable for crystallographic studies. *J Mol Biol* **1995,** *249* (2), 398-408.
186. Kao, C.; Zheng, M.; Rudisser, S., A simple and efficient method to reduce nontemplated nucleotide addition at the 3 terminus of RNAs transcribed by T7 RNA polymerase. *RNA* **1999,** *5* (9), 1268-72.
187. Lyakhov, D. L.; He, B.; Zhang, X.; Studier, F. W.; Dunn, J. J.; McAllister, W. T., Mutant bacteriophage T7 RNA polymerases with altered termination properties. *J Mol Biol* **1997,** *269* (1), 28-40.
188. Wolfson, A. D.; Uhlenbeck, O. C., Modulation of tRNAAla identity by inorganic pyrophosphatase. *Proc Natl Acad Sci U S A* **2002,** *99* (9), 5965-70.
189. McGann, R. G.; Deutscher, M. P., Purification and characterization of a mutant tRNA nucleotidyltransferase. *European journal of biochemistry* **1980,** *106* (1), 321-8.
190. Hadd, A.; Perona, J. J., Coevolution of specificity determinants in eukaryotic glutamyl- and glutaminyl-tRNA synthetases. *J Mol Biol* **2014,** *426* (21), 3619-33.
191. Rodriguez-Hernandez, A.; Spears, J. L.; Gaston, K. W.; Limbach, P. A.; Gamper, H.; Hou, Y. M.; Kaiser, R.; Agris, P. F.; Perona, J. J., Structural and mechanistic basis for enhanced translational efficiency by 2-thiouridine at the tRNA anticodon wobble position. *J Mol Biol* **2013,** *425* (20), 3888-906.
192. Dulic, M.; Cvetesic, N.; Perona, J. J.; Gruic-Sovulj, I., Partitioning of tRNA-dependent editing between pre- and post-transfer pathways in class I aminoacyl-tRNA synthetases. *The Journal of biological chemistry* **2010,** *285* (31), 23799-809.
193. Schneider, C. A.; Rasband, W. S.; Eliceiri, K. W., NIH Image to ImageJ: 25 years of image analysis. *Nat Methods* **2012,** *9* (7), 671-5.
194. Bhaskaran, H.; Taniguchi, T.; Suzuki, T.; Suzuki, T.; Perona, J. J., Structural dynamics of a mitochondrial tRNA possessing weak thermodynamic stability. *Biochemistry* **2014,** *53* (9), 1456-65.
195. Avis, J. M.; Day, A. G.; Garcia, G. A.; Fersht, A. R., Reaction of modified and unmodified tRNA(Tyr) substrates with tyrosyl-tRNA synthetase (Bacillus stearothermophilus). *Biochemistry* **1993,** *32* (20), 5312-20.
196. First, E. A.; Fersht, A. R., Involvement of threonine 234 in catalysis of tyrosyl adenylate formation by tyrosyl-tRNA synthetase. *Biochemistry* **1993,** *32* (49), 13644-50.
197. Fechter, P.; Rudinger-Thirion, J.; Tukalo, M.; Giege, R., Major tyrosine identity determinants in Methanococcus jannaschii and Saccharomyces cerevisiae tRNA(Tyr) are conserved but expressed differently. *European journal of biochemistry* **2001,** *268* (3), 761-7.
198. Brevet, A.; Chen, J.; Leveque, F.; Plateau, P.; Blanquet, S., In vivo synthesis of adenylylated bis(5'-nucleosidyl) tetraphosphates (Ap4N) by Escherichia coli aminoacyl-tRNA synthetases. *Proc Natl Acad Sci U S A* **1989,** *86* (21), 8275-9.

199. Kobayashi, T.; Nureki, O.; Ishitani, R.; Yaremchuk, A.; Tukalo, M.; Cusack, S.; Sakamoto, K.; Yokoyama, S., Structural basis for orthogonal tRNA specificities of tyrosyl-tRNA synthetases for genetic code expansion. *Nat Struct Biol* **2003,** *10* (6), 425-32.
200. Jackson, J. C.; Hammill, J. T.; Mehl, R. A., Site-specific incorporation of a (19)F-amino acid into proteins as an NMR probe for characterizing protein structure and reactivity. *J Am Chem Soc* **2007,** *129* (5), 1160-6.
201. Rodriguez-Hernandez, A.; Perona, J. J., Heat maps for intramolecular communication in an RNP enzyme encoding glutamine. *Structure* **2011,** *19* (3), 386-96.
202. Hadd, A.; Perona, J. J., Recoding aminoacyl-tRNA synthetases for synthetic biology by rational protein-RNA engineering. *ACS Chem Biol* **2014,** *9* (12), 2761-6.
203. Knyushko, T. V.; Sharov, V. S.; Williams, T. D.; Schoneich, C.; Bigelow, D. J., 3-Nitrotyrosine modification of SERCA2a in the aging heart: a distinct signature of the cellular redox environment. *Biochemistry* **2005,** *44* (39), 13071-81.
204. Squier, T. C.; Bigelow, D. J., Protein oxidation and age-dependent alterations in calcium homeostasis. *Frontiers in bioscience : a journal and virtual library* **2000,** *5*, D504-26.
205. Stewart, T. A.; Yapa, K. T.; Monteith, G. R., Altered calcium signaling in cancer cells. *Biochimica et biophysica acta* **2015,** *1848* (10 Pt B), 2502-11.
206. Wehrens, X. H.; Lehnart, S. E.; Marks, A. R., Intracellular calcium release and cardiac disease. *Annual review of physiology* **2005,** *67*, 69-98.
207. Black, D. J.; Tran, Q. K.; Persechini, A., Monitoring the total available calmodulin concentration in intact cells over the physiological range in free Ca2+. *Cell calcium* **2004,** *35* (5), 415-25.
208. Benaim, G.; Villalobo, A., Phosphorylation of calmodulin. Functional implications. *European journal of biochemistry* **2002,** *269* (15), 3619-31.
209. Persechini, A.; Cronk, B., The relationship between the free concentrations of Ca2+ and Ca2+-calmodulin in intact cells. *The Journal of biological chemistry* **1999,** *274* (11), 6827-30.
210. Persechini, A.; Stemmer, P. M., Calmodulin is a limiting factor in the cell. *Trends in cardiovascular medicine* **2002,** *12* (1), 32-7.
211. Porter, J. J.; Mehl, R. A., Genetic Code Expansion: A Powerful Tool for Understanding the Physiological Consequences of Oxidative Stress Protein Modifications. *Oxidative medicine and cellular longevity* **2018,** *2018*, 7607463.
212. Huhmer, A. F.; Gerber, N. C.; de Montellano, P. R.; Schoneich, C., Peroxynitrite reduction of calmodulin stimulation of neuronal nitric oxide synthase. *Chemical research in toxicology* **1996,** *9* (2), 484-91.
213. Lourette, N.; Smallwood, H.; Wu, S.; Robinson, E. W.; Squier, T. C.; Smith, R. D.; Pasa-Tolic, L., A top-down LC-FTICR MS-based strategy for characterizing oxidized calmodulin in activated macrophages. *Journal of the American Society for Mass Spectrometry* **2010,** *21* (6), 930-9.

214. Weber, T. J.; Negash, S.; Smallwood, H. S.; Ramos, K. S.; Thrall, B. D.; Squier, T. C., Calmodulin involvement in stress-activated nuclear localization of albumin in JB6 epithelial cells. *Biochemistry* **2004,** *43* (23), 7443-50.
215. Madamanchi, N. R.; Vendrov, A.; Runge, M. S., Oxidative stress and vascular disease. *Arteriosclerosis, thrombosis, and vascular biology* **2005,** *25* (1), 29-38.
216. Wu, G.; Gao, Z.; Dong, A.; Yu, S., Calcium-induced changes in calmodulin structural dynamics and thermodynamics. *International journal of biological macromolecules* **2012,** *50* (4), 1011-7.
217. Bossuyt, J.; Bers, D. M., Visualizing CaMKII and CaM activity: a paradigm of compartmentalized signaling. *Journal of molecular medicine (Berlin, Germany)* **2013,** *91* (8), 907-16.
218. Gilli, R.; Lafitte, D.; Lopez, C.; Kilhoffer, M.; Makarov, A.; Briand, C.; Haiech, J., Thermodynamic analysis of calcium and magnesium binding to calmodulin. *Biochemistry* **1998,** *37* (16), 5450-6.
219. Johnson, J. D.; Wittenauer, L. A., A fluorescent calmodulin that reports the binding of hydrophobic inhibitory ligands. *Biochem J* **1983,** *211* (2), 473-9.
220. Piazza, M.; Taiakina, V.; Guillemette, S. R.; Guillemette, J. G.; Dieckmann, T., Solution structure of calmodulin bound to the target peptide of endothelial nitric oxide synthase phosphorylated at Thr495. *Biochemistry* **2014,** *53* (8), 1241-9.
221. Kincaid, R. L.; Vaughan, M.; Osborne, J. C., Jr.; Tkachuk, V. A., Ca2+-dependent interaction of 5-dimethylaminonaphthalene-1-sulfonyl-calmodulin with cyclic nucleotide phosphodiesterase, calcineurin, and troponin I. *The Journal of biological chemistry* **1982,** *257* (18), 10638-43.
222. Abdiche, Y.; Malashock, D.; Pinkerton, A.; Pons, J., Determining kinetics and affinities of protein interactions using a parallel real-time label-free biosensor, the Octet. *Analytical biochemistry* **2008,** *377* (2), 209-17.
223. Matsubara, M.; Hayashi, N.; Titani, K.; Taniguchi, H., Circular dichroism and 1H NMR studies on the structures of peptides derived from the calmodulin-binding domains of inducible and endothelial nitric-oxide synthase in solution and in complex with calmodulin. Nascent alpha-helical structures are stabilized by calmodulin both in the presence and absence of Ca2+. *The Journal of biological chemistry* **1997,** *272* (37), 23050-6.
224. Spratt, D. E.; Taiakina, V.; Palmer, M.; Guillemette, J. G., FRET conformational analysis of calmodulin binding to nitric oxide synthase peptides and enzymes. *Biochemistry* **2008,** *47* (46), 12006-17.
225. Venema, R. C.; Sayegh, H. S.; Kent, J. D.; Harrison, D. G., Identification, characterization, and comparison of the calmodulin-binding domains of the endothelial and inducible nitric oxide synthases. *The Journal of biological chemistry* **1996,** *271* (11), 6435-40.
226. Gorlach, A.; Bertram, K.; Hudecova, S.; Krizanova, O., Calcium and ROS: A mutual interplay. *Redox Biol* **2015,** *6*, 260-71.
227. Adams, L.; Franco, M. C.; Estevez, A. G., Reactive nitrogen species in cellular signaling. *Experimental biology and medicine (Maywood, N.J.)* **2015,** *240* (6), 711-7.
228. Olsen, J. V.; Vermeulen, M.; Santamaria, A.; Kumar, C.; Miller, M. L.; Jensen, L. J.; Gnad, F.; Cox, J.; Jensen, T. S.; Nigg, E. A.; Brunak, S.; Mann, M.,

Quantitative phosphoproteomics reveals widespread full phosphorylation site occupancy during mitosis. *Science signaling* **2010,** *3* (104), ra3.
229. Lafitte, D.; Tsvetkov, P. O.; Devred, F.; Toci, R.; Barras, F.; Briand, C.; Makarov, A. A.; Haiech, J., Cation binding mode of fully oxidised calmodulin explained by the unfolding of the apostate. *Biochimica et biophysica acta* **2002,** *1600* (1-2), 105-10.
230. Babu, Y. S.; Bugg, C. E.; Cook, W. J., Structure of calmodulin refined at 2.2 A resolution. *J Mol Biol* **1988,** *204* (1), 191-204.
231. Mukherjea, P.; Maune, J. F.; Beckingham, K., Interlobe communication in multiple calcium-binding site mutants of Drosophila calmodulin. *Protein Sci* **1996,** *5* (3), 468-77.
232. Sessa, W. C., eNOS at a glance. *Journal of cell science* **2004,** *117* (Pt 12), 2427-9.
233. Campbell, M. G.; Smith, B. C.; Potter, C. S.; Carragher, B.; Marletta, M. A., Molecular architecture of mammalian nitric oxide synthases. *Proc Natl Acad Sci U S A* **2014,** *111* (35), E3614-23.
234. Stuehr, D. J.; Tejero, J.; Haque, M. M., Structural and mechanistic aspects of flavoproteins: electron transfer through the nitric oxide synthase flavoprotein domain. *The FEBS journal* **2009,** *276* (15), 3959-74.
235. Bers, D. M.; Patton, C. W.; Nuccitelli, R., A practical guide to the preparation of Ca(2+) buffers. *Methods in cell biology* **2010,** *99*, 1-26.
236. Boo, Y. C.; Tressel, S. L.; Jo, H., An improved method to measure nitrate/nitrite with an NO-selective electrochemical sensor. *Nitric oxide : biology and chemistry* **2007,** *16* (2), 306-12.
237. Chen, H.; Venkat, S.; McGuire, P.; Gan, Q.; Fan, C., Recent Development of Genetic Code Expansion for Posttranslational Modification Studies. *Molecules (Basel, Switzerland)* **2018,** *23* (7).
238. MacMillan-Crow, L. A.; Thompson, J. A., Tyrosine modifications and inactivation of active site manganese superoxide dismutase mutant (Y34F) by peroxynitrite. *Arch Biochem Biophys* **1999,** *366* (1), 82-8.
239. MacMillan-Crow, L. A.; Crow, J. P.; Kerby, J. D.; Beckman, J. S.; Thompson, J. A., Nitration and inactivation of manganese superoxide dismutase in chronic rejection of human renal allografts. *Proc Natl Acad Sci U S A* **1996,** *93* (21), 11853-8.
240. Pennington, K. L.; Chan, T. Y.; Torres, M. P.; Andersen, J. L., The dynamic and stress-adaptive signaling hub of 14-3-3: emerging mechanisms of regulation and context-dependent protein-protein interactions. *Oncogene* **2018,** *37* (42), 5587-5604.
241. Nuriel, T.; Whitehouse, J.; Ma, Y.; Mercer, E. J.; Brown, N.; Gross, S. S., ANSID: A Solid-Phase Proteomic Approach for Identification and Relative Quantification of Aromatic Nitration Sites. *Frontiers in chemistry* **2015,** *3*, 70.
242. Ghesquiere, B.; Colaert, N.; Helsens, K.; Dejager, L.; Vanhaute, C.; Verleysen, K.; Kas, K.; Timmerman, E.; Goethals, M.; Libert, C.; Vandekerckhove, J.; Gevaert, K., In vitro and in vivo protein-bound tyrosine nitration characterized by diagonal chromatography. *Mol Cell Proteomics* **2009,** *8* (12), 2642-52.

243. Zhao, Y.; Zhang, Y.; Sun, H.; Maroto, R.; Brasier, A. R., Selective Affinity Enrichment of Nitrotyrosine-Containing Peptides for Quantitative Analysis in Complex Samples. *Journal of Proteome Research* **2017,** *16* (8), 2983-2992.
244. Arbely, E.; Torres-Kolbus, J.; Deiters, A.; Chin, J. W., Photocontrol of tyrosine phosphorylation in mammalian cells via genetic encoding of photocaged tyrosine. *J Am Chem Soc* **2012,** *134* (29), 11912-5.
245. Italia, J. S.; Zheng, Y.; Kelemen, R. E.; Erickson, S. B.; Addy, P. S.; Chatterjee, A., Expanding the genetic code of mammalian cells. *Biochem Soc Trans* **2017,** *45* (2), 555-562.
246. Zheng, Y.; Lewis, T. L., Jr.; Igo, P.; Polleux, F.; Chatterjee, A., Virus-Enabled Optimization and Delivery of the Genetic Machinery for Efficient Unnatural Amino Acid Mutagenesis in Mammalian Cells and Tissues. *ACS Synth Biol* **2017,** *6* (1), 13-18.
247. Nikic, I.; Estrada Girona, G.; Kang, J. H.; Paci, G.; Mikhaleva, S.; Koehler, C.; Shymanska, N. V.; Ventura Santos, C.; Spitz, D.; Lemke, E. A., Debugging Eukaryotic Genetic Code Expansion for Site-Specific Click-PAINT Super-Resolution Microscopy. *Angew Chem Int Ed Engl* **2016,** *55* (52), 16172-16176.
248. Fukui, M.; Zhu, B. T., Mitochondrial superoxide dismutase SOD2, but not cytosolic SOD1, plays a critical role in protection against glutamate-induced oxidative stress and cell death in HT22 neuronal cells. *Free Radic Biol Med* **2010,** *48* (6), 821-30.
249. Connor, K. M.; Subbaram, S.; Regan, K. J.; Nelson, K. K.; Mazurkiewicz, J. E.; Bartholomew, P. J.; Aplin, A. E.; Tai, Y. T.; Aguirre-Ghiso, J.; Flores, S. C.; Melendez, J. A., Mitochondrial H2O2 regulates the angiogenic phenotype via PTEN oxidation. *The Journal of biological chemistry* **2005,** *280* (17), 16916-24.
250. Arulpragasam, A.; Magno, A. L.; Ingley, E.; Brown, S. J.; Conigrave, A. D.; Ratajczak, T.; Ward, B. K., The adaptor protein 14-3-3 binds to the calcium-sensing receptor and attenuates receptor-mediated Rho kinase signalling. *Biochem J* **2012,** *441* (3), 995-1006.
251. Chatterjee, S.; Lardinois, O.; Bonini, M. G.; Bhattacharjee, S.; Stadler, K.; Corbett, J.; Deterding, L. J.; Tomer, K. B.; Kadiiska, M.; Mason, R. P., Site-specific carboxypeptidase B1 tyrosine nitration and pathophysiological implications following its physical association with nitric oxide synthase-3 in experimental sepsis. *J Immunol* **2009,** *183* (6), 4055-66.
252. Hu, S.; Liu, H.; Ha, Y.; Luo, X.; Motamedi, M.; Gupta, M. P.; Ma, J. X.; Tilton, R. G.; Zhang, W., Posttranslational modification of Sirt6 activity by peroxynitrite. *Free Radic Biol Med* **2015,** *79*, 176-85.
253. Aggarwal, S.; Gross, C. M.; Rafikov, R.; Kumar, S.; Fineman, J. R.; Ludewig, B.; Jonigk, D.; Black, S. M., Nitration of tyrosine 247 inhibits protein kinase G-1alpha activity by attenuating cyclic guanosine monophosphate binding. *The Journal of biological chemistry* **2014,** *289* (11), 7948-61.
254. Shi, Q.; Xu, H.; Yu, H.; Zhang, N.; Ye, Y.; Estevez, A. G.; Deng, H.; Gibson, G. E., Inactivation and reactivation of the mitochondrial alpha-ketoglutarate dehydrogenase complex. *The Journal of biological chemistry* **2011,** *286* (20), 17640-8.

255. Takakusa, H.; Mohar, I.; Kavanagh, T. J.; Kelly, E. J.; Kaspera, R.; Nelson, S. D., Protein tyrosine nitration of mitochondrial carbamoyl phosphate synthetase 1 and its functional consequences. *Biochemical and biophysical research communications* **2012,** *420* (1), 54-60.
256. Viera, L.; Radmilovich, M.; Vargas, M. R.; Dennys, C. N.; Wilson, L.; Barnes, S.; Franco, M. C.; Beckman, J. S.; Estevez, A. G., Temporal patterns of tyrosine nitration in embryo heart development. *Free Radic Biol Med* **2013,** *55*, 101-8.
257. Zhang, Y.; Werling, U.; Edelmann, W., SLiCE: a novel bacterial cell extract-based DNA cloning method. *Nucleic acids research* **2012,** *40* (8), e55.
258. Italia, J. S.; Latour, C.; Wrobel, C. J. J.; Chatterjee, A., Resurrecting the Bacterial Tyrosyl-tRNA Synthetase/tRNA Pair for Expanding the Genetic Code of Both E. coli and Eukaryotes. *Cell chemical biology* **2018,** *25* (10), 1304-1312.e5.
259. Rauch, B. J.; Porter, J. J.; Mehl, R. A.; Perona, J. J., Improved Incorporation of Noncanonical Amino Acids by an Engineered tRNA(Tyr) Suppressor. *Biochemistry* **2016,** *55* (3), 618-28.
260. Hornsby, M.; Paduch, M.; Miersch, S.; Saaf, A.; Matsuguchi, T.; Lee, B.; Wypisniak, K.; Doak, A.; King, D.; Usatyuk, S.; Perry, K.; Lu, V.; Thomas, W.; Luke, J.; Goodman, J.; Hoey, R. J.; Lai, D.; Griffin, C.; Li, Z.; Vizeacoumar, F. J.; Dong, D.; Campbell, E.; Anderson, S.; Zhong, N.; Graslund, S.; Koide, S.; Moffat, J.; Sidhu, S.; Kossiakoff, A.; Wells, J., A High Through-put Platform for Recombinant Antibodies to Folded Proteins. *Mol Cell Proteomics* **2015,** *14* (10), 2833-47.
261. Muyldermans, S., Nanobodies: natural single-domain antibodies. *Annu Rev Biochem* **2013,** *82*, 775-97.
262. Brown, W.; Liu, J.; Deiters, A., Genetic Code Expansion in Animals. *ACS Chem Biol* **2018,** *13* (9), 2375-2386.
263. Elsasser, S. J.; Ernst, R. J.; Walker, O. S.; Chin, J. W., Genetic code expansion in stable cell lines enables encoded chromatin modification. *Nat Methods* **2016,** *13* (2), 158-64.